THE THREE-DIMENSIONAL STRUCTURE OF THE EPSTEIN-BARR VIRUS GENOME VARIES BY LATENCY TYPE AND IS REGULATED BY PARP1 ENZYMATIC ACTIVITY

A Dissertation Submitted to the

Temple University Graduate Board

In Partial Fulfillment of the Requirements for the Degree

DOCTOR OF PHILOSOPHY

by

Sarah Johnson

May 2021

Examining Committee:

Kelly Whelan, Ph.D. (Advisor), Department of Pathology and Laboratory Medicine

Italo Tempera, Ph.D., The Wistar Institute Cancer Center, Gene Expression & Regulation Program

Stefania Gallucci, Ph.D., Department of Microbiology and Immunology

Bassel Sawaya, Ph.D., Department of Neurology

Vincent Tam, Ph.D. (External Examiner), Department of Microbiology and Immunology

ABSTRACT

Epstein-Barr virus (EBV) establishes life-long latency in human B-cells by maintaining its chromatinized episomes within the nucleus. These circularized mini-chromosomes do not integrate into the host genome. Therefore, it is essential for EBV to organize its chromatin in a manner suitable for genomic stability, DNA replication, and efficient gene expression. Poly [ADP-ribose] polymerase 1 (PARP1) activity is significantly higher in B-cells infected with EBV than those without, and considerably higher in the transcriptionally active type III latency compared to the immunoevasive type I. In addition to its role in DNA damage response, PARP1 has been implicated in transcriptional regulation and structural maintenance of both the human and EBV genome at specific regions. To better understand PARP1's role in the regulation of the EBV episome, we have functionally characterized the effect of PARP enzymatic inhibition on total episomal structure through *in situ* Hi-C mapping, generating the first complete 3D structure of the EBV genome. We have also mapped intragenomic contact changes after PARP inhibition to global binding of the chromatin looping factors CTCF and cohesin across the EBV genome. In doing so, we found that PARP inhibition stabilizes cohesin-chromatin binding while decreasing CTCF binding. PARP inhibition resulted in widespread alterations to chromatin structure, with fewer overall unique intragenomic interactions. Despite this, some areas have new chromatin loops not seen in the untreated EBV episome. Additionally, PARP inhibition was shown to alter gene expression at the regions where chromatin looping was most affected. The altered expression profile after the structural rearrangement induced by PARP inhibition also supports the idea that PARP1 helps maintain EBV latency programs, as many of the significantly upregulated genes were indicative of lytic reactivation. The data presented herein allows us to conclude that PARP1 does have an essential role in the regulation of global EBV chromatin structure. And furthermore, it provides the first study showing that PARP enzymatic activity alone can regulate 3D chromatin structure on a global scale.

ACKNOWLEDGEMENTS

I would like to thank my thesis advisor Dr. Italo Tempera for his continued support and guidance throughout this program. I would also like to thank him for giving me the freedom to explore questions that piqued my own curiosity and learn new techniques that interested me. Without his efforts, I would not have been able to pursue the career trajectory I have always dreamed of and for this I am truly grateful. After Dr. Tempera moved his lab to the Wistar Institute, Dr. Kelly Whelan stepped in as my advisor, allowing me to finish my doctorate. For this I am also incredibly grateful.

My committee members Dr. Kelly Whelan, Dr. Stefania Gallucci, and Dr. Bassel Sawaya, have also facilitated my development as a scientist and a speaker. They asked me tough questions that strengthened my work tremendously and gave me honest feedback that has allowed me to develop my confidence as a professional.

I would also like to thank my colleagues in the Tempera lab, particularly Dr. Lisa Caruso and Dr. Michael Hulse. Lisa was an incredibly involved mentor to me during my early years in the lab, while Michael went above and beyond in teaching me how to navigate life as a graduate student at Temple and advising me during important milestones in my career thus far.

Additionally, I genuinely do not believe I would have had the mental fortitude to tackle the challenges I have faced in my graduate career without Dr. Kelly Whelan and Dr. Nora Engel. They have been always been available to listen to my problems, both professionally and personally, and provide me with invaluable advice as amazing women in science. I am so grateful to have known them and hope to be a mentor like them in the future.

Finally, I would like to thank my parents for always being on my side, and my best friend Carolyn Dann for being a constant inspiration to follow my dreams and never be discouraged.

TABLE OF CONTENTS

Page

LIST OF FIGURES

CHAPTER 1

INTRODUCTION

Chromatin Organization and Transcriptional Regulation

The ability to store and faithfully replicate genetic information is vital for successful long-term division of cells. To protect and spatially accommodate roughly 3 billion base pairs (bp), DNA must compact. With the help of proteins called histones, DNA folds into 30nm fibers of chromatin (1). DNA is negatively charged, enabling a strong interaction with the positively charged "tails" of histones. Numerous studies have shown the functional importance of N-terminal histone tails in chromatin conformation. The N-terminal tails of H2A, H3, and H4 variants help form chromatin structures more complex than the 30nm fiber, called "higher-order" structures, while the H2B N-terminal tail is essential for any form of chromosome compaction (2). Deletion of histone tails *in vitro* destabilizes nucleosome formation and opens DNA structures, making DNA more accessible (2). Nucleosomes, formed by two copies each of H2A, H2B, H3, and H4, are wrapped by 145-146bp of DNA in roughly 1.7 helical turns (2). The DNA-bound octamers are connected by 10-100 bp of DNA, known as "linker DNA", associated with histone variant H1 (1).

While the exact structure is still debated, it is generally accepted that chromatin is heterogenous in living nuclei, with more and less compact regions to enable a functional relationship between chromatin and the numerous DNA-binding proteins necessary to maintain cellular function and viability (1). Transcriptionally inactive chromatin is highly compact with a regular folding pattern (1). However, a small amount of the mammalian genome has irregular folding enabling binding of proteins such as those involved in the DNA-damage response, transcription, and replication (1). At a given time in any cell, it is estimated that only 1% of DNA is in an open, accessible state which permits protein binding (3). Maintenance of chromatin structure and compaction is a dynamic process under numerous layers of regulation that we are only just beginning to understand. After the initial formation of nucleosomes, it is thought that the chromatin is further condensed by interactions between linker DNA and the highly basic histone tails, as well as the interactions between histone tails and acidic patches of neighboring nucleosomes (2). This second layer of

DNA compaction is considerably less accessible to trans-acting proteins than nucleosomal DNA and is thus considered the first step in chromatin-mediated regulation of transcription (4).

The exact formation of nucleosomal DNA within the 30nm fiber is still unknown, mainly due to limitations in resolution of X-ray crystallography (4). Early studies attempting to elucidate the inner structure of chromatin aimed to extract DNA from nuclei where it is presumably in its native conformation, thus providing a physiologically relevant template for analysis (4). This methodology contained inherent flaws in that native chromatin is remarkably heterogenous, making it difficult to determine fine details of nucleosomal arrays that would be applicable as general characteristics across the genome (4). Awaiting the emergence of better methods to visualize chromatin *in situ*, mathematical modeling combined with *in vitro* assays which systematically reconstitute nucleosomal arrays has provided two formation model classes that spatially fit the 30nm fiber diameter (4). The “solenoid” model consists of a linearly arranged nucleosome stack arising from one starting point connected by spiraling linker DNA, while the “zig-zag” model proposes two starting points of parallel nucleosome stacks connected by straight lines of linker DNA (4).

Past the elusive organization within the DNA fiber, chromatin is further compact as a heterogenous pattern of “euchromatin” and “heterochromatin” during interphase, the phase of the cell cycle in which DNA is actively replicated and transcribed. Euchromatin is considerably less compact and thus more accessible to replication and transcription machinery while heterochromatin is densely packed and formed by the 30nm fiber folding back onto itself as a series of tightly wound loops (5). Because of this, euchromatin is generally characterized as transcriptionally active with the opposite true for heterochromatin. In addition to state of compaction, chromatin can also be characterized by its regional histone modifications, which can also significantly impact DNA accessibility and thus transcriptional activity (6). Covalently bound post-translational modifications of core and linker histones have long been studied for their impact on transcriptional activity and have more recently been implicated as essential components of the DNA damage response, cell cycle checkpoint program, spermatogenesis, and apoptosis in humans (7-11). The most extensively studied histone

tail markings include lysine acetylation, serine/threonine/tyrosine phosphorylation, and lysine methylation. Acetylation and phosphorylation are negatively charged PTMs generally characterized as transcriptional activators that work by neutralizing the positive charge of histone tails (and a handful of histone core examples) thus destabilizing the nucleosome structure (12, 13). Like the previous PTMs, most methyl marks occur on N-terminal histone tails (12). However, methyl modifications were traditionally characterized as transcriptionally repressive as they do not carry a negative charge, so the electrostatic interactions within the nucleosome are preserved allowing chromatin to remain compact (12). Methyl groups can also be added as a chain of two to three, generating possible steric interference against transcriptional machinery (12, 13). Despite this, methylated histones can be found in euchromatin and heterochromatin, proving methylation to be more enigmatic than previously thought (2, 13). Less characterized classes of histone PTMs include ubiquitination, SUMOylation, and poly-ADP-ribosylation (PARylation), all of which are significantly larger than their better characterized counterparts and exert a more dynamic effect on chromatin and gene regulation (12). The study of how PTMs impact DNA structure and accessibly, and thus gene expression, is the basis for the field of epigenetics.

To accommodate the cellular processes necessary for cell survival and replication, there are numerous mechanisms to unpack chromatin. This process is mediated by two general classes of proteins, the first of which is chromatin modifying enzymes (CME) that can post-translationally modify (PTM) histones directly to alter their electrostatic interactions with DNA, ultimately perturbing chromatin structure through addition of the various groups described above (12). The PTM of histones can also exert a secondary effect of altering the ability of other proteins to bind DNA by providing docking sites that can be bound by specific protein domains (12). The second class, chromatin remodeling enzymes (CRE), work by repositioning histones along DNA or by replacing core histones with histone variants (14, 15). By sliding nucleosomes to neighboring regions of DNA, these ATP-dependent protein complexes can allow access to promoter regions or other regulatory sequences to affect gene expression (16). CRE can also affect transcription by recruiting additional regulatory complexes through substitution of histone variants which can provide docking sites to

these proteins (16). Histone modifications and variants can help establish boundary regions of different types of DNA with varying transcriptional activity, as mentioned previously in distinguishing heterochromatin and euchromatin (14, 16).

Chromatin is also separated into “compartments” and “topologically-associating domains”. Compartments fall into an “A” or “B” category, with A referencing transcriptionally active chromatin and B referencing transcriptionally inactive chromatin- both of which can span numerous megabases of the genome in an irregular pattern (6). Both A and B compartments preferentially interact with other compartments of the same type, allowing chromatin with similar transcriptional activity to physically associate in 3D space within the nucleus (6). Topologically-associating domains (TADs) are sub-megabase regions of chromatin that interact preferentially within themselves (6, 17). In general, compartments are composed of numerous TADs (6, 17). The smallest categorization of chromatin used frequently in literature is the “subTAD”, also known as “contact domains”, which can be found within TADs (6, 17).

Physical interactions of chromatin within the nucleus can span millions of bases and have a direct impact on gene regulation. Numerous studies can be cited amongst mammalian genomes illustrating the functional role of TADs in facilitating enhancer-promoter communication (18). The murine Sonic Hedgehog (*shh*) gene promoter, for example, is regulated by an enhancer nearly a megabase away known as the Zone Of Polarizing Activity Regulatory Sequence (ZRS) (19, 20). When sequences within the TAD comprising the *shh* promoter and ZRS enhancer were inverted resulting in the disruption of folding and local contacts within the TAD, *shh* expression decreased (20). In this way, TADs regulate gene expression in *cis* by enabling regulatory sequences to act upon genes that may be located numerous megabases away by physically folding the chromosome.

Interestingly, there are also examples of interchromosomal *trans* interactions allowing a regulatory sequence of one chromosome to influence expression of a gene located on a different

chromosome, such as the regulatory regions of the TH2 cytokine locus located on murine chromosome 11 and the interferon-gamma promoter region of chromosome 10 (21, 22).

Current methods of study

As mentioned previously, chromatin is largely organized in three-dimensional space within the nucleus according to relative transcriptional activity. Chromatin tends to colocalize in topologically associating domains (TADs) which preferentially interact within themselves. Numerous transcriptionally active TADs that physically associate are referred to as “A compartments”, while inactive TADs are grouped into “B compartments” (6). The TADs making up these compartments can be separated by many megabases (6). The relatively transcriptionally silent B compartments tend to localize around the nuclear periphery, physically interacting with the nuclear lamina (23). The roughly .5Mb chromatin regions interacting with the nuclear lamina are known as “lamina-associated domains (LADs)” (23). Beyond the TAD level, entire chromosomes are also reproducibly found in interphase cells at specific “chromosome territories” that are arranged according to gene density, size, and proximity to other chromosomes, in a cell-type specific manner (24-30).

Technological advances in the study of chromatin organization and structure, and the consequent influence on gene expression, have made great strides in recent years. A comprehensive catalog of published genome-wide association studies (GWAS) has relieved that the majority of disease-associated loci lie within non-coding regions of the human genome (31). As many of these loci are distal from the protein-coding genes associated with their respective disease, it is plausible that they have regulatory functions that require chromatin folding to bring the two regions in appropriate proximity (31, 32). In fact, the study of chromatin structure and its implication on gene expression has led to the formation of the “4D Nucleome Network” which aims to generate single cell and population models of spatial genome organization (32). The formation of this publicly available data-sharing network would incorporate data gathered from numerous types of chromatin conformation assays.

The oldest forms of chromatin conformation assays relied on fluorescent microscopy (33, 34). DNA fluorescence in situ hybridization (DNA-FISH) is a method to visualize the physical location of a specific segment of DNA within a single nucleus via hybridization with probe DNA or RNA that has been fluorescently labeled (35, 36). DNA-FISH was introduced in 1969 yet is still widely used today for its ability to locate exact regions of interest in a single-cell format. Since then, researchers wanting to study all chromatin within a single cell can use an array of high-resolution, fluorescent microscopy techniques including: chromatin electron microscopy tomography, stimulated-emission-depletion fluorescence, structured illumination, sub-diffraction-limit imaging by stochastic optical reconstruction, and direct stochastic optical reconstruction (37-41). These techniques, dubbed “fluorescent nanoscopy”, have the potential to generate chromatin images *in situ* at 1nm resolution while preserving the native conformation of the DNA (42).

For population studies, chromatin conformation capture (3C) or “proximity-based” techniques are preferable (33, 34). In general, this group of techniques relies on chemical crosslinking of DNA-DNA and DNA-protein interactions, followed by fragmentation of the chromatin and subsequent ligation (33). Figure 1, from an excellent review by Kempfer and Pombo on 3C technologies, provides a graphical overview of these methodologies (34). The original 3C method relies on prior knowledge of the sequence of a region of interest within the genome to generate an “anchor primer” which remains in a fixed orientation (43). The PCR primers in the opposite orientation are of variable distance from the anchor primer (43). In this way, researchers are able to determine which region was physically interacting with the anchor primer at the time of chemical crosslinking (43). This targeted approach was further developed into “chromosome conformation capture-on-chip” (4C), or circularized 3C, enabling the identification of all regions interacting with one region of interest without the need for systematic generation of variable primers opposing the anchor primer within the region of interest (44, 45). The advent of “chromatin conformation capture carbon copy” (5C) enabled the ligation product libraries generated in 3C to be amplified and hybridized to microarrays or sequenced in totality, generating DNA-DNA contact maps for cell populations (46). 5C still however only enabled visualization of relatively high-frequency ligation products (47). To overcome

this, Lieberman-Aiden *et al* developed “Hi-C”, a method that incorporates a biotin tag during the ligation of DNA-DNA contacts, allowing ligation products to first be pooled into a purified library before massively-parallel sequencing (48). To date, Hi-C technologies are still being improved upon. All methods described to this point had primarily formaldehyde fixed pre-lysed nuclear solutions. In 2014, Rao *et al* developed *in situ* Hi-C, where DNA-DNA interactions were covalently bound within intact nuclei in the hopes of preserving native chromatin conformation to generate a more accurate view of chromatin folding within live cell populations at kilobase resolution (49). Of course, even *in situ* Hi-C still has the major limitation of all population studies, in that the contact maps generated can only provide a generalized view of the most frequent DNA-DNA contacts within the population. While single cell Hi-C methods are in development, current coverage of genome-wide datasets only reach ~2.5% (50, 51).

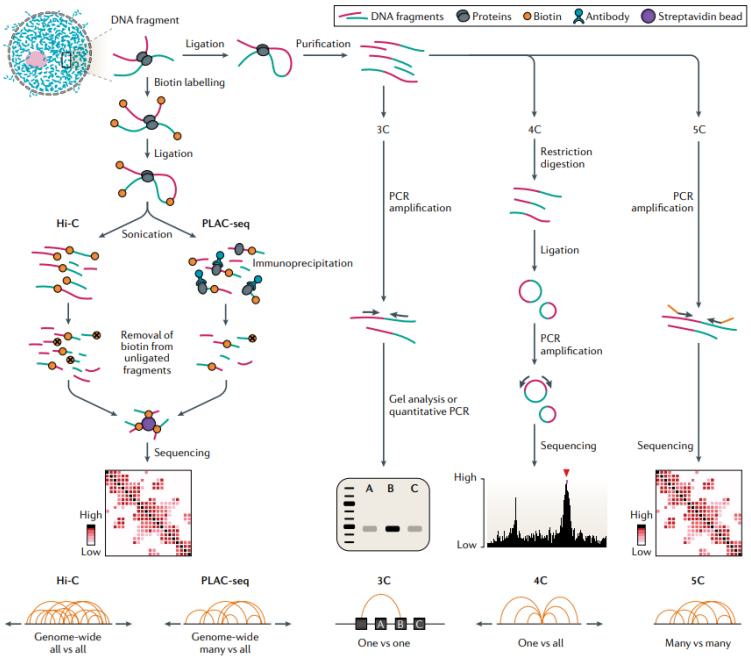

Kempfer and Pombo. In “Methods for mapping 3D chromosome architecture.” Figure 3. Nature Reviews, 2020.

Figure 1. 3C and its derivatives. All methods begin with chemical crosslinking, followed by DNA fragmentation and ligation. Hi-C differs in the incorporation of a biotin tag in the ligation. 3C and 4C require the use of known primer sequences for amplification, while Hi-C and 5C utilize universal primers and Next-Generation sequencing.

CTCF, cohesin, and the loop extrusion model

As mentioned previously, mammalian genomes are separated into large compartments, denoted “A” or “B” based upon transcriptional activity, with A as transcriptionally active and B as inactive. A

compartments tend to physically interact with other A compartments, and B with B (6). Located within compartments are topologically-associating domains (TADs), sub-megabase regions of chromatin that interact preferentially within themselves (6, 17, 52, 53). TADs are in general, though not always, separated by boundaries enriched in transcriptionally active genes and binding sites for the DNA-binding protein CCCTC-binding factor (CTCF) (54-56). In the sub-megabase range are preferentially interacting regions which can be present inside, between, or overlapping CTCF loops in mammalian genomes, known as subTADs or contact domains (6, 57).

By binding to at least 60,000 sites across mammalian genomes with its central domain containing 11-zinc finger motifs, CTCF has a dynamic role in regulation of gene expression. CTCF has been shown over numerous decades to function as an insulator to physically separate different regulatory regions of chromatin and to directly impact gene transcription, activating or repressing expression in a context dependent manner (58). When the specific consensus sequence "CCGCGNGGNGGCAG" is unmethylated and located within an insulator region of DNA, CTCF is able bind and prevent the effects of cis-acting enhancers, thus preventing transcription of specific genes (59). For example, when CTCF binds to its consensus sequence within the chicken β-globin locus, it blocks association of the gene's enhancer with the β-globin promoter region, thus decreasing expression of the gene by physically isolating the enhancer region within a chromatin loop (59, 60). CTCF also functions as an insulator in a different sense by preventing the spread of aberrant histone marks. For example, CTCF binding is known to prevent the spread of the activating histone mark H3K4me3 to regions of low gene expression and conversely prevent the spread of the repressive histone mark H3K27me3 to regions of active gene expression (61, 62). As mentioned previously, CTCF binding is also essential to higher order chromatin structure. Two CTCF proteins binding in a convergent orientation often leads to the formation of a chromatin loop between the regions (49, 63). Infrequently, CTCF-mediated chromatin loops can also form when two CTCF binding sites are in the forward-forward or reverse-reverse orientation, but almost never occur when the binding sites are in the divergent "reverse/forward" orientation (64). Regardless of insulation or loop-formation, the binding of CTCF is contingent on DNA being unmethylated.

In the human genome, CTCF shares the majority of its conserved binding sites with the multimeric protein complex cohesin, composed of a V-shaped SMC1/3 heterodimer bound by RAD21 and SA1/2 (STAG1/2) to form a ring-like structure (6, 58, 65). Weak-affinity cohesin binding sites are often found within active promoter or enhancer regions where it colocalizes with its loading factor NIPBL, mediator components, and transcription factors (6). Strong cohesin binding sites generally map to CTCF binding sites and are thought to be “recruited” by CTCF via the extrusion model to form TADs (66, 67). The loop extrusion model suggests that the cohesin structural maintenance of chromosomes proteins (SMCs) progressively extrude chromatin through their ring-shaped protein structure until blocked by CTCF proteins bound in the correct orientation (66-68). Recent *in silico* models have suggested that nucleosomes existing in a high enough concentration above linker histones may aid CTCF in the formation of a “cohesin barrier”, barring further cohesin movement (69). Once colocalized, the cohesin complex physically encloses the two chromatin fibers together (63, 66, 67). CTCF depletion reduces cohesin enrichment at colocalization sites but does not disrupt the binding of cohesin to chromatin overall, implying that the persistence of CTCF binding is necessary for proper distribution of cohesin but not its loading or physical interaction with chromatin (70). CTCF depletion also results in loss of CTCF-mediated TADs and contact domains, while the larger compartments which are primarily mediated by transcriptional activity remain intact (71, 72). The megabase-scale compartments were surprisingly better segregated when cohesin was depleted, while CTCF-mediated chromatin loops were lost and CTCF binding remained unchanged (71, 73, 74). Chromosomal folding at the compartment level can only be disrupted by the depletion of both CTCF and cohesin, resulting in overall chromatin compaction and cell death (75).

While it is widely accepted that the cohesin complex physically forms chromatin loops utilizing CTCF anchor points, how cohesin mechanistically moves along DNA is less concrete. Models including diffusion via Brownian motion would largely depend on the DNA-bound concentration of cohesin complex and its loading factor, NIPBL (73, 76). A recent report combining Brownian 3D

dynamics simulations with exactly solvable 1D nonequilibrium models of “slip link molecules” mimicking cohesin behavior demonstrated that simple diffusion along DNA can account for observed *in vitro* cohesin motility (76). This model also showed a strong bias for chromatin loop formation with convergently oriented CTCF anchors (76). However, it cannot be overlooked that the SMCs within the cohesin complex contain intrinsic ATPase activity. Utilizing live, single-molecule imaging, Kim *et al* illustrated cohesin-NIPBL complex compacting both naked and nucleosome-bound DNA in an ATP-dependent process (77). Indeed, after depletion and subsequent reintroduction of cohesin *in vitro*, an independent study found that ATP deprived cells are unable to form cohesin-mediated CTCF loops, while chromatin loops within cells provided ATP are quickly re-established (78). It is also possible that these models are not mutually exclusive, as the same study also found that hundreds of CTCF-independent loops formed in the absence of ATP (78). Finally, a third model also proposes that cohesin may be pushed along DNA by RNA polymerase, as cohesin motility has been correlated with transcriptional activity *in vitro* and *in vivo* (70, 79-81).

Cohesin also likely has essential functions in transcriptional regulation that are independent of its role in chromatin looping. As mentioned previously, weak-affinity cohesin binding sites often do not overlap its high-affinity CTCF colocalization sites (6). The independent binding sites are generally within promoter or enhancers and are bound specifically by SA2 variant containing cohesin complex, while CTCF anchor sites are bound by either variant (82). Interestingly, SA1-containing complex cannot be substituted for cohesin-SA2 in its absence, suggesting that cohesin-SA1 has a larger role in chromatin looping while cohesin-SA2 has a unique role in facilitation of enhancer-promoter contacts (82). Cohesin-SA2 binding sites are also cell-type specific, underscoring an essential role in fine-tuning gene expression (82). As cohesin binding tends to correlate to regions of chromatin with higher transcriptional activity, and the binding at these sites is SA2 specific, it is also possible that cohesin has other functions in regulation of gene expression that have yet to be established.

While the importance of CTCF and cohesin as synergistic structural proteins in chromatin organization is well established, there is much work to be done in illustrating their roles in transcriptional regulation. There are numerous examples of targeted deletion or inversion of CTCF binding sites impacting expression of neighboring genes, such as the chicken β-globin and protocadherin β loci and the Igf2/H19 Imprinting Control Region (59, 64, 83, 84). However, knockdown of CTCF in HEK293T cells only significantly alters expression of 161 genes after 24 hours in culture (85). Though total cohesin or CTCF depletion results in cell death in culture after approximately four days, the immediate impacts on transcriptional regulation are not dramatic (74). After 24 hours of nearly complete CTCF knockout, 370 genes are differentially expressed, with only 43 reaching at least five-fold dysregulation (72). Knockdown of the RAD21 component of cohesin only results in five-fold dysregulation of two genes (73). Adding to the complexity, at least three separate classes of post-translational modifications (PTMs) have been identified on CTCF, all of which differentially impact its function. Poly-[ADP]-ribosylated (PARylated) CTCF was shown to bind to the Igf2/H19 imprinting control region with much higher affinity than un-PARylated CTCF, as well as be preferentially localized within nucleoli (86, 87). CTCF can also be phosphorylated on five separate, validated serine residues, which prevents its enhancer-blocking activity at the mammalian c-myc locus and may be essential to cell cycle progression (88, 89). Finally, SUMOylation enhances global CTCF repressor function and general chromatin condensation in a large transgene array study (90).

Beyond CTCF PTMs, cohesin also can be modified in a variety of ways including phosphorylation, acetylation, SUMOylation, and methylation. As cohesin was first identified as the integral protein in sister chromatid cohesion, its PTMs have primarily been characterized from this standpoint. Acetylation of SMC3 is essential for sister chromatin cohesion and for cohesin's association to DNA in general, though it remains unclear if acetylation is necessary for initial loading or persistence on DNA (91). SMC3 acetylation is also essential for proper replication fork progression, as acetylation destabilizes SMC3 interaction with its associating protein PDS5A and release factor WAPL (92). Destabilization of the binding of these proteins allowed the replication fork machinery to pass by

more quickly than in SMC3 mutants unable to be acetylated (92). Conversely, the SA1/SA2 (STAG1/2) and RAD21 components of cohesin must be phosphorylated in order to separate from sister chromatids during mitosis (93, 94). Cohesin is also known to be recruited to sites of DNA damage, particularly in the double-strand break response. Both SMC1 and SMC3 cohesin components are known to be phosphorylated in response to DNA damage, and cells deficient in phosphorylation of either of these proteins display improper regulation of S and G2/M checkpoints (95-100). Also following DNA damage, sister chromatid tethering was dependent upon SUMOylation of at least RAD21, though all subunits appeared to be SUMOylated after exposure to DNA damaging agents (101). Finally, in the yeast SMC1 homologue, Psm1, must be methylated for proper homologous recombination to occur following DNA damage (102). As the consequences of both cohesin and CTCF PTMs have primarily been studied in a locus-specific manner, there is much work to be done to determine what roles PTMs play in their function in general.

PARP1 and chromatin organization

Poly [ADP-ribose] polymerase 1, also referred to as ADP-ribosyltransferase D-type 1 (ARTD1), is one of eighteen proteins in the PARP family. PARPs facilitate the addition of poly-ADP ribose (PAR) onto various target proteins, including themselves, via poly-ADP ribosylation (PARylation) using NAD+ as substrate. The first PAR unit is covalently bound to a target's aspartic acid, glutamic acid, or lysine residue, followed by 2′,1″-O-glycosidic bonding of subsequent PAR units to form a straight or branched chain (103). However, only four members have definitive poly-ADP-ribose transferase activity, namely PARP1, 2, 5a, and 5b, with PARP1 accounting for at least 90% of PARylation induced by DNA damage (103, 104). The other members of the PARP family only have the ability to covalently bond the first ADP-ribose unit (mono-ADP-ribosylation/MARylation), or no catalytic activity at all (104). PARP1 has critical roles in response to numerous types of DNA damage including single-strand breaks via base-excision repair and double-strand breaks via homologous recombination or nonhomologous DNA end joining, primarily through recruitment of other proteins with PAR-binding motifs (103). Despite PARP1's established role in the DNA damage response, PARP1-KO mice are surprisingly viable, as PARP2 can compensate for PARP1's absence if

necessary (105). It is important to note, however, that PARP1-KO mice are more susceptible to DNA damaging agents and are prone to genomic instability, including chromosome breaks, chromosome fusions, aneuploidy, and telomere shortening (106-108).

PARP1 has numerous established roles outside of the DNA damage response, including cell growth, stress response, apoptosis, metabolic regulation, spermatogenesis, embryogenesis, and differentiation (109). More recently, PARP1 has been implicated in chromatin remodeling and epigenetic gene regulation. PARP1 has a dynamic role in these processes that can occur through numerous mechanisms resulting in positive or negative impacts on expression which are often cell type- and context-specific. Early studies of PARP1 in gene expression were conducted in *drosophila*, where PARP1 is activated by colocalization with the transcriptional activator heat shock factor (HSF) at the Hsp70 loci, inducing widespread PARylation throughout the region and loosened "puffed" polytene chromatin (110, 111). Additionally, PARylation of H1 histones within rat pancreatic polynucleosomes resulted in global de-condensation *in vitro*, while later studies found that histone H2B can also be PARylated in the absence of H1 (112, 113). However, contradictory studies utilizing purified polynucleosomes found that PARP1 not only could prevent MNase digestion but could also replace linker histone H1 function to form nucleosomal repeats (i.e. condensed chromatin) (114). Both studies concluded, however, that PARP1 catalytic activity is activated by association with nucleosomes. Despite PARP1 and H1 resulting in similar chromatin structure, the group also noted that PARP1 and H1 tend bind DNA in a mutually exclusive manner in live cells (114). This was not only validated by other groups, but shown to have distinct outcomes on transcription, with H1 found in regions of repressed transcription and PARP1 found around actively transcribed genes (115). Only adding to the complexity, when auto-PARylated, PARP1 may also serve as a histone chaperone by recruiting histones and efficiently facilitating nucleosome formation *in vitro* and in live cells (116).

PARP1 also has indirect effects on chromatin structure by modification of other chromatin remodeling enzymes. For example, PARP1 mediated PARylation of DNA-methyltransferase 1

inhibits its catalytic function, thereby allowing the structural protein CTCF to bind to sites that would normally be methylated and thus inaccessible to CTCF (117, 118). In fact, when PARP1 is pharmacologically inhibited or depleted, or site-directed-mutagenesis of CTCF prevents its PARylation, CTF is no longer able to bind to insulator regions that regulate expression of genes coding for E-cadherin, the tumor suppressors p16 and p19ARF, or Igf2 (119, 120). PARP1 also negatively regulates the expression and catalytic activity of the histone methyltransferase EZH2, the catalytic component of the PRC2 complex responsible for the repressive histone mark H3K27me3 (121, 122). The histone demethylase KDM5B is also negatively regulated by PARylation at least at specific loci, thereby maintaining an open chromatin landscape by preventing the removal of the activating histone park H3K4me3 while still preventing the inclusion of H1 (123). PARP1 also directly PARylates the *drosophila* SWI/SNF homologue, ISWI, thereby preventing nucleosome remodeling and chromatin loop formation *in vitro* and *in vivo* (124).

PARP1 also has more direct impacts on transcriptional activity than just modulation of local chromatin environment. Direct PARylation of TATA-binding protein prevents the formation of the pre-initiation complex, while PARylation of transcription factors like YY1, p53, CREB, Sp1, SRY, SOX2, and NFκB, impair their ability to bind to DNA, all of which have a negative impact on transcription (125). Interestingly, PARP1 negatively regulates its own expression by binding and stabilizing stem-loop structures upstream of its initiation site in a catalytically independent manner (126-128). PARP1 also can activate transcription in some circumstances by PARylation of transcriptional repressors. When phosphorylated, and thus activated, PARP1 PARylates itself, TLE/Groucho, TopoIIβ, nucleophosmin, nucleolin, and Rad50, as they are all part of a repressive complex preventing the differentiation of neuronal stem cells (129). As a result, local transcription is initiated and differentiation begins. PARP1 is also thought of as a general activator of transcription as it is often found colocalized with RNA-polymerase II. Positive transcription factors such as E2F1 and NFκB require PARP1 as a cofactor, with the latter specifically binding acetylated PARP1 (125).

Recently, PARP1 was found to regulate gene expression *in trans* via recruitment of circadian loci to the nuclear lamina. Upon the realization that PARP1 enzymatic activity follows a 24 hour schedule and seemed to be regulated by feeding in mice, Asher *et al* discovered that PARP1 deficient mice had impaired circadian rhythms (130). Further investigation revealed direct PARylation of the positive transcription factors CLOCK and BMAL at circadian loci, leading to their association with repressor proteins PER and CRY (130). Zhao *et al* later found that PARP1 also regulates the recruitment of circadian loci to the repressive environment of the nuclear lamina by its association with CTCF, thereby physically segregating the active compartments containing the loci (131). This finding also provides the first example of PARP1 mediating 3D chromatin structure, rather than just local chromatin accessibility.

Viral Chromatin Control

CTCF is not only indispensable in proper chromatin organization and gene regulation in mammalian genomes, but also in numerous viral genomes including: human herpesvirus 1 (HSV1), Kaposi's sarcoma-associated herpesvirus (KSHV), Epstein-Barr virus (EBV), human cytomegalovirus (HCMV), and human papillomavirus (HPV) (132-142). HSV1 has seven CTCF binding sites across its genome, which seem to be crucial in regulating the shift from latency to lytic reactivation in the virus (133-135). *In vitro* and *in vivo* models have shown that depletion of CTCF results in lytic reactivation, as CTCF occupancy normally diminishes across the viral genome early in the lytic cycle in a transcription-dependent manner (133-135). However, CTCF may also be required for structural maintenance of the lytic HSV1 genome, as its knockout *in vitro* resulted in dysregulated transcription of lytic genes, reduced viral copy number, and ablated mature virus production (132). In the lytic HSV1 genome, CTCF seems to insulate lytic transcripts from the spread of repressive chromatin marks H3K27me3 and H3K9me3, as well as possibly recruit RNA pol II (132). EBV also displays ubiquitous CTCF binding across its latency types, but with site-specific affinity and possibly different functions (137). Deletion of a CTCF binding site within the Q-promoter (Qp) utilized by EBV's minimally transcriptionally active type I latency in EBV bacmids lead to local repressive H3K9

methylation and an increase in expression of genes typically seen in the more transcriptionally active type III latency (136). However, other studies have shown that stable CTCF knockdown did not have the same effect, as genes typical of type III transcription were not upregulated in type I cell lines following knockdown, indicating that endogenous viral regulation may be more complex (139). In HCMV and HPV, CTCF knockdown and binding site mutagenesis, respectively, resulted in significantly higher viral replication (140, 141). Additional work in HPV has shown that CTCF is necessary for the recruitment of polycomb repressive complex which is responsible for deposition of repressive histone marks, resulting in decreased expression of viral proteins critical to the initiation of viral genome replication (142). The same work also showed that CTCF forms chromatin loops in the HPV genome that contribute to repressed viral replication(142) . It is of note that all examples provided here at least in part are a result of the direct binding of CTCF to the viral genome, rather than downstream effects from CTCF's regulation of host trans-acting factors on the virus.

CTCF shares roughly half of its binding sites in the human genome with cohesin, but this is not always the case for viral genomes. In EBV, cohesin is always found colocalized with CTCF, but CTCF has some independent binding sites without cohesin (143, 144). The same can be said for KSHV, where cohesin binding is dependent on CTCF colocalization, whereas CTCF can bind without the presence of cohesin (145). However, CTCF-cohesin interaction is essential for transcriptional regulation in the virus's latent and lytic cycles (145-148). When a CTCF binding site within the latency control region was deleted from EBV-bacmids, cohesin was no longer able to bind either, culminating in increased expression of lytic transcripts and a loss in colony formation ability (146). A follow-up study revealed that CTCF/cohesin binding on the viral genome fluctuates with the host cell cycle (147). Overexpression of the cohesin subunit RAD21 repressed transcription of lytic genes, as did ectopic expression of a CTCF-cohesin fusion protein, indicating a strong role for cohesin in maintenance of KSHV latency (147). Furthermore, CTCF and cohesin were found to form chromatin loops in the KSHV genome that fluctuated with the host cell cycle, providing a functional outcome for the previous study (148). The chromatin looping was also altered during lytic

reactivation of the virus (148). Both CTCF and cohesin were additionally found to be required for genomic stability and replication in human papillomavirus, with knockdown of CTCF or cohesin component SMC1 preventing viral replication (149).

As mentioned previously PARP1 and CTCF share numerous binding sites across the yeast and mammalian genome, particularly at sites of active transcription and insulator regions (103, 104). The same is true for EBV, where PARP1 binds at all CTCF sites in addition to one to two independent sites (150). EBV infection of B-cells, in particular expression of latent membrane protein 1 (LMP1), induces markedly increased intracellular PAR levels through activation of PARP1 (151). After which, PARP1 is necessary to stabilize CTCF binding in type III latency at the C-promoter (150). When PARP1 is pharmacologically inhibited or knocked down, CTCF binding is ablated, expression of neighboring transcripts is decreased, and repressive histone marks spread to the region while activating marks decrease (150). PARP1 binding is necessary at the EBV lytic promoter to repress its activation and maintain latency (152). If PARP1 is inhibited, lytic transcript expression is increased as well as viral copy number (152, 153). In KSHV, PARP1 is also critical for viral replication in latency and suppression of lytic reactivation (154). *In vitro*, KSHV viral processivity factor 8 (PF-8) facilitates degradation of PARP1, presumably to avoid immune detection and maintain genomic stability upon lytic reactivation (155). PARP1 is also a transcriptional repressor of lytic genes in the related murine gamma-herpesvirus 68 (MHV68), as such lytic replication is activated upon PARP1 knockout (156). In the unrelated influenza A virus (IAV), PARP1 is required for synthesis of viral nucleoprotein, yet inhibition of its enzymatic function increased viral titer and general expression of viral transcripts, indicating that the presence of PARP1 itself and PARylation may have independent roles (157). Finally, PARP1 knockout cells infected with human immunodeficiency virus (HIV) had almost complete protection due to prevention of viral integration with the host genome, though this work has been contradicted by subsequent studies (158-160). Once integrated, however, PARP1 binding suppressed viral transcription independent of its enzymatic activity (161).

Finally, at least in the context of EBV, chromatin conformation seems to alter by latency type at key regulatory regions. EBV utilizes different promoters per latency program, with transcription initiated by the Q-promoter (Qp) characteristic of type I latency, and the C-promoter (Cp) in type III. When assessed by 3C, it was found that the viral origin of replication (OriP) and Qp physically interact in type I latency, while in type III latency OriP preferentially interacts with Cp (162). This altered chromatin looping was at least in part mediated by CTCF binding, as mutation of the CTCF binding site within Qp disrupted the OriP-Qp latency I loop (162). This disturbance also correlated with alternative Cp usage in type I cells and diminished Qp transcription (162). In 293 cells infected with EBV-bacmid, mutation of the CTCF binding site within Qp as well as siRNA depletion of CTCF ablated chromatin looping with OriP (162).

Epstein-Barr Virus and Associated Malignancies

Epstein-Barr virus (EBV) is a ubiquitous gamma-herpesvirus infecting at least 90% of the global population (163). As with all human herpesviruses, EBV persists in varying latency types throughout the lifetime of its host, with numerous stressors able to induce lytic reactivation (163). EBV typically establishes primary infection during early childhood generally resulting in asymptomatic infection. If primary infection is established later in life, typically between the ages of 10-30, it leads to the development of infectious mononucleosis (IM) (163). Beginning after a uniquely long six-week incubation period, IM is characterized by lymphocytosis, sore throat, lymphadenopathy, and fatigue (163). Symptomatic infection lasts an average of 18 days, with some cases still symptomatic up to 54 days post symptom-onset (163). EBV is primarily spread through kissing and sharing of food, however there are less common modes of transmission including blood and allograft transplants (163).

After initial contact with infectious fluids, EBV primarily infects the epithelial cells of the oropharynx region. EBV then rapidly proliferates within the epithelia and viral shedding begins (164). These virions go on to infect host naïve B-lymphocytes, where the virus then enters a “latency III” transcriptional program inducing rapid cellular proliferation known as a “blast phase” (164). In route to the lymphoid follicles where infected B-lymphocytes will form germinal centers, EBV begins

expressing less latency proteins thus entering “latency II” (164). Expression of latent membrane proteins encoded by EBV allows the naïve B-lymphocytes to survive the germinal center reaction and become memory B-cells (164). Resting memory B-cells then circulate in the periphery with EBV expressing “latency 0”, with nearly no viral transcription (164). When B-cells divide, EBV enters “latency I”, which encodes only the proteins necessary for the EBV episome to replicate and persist within the daughter cells (164).

In healthy adults, EBV exists in its proper latent form, "latency 0", or the minimally transcriptionally active form "latency I" within resting memory B-cells (165). During latency 0, only non-coding RNA is transcribed from the episome, including the BART, BHRF1, and EBER microRNAs (165). Type I latency only differs in the expression of one viral protein, EBV nuclear antigen protein 1 (EBNA1), which acts as a transcription factor to replicate the episome during host cell division (165). An intermediate transcriptional profile, “latency II”, expressing EBNA1 and the non-coding RNAs in addition to latent membrane proteins (LMP1, 2a, and 2b) has been occasionally reported within the germinal center of healthy individuals and the epithelial cells of the oropharynx (165). The final and most transcriptionally active latency program, “latency III”, expresses all previously mentioned genes in addition to various other latency transcripts (165).

In 1964, EBV became the first virus implicated in human cancer development (166). Since then, numerous EBV-associated cancers and lymphoproliferative disorders have been characterized, all of which are associated with the virus’s latency cycle (166). There are numerous malignancies associated with type I latency, which typically arise in immunocompetent individuals, including Burkitt’s lymphoma and gastric carcinoma (167). Type II latency is also associated with several malignancies, including nasopharyngeal carcinoma, Hodgkin's disease, and nasal T/natural killer-cell lymphomas (167). Latency III-associated malignancies are generally found in immunocompromised individuals, including AIDS-associated non-Hodgkin’s lymphoma and post-transplant lymphoma, in addition to various lymphoproliferative disorders (167). Because 1-2% of all human cancers are associated with EBV infection, there is an apparent need for EBV-specific treatments of these diseases, as these amount to 100-200,000 deaths annually (168-170).

The current standard of care for each EBV-positive malignancy does not account for potential viral driving factors or etiology (171). In children, Burkitt's lymphoma is typically treated with the chemotherapy combination cyclophosphamide, doxorubicin hydrochloride (hydroxydaunorubicin), vincristine sulfate (Oncovin), and prednisone, often abbreviated as CHOP (172). In adult cases, addition of rituximab to chemotherapy cocktails through central nervous system prophylaxis is also required, as adults have a significantly worse prognosis than children (172). In Hodgkin's lymphoma, early-stage patients are treated with combination chemotherapy and radiation (173). In very advanced cases, chemotherapy is followed by autologous stem cell transplant, and brentuximab vedotin as a last resort (173). AIDS-associated non-Hodgkin's lymphoma, known to be driven by rapid proliferation of EBV+ B-cells in immunocompromised patients, has a similar standard of care but with lower dosage to compensate for the combined effects of highly active antiretroviral therapy (HAART) and low blood cell counts (171). Nasal/natural killer cell lymphoma is specifically treated with l-asparaginase-based chemotherapy and high-dose radiation therapy in addition to autologous transplantation in late-stage disease (174). Alarmingly, there is no approved standard of care for post-transplant lymphoproliferative disorder, which is often caused by rapid EBV-driven proliferation of B-cells in the immunosuppressed patient (175). Treatment in most cases involves reduction of immunosuppression, compromising the success rate of the transplant (175). Chemotherapeutic and immunomodulatory agents are added sequentially once the patient is stabilized (175). Treatment for gastric carcinoma and nasopharyngeal carcinoma varies greatly, including surgery, medications, radiation, and chemotherapy depending on cell-type of origin, location, and progression (176, 177). In the case of nasopharyngeal cancer, however, screening for EBV DNA in plasma of many Asian populations as led to a decline in cases, despite a lack of understanding behind its viral etiology (177). As each of the malignancies listed is associated with a particular EBV latency program, understanding how EBV maintains latency type may provide opportunities for novel, targeted therapeutics.

Project Outline and Aims

Previous work has shown that EBV adopts alternative chromatin looping between the Q-promoter or C-promoter and the viral origin of replication dependent upon latency type (162). It is also known that PARP1 enzymatic activity varies by latency type, with the transcriptionally active type III latency having significantly higher intracellular PAR levels than the relatively silent type I latency (151). As PARP1 has known chromatin remodeling roles in the human and EBV genome, and speculative importance for 3D chromatin structure, we set out to assess if and to what degree PARylation regulates global chromatin conformation of the EBV genome (Fig 2). PARP1 binding and PARylation have also been shown to regulate CTCF function and binding in both genomes. As CTCF and cohesin are established chromatin structural regulators and are known to bind and regulate gene expression in the EBV genome, we also assessed if altered PARylation had impact on their chromatin binding or function (Fig 2). Alterations to chromatin structure were then analyzed for correlation to sites of altered transcription and altered CTCF/cohesin binding.

Aim 1: Global episomal conformation varies by latency type.

Sub-aim 1.1: ChIP-seq to generate CTCF and cohesin binding profiles in type I and type III latently infected B-cells.

Sub-aim 1.2: *In situ* Hi-C to generate global contact maps of type I and type III genomes.

In Aim 1, we set out to validate the results of a prior study demonstrating alternative chromatin looping between the EBV OriP and Qp in type I latency and the OriP and Cp in type III latency. Beyond this, we wanted to generate a global contact map for each latency type. To accomplish this, we performed *in situ* Hi-C on isogenic type I and type III EBV genomes, with an additional step to purify all EBV-EBV ligation products. This additional step to the traditional Hi-C protocol enabled the production of detailed contact maps with resolution approaching 2kb. We then overlaid these contact maps to ChIP-seq binding profiles for CTCF and the RAD21 component of cohesin for both latency types allowing us to interpret how these known chromatin regulatory proteins contribute to EBV episome structure. These data taken together also allowed us to draw conclusions as to how

differences in chromatin binding by each factor may contribute to any differences observed in episomal structure per latency type.

Aim 2. PARylation alters 3D structure of the EBV epsiome.

Sub-aim 2.1: ChIP-seq to generate CTCF and cohesin binding profiles after PARP inhibition in type I and type III latency.

Sub-aim 2.2: *In situ* Hi-C to generate global contact maps of type I and type III genomes after PARP inhibition.

In aim 2, the same protocols were performed after 72-hour exposure to olaparib, a drug known to inhibit PARP1 enzymatic activity. *In situ* Hi-C allowed us to compare differences in 3D structure of the EBV episome after PARP enzymatic inhibition for each latency type, illustrating PARP1's importance as a chromatin structural remodeler. This also enabled us to determine the extent to which each latency type depends upon PARylation for genomic stability. Additionally, ChIP-seq of CTCF and RAD21 after olaparib treatment allowed for the comparison of their binding in the absence of PARylation, demonstrating an importance of the PAR PTM for their binding and function.

Aim 3. Gene expression is dysregulated by altered chromatin structure.

Sub-aim 3.1: RNA-seq of type I and type III latently infected B-cells before and after PARP inhibition.

Sub-aim 3.2: Correlational analysis of altered chromatin contacts to transcriptional regulatory regions.

Sub-aim 3.3: Correlational analysis of altered cohesin/CTCF binding to transcriptional regulatory regions.

In aim 3, we set out to determine the impact of structural rearrangement on viral gene expression. To accomplish this, RNA-seq was performed on type I and type III B-cells with and without olaparib

treatment. By mapping differentially expressed transcripts back to the EBV episome, we established a correlation of altered gene expression to altered DNA-DNA interactions in the same regions, as well as altered transcription to altered cohesin/CTCF binding. This aim also allowed us to establish a correlation between PARylation and maintenance of latency-specific gene expression programs.

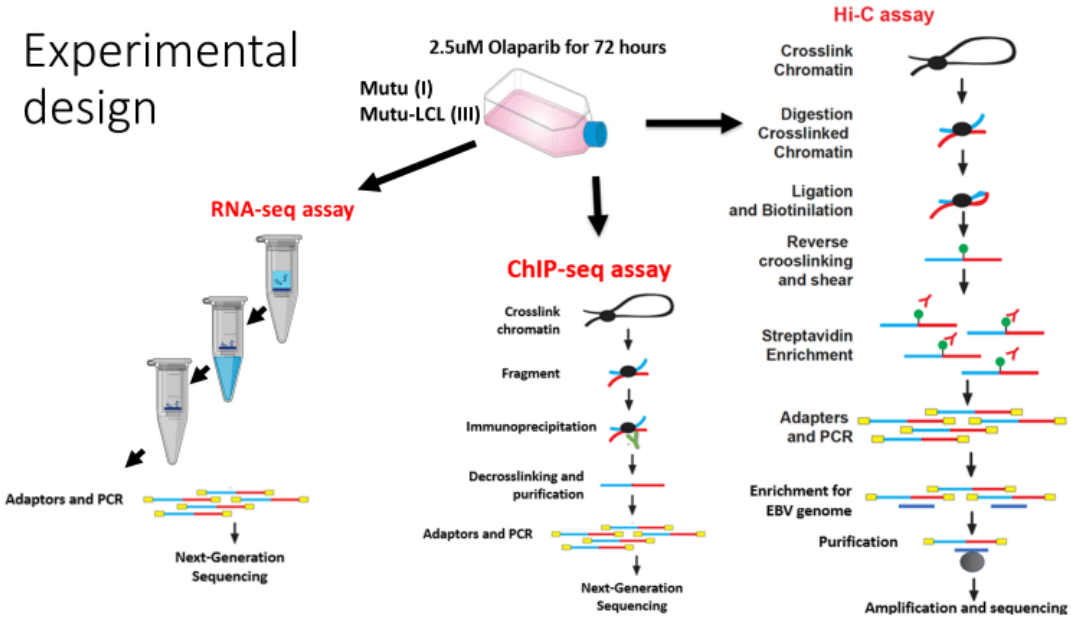

Figure 2: Project experimental Design. Type I cells (Mutu I) and type III cells (Mutu-LCL) were treated with PARP inhibitor (olaparib, 2.5uM) for 72 hours. Cells were either collected immediately for RNA extraction and sequencing (RNA-seq) or fixed to crosslink closely interacting genomic regions. Fixed chromatin was assayed via chromatin-immunoprecipitation with antibody against CTCF or the RAD21 component of cohesin, and subsequently sequenced (ChIP-seq). The fixed chromatin was also assayed via Hi-C, in which all intragenomic interactions are mapped to the EBV genome. To accomplish this, fixed chromatin is fragmented, and subsequently ligated with a biotin tag within the newly formed junction. These ligation junctions are then purified via their biotin tag. All ligations are then incubated with EBV specific “baits” to remove EBV genomic ligations from human ligation products. These EBV-specific ligations are subsequently sequenced and mapped against the genome to visualize all intragenomic interactions in the EBV episome.

CHAPTER 2

METHODS

Cell culture and drug treatment

The type I latency “Mutu I” Burkitt Lymphoma cell line and the type III latency lymphoblastoid cell line “Mutu-LCL” were maintained in a humidified incubator at 37°C and 5% CO2 in RPMI 1640 medium supplemented with 1% penicillin/streptomycin and 15% fetal bovine serum. Treatment with PARP inhibitor olaparib (Selleck Chemicals, Catalog No. S1060) was given 72 hours before collection at a concentration of 2.5uM. PARP inhibition was validated via PAR ELISA as per manufacturer’s protocol (PARP In Vivo Pharmacodynamic Assay II, Trevigen, Catalog No. 4520-096-K). Relative luminescence was measured on the EnVision 2104 Multilabel Reader (PerkinElmer).

Chromatin immunoprecipitation assays

Chromatin Immunoprecipitation-Sequencing (ChIP-seq)

After a 72 hour incubation with 2.5uM olaparib or equal volume DMSO, 25 million cells per immunoprecipitation were collected and fixed with 1% formaldehyde to preserve all DNA-protein interactions for 15 minutes and then quenched with .25M glycine for 10 minutes on ice. Pellet was resuspended after centrifugation in 10mL each of a series of three lysis buffers before fragmentation in Qsonica sonicator (90AMP, 25 sonication cycles, 30 seconds on/30 seconds off) to generate chromatin fragments roughly 200-500bp in size. Chromatin was centrifuged to clear of debris and a sample of this cleared chromatin (1% of total material) was kept as a standard input for comparison against immunoprecipitations. Chromatin was incubated rotating at 4˚ overnight with 25ug of antibody against RAD21 (Abcam, Product No. ab992). Chromatin-antibody complexes were precipitated using 50uL of Dynabeads Protein A (ThermoFisher, Product No. 10001D) incubated rotating at 4˚ overnight. Beads were collected on a magnetic rack and resuspended in 1mL modified RIPA buffer and were rotated for one minute at room temperature. Beads were collected on magnetic rack, wash was repeated four additional times, with the final wash in TE buffer. After final wash step, beads were resuspended in 60uL elution buffer and incubated for 15

minutes in 65˚ thermomixer at max RPM. Eluant was collected and .2M NaCl was added to each sample (including input chromatin). All samples were incubated in 65˚ water bath overnight to reverse crosslink. DNA was purified using Promega Wizard SV Gel and PCR Clean-up Kit (Product No. A9285). Libraries for sequencing were made NEBNext® Ultra™ II DNA Library Prep Kit (New England Biolabs, Product No. E7103) and sequenced on the hiseq2500 (Illumina).

Reads were mapped against the ***human gammaherpesvirus 4 (HHV4) NC_007605.1 genome*** assembly using bowtie2 (178). We used MACS2 (179, 180) software packages to call reads enrichment in pull down samples compared to input samples as peaks. Analysis of peak distribution under differentiated conditions were performed with the bedtools software package for genome arithmetic (181), and for data visualization we used deepTools (182). RNA-seq an ChIP-seq data were deposited for public access at Gene Expression Omnibus (GEO).

Chromatin immunoprecipitation-qPCR (ChIP-qPCR)

After 72-hour incubation with 2.5uM olaparib or equal volume DMSO, 2-3 million cells per immunoprecipitation were collected and fixed with 1% formaldehyde to preserve all DNA-protein interactions for 15 minutes and then quenched with .25M glycine for 10 minutes on ice. After centrifugation, pellet was resuspended in 120uL lysis buffer and sonicated using Covaris S2 (Duty Cycle: 10%, Intensity: 5, Cycles/Burst: 200, Time: 120 seconds (60s *2 cycles) to generate chromatin fragments roughly 200-500bp in size. A sample of “input chromatin” was collected at this point as a standard for comparison against immunoprecipitations (1% of total material). Chromatin was then incubated overnight rotating at 4˚ with 5ug of antibody against each cohesin component, CTCF, or IgG, respectively (RAD21: Abcam Product No. ab992, SMC3: Abcam Product No. ab9263, CTCF: Active Motif Catalog No. 61311, IgG: Jackson ImmunoResearch, Product No. 111-005-003). Chromatin-antibody complexes were precipitated via two-hour incubation with 50uL of Dynabeads Protein A rotating at 4˚. Beads were washed with 1mL of a series of three wash buffers, followed by two washes with TE buffer. Washed beads were resuspended in 150uL SDS-TE and incubated for 15 minutes in a 65˚ thermomixer at max RPM. Beads were cleared on magnetic rack and eluant was incubated in a 65˚ water bath overnight to reverse DNA-protein crosslink.

Proteinase K (Ambion, Product No. AM2546) was then added at 20mg/mL and incubated in 55˚ water bath for three hours. DNA was then recovered using Promega Wizard SV Gel and PCR Clean-up Kit (Product No. A9285). Realtime PCR was performed with a master mix containing 1X Maxima SYBR Green (Thermoscientific, REF No. K0223) 0.25 μM primers and 1% of ChIP or input DNA per well. Data were analyzed by the ΔΔCT method relative to DNA input and normalized to the IgG control. Treatment and control groups were compared via student's T-test with two-tailed distribution and equal variance.

Hi-C

After 72 hour incubation with or without olaparib, five million cells per condition were collected for *in situ* Hi-C (49), with minor modifications. Libraries of total ligation products were produced using Ultralow Library Systems V2 (Tecan Genomics, part no. 0344NB-32) as per manufacturer's protocol with minor modifications. Purified libraries were then enriched for only EBV genome ligation products using myBaits enrichment kit as per manufacturer's protocol. Enriched libraries were sequenced using hiseq2500 (Illumina) with paired-end 75bp read length. Complete protocol with all minor alterations will be happily supplied by corresponding author per request.

Hi-C data were processed as described previously (183). Briefly, 75-bp paired reads were separately aligned to the EBV genome (V01555.2) using Bowtie2 (version 2.2.9) with iterative alignment strategy (183). Redundant paired reads derived from a PCR bias, reads aligned to repetitive sequences, and reads with low mapping quality (MapQ < 30) were removed. Reads potentially derived from self-ligation and undigested products were also discarded. EBV genome were divided into 5 kb windows with 1 kb sliding. Raw contact matrices were constructed by counting paired reads assigned to two 5 kb windows. Hi-C biases in contact matrices were corrected using the ICE method (184). The ICE normalization was repeated 30 times. Significant associations were determined based on the distance between two 5kb windows, all combinations were categorized into 20 groups. We assumed Hi-C score as Poisson distribution with a parameter λ matching the mean score. We then assigned a P values for each group and applied an FDR correction for multiply hypotheses (185). FDR < 0.05 were defined as significant associations.

Significant associations were plotted as circos graph using the circlize package (version 0.3.3) of R (version 3.6.1).

Gene Expression Assays

Real-time quantitative PCR (RT-qPCR)

Five million cells were collected for three biological replicates of both Mutu-LCL untreated and Mutu-LCL 2.5uM olaparib treated for 72 hours. Cells were centrifuged, washed twice with PBS, and resuspended in trizol. RNA was extracted using chloroform and isopropanol. After DNAse treatment, cDNA was prepared using SuperScript™ III First-Strand Synthesis System (Invitrogen, Catalog No. 18080051). Realtime PCR was then performed with a master mix containing 1X Maxima SYBR Green (Thermoscientific, REF No. K0223) 0.25 μM primers and 25% cDNA. Data were analyzed by the ΔCT method relative to 18S-ribosomal subunit control. Treatment and control groups were compared via student's T-test with two-tailed distribution and equal variance.

RNA-sequencing (RNA-seq)

Five million cells each for two biological replicates were collected per control and olaparib treatment groups for RNA sequencing. RNA was purified using the PureLink RNA Mini Kit from Thermofisher (cat no. 12183018A). Libraries for sequencing were made using NEBNext Ultra™ Directional RNA Library Prep Kit for RNAseq (Cat #E4720L) and sequenced on the hiseq2500 (Illumina).

Sequenced reads were aligned to the ***human gammaherpesvirus 4 (HHV4) NC_007605.1 genome*** assembly using the STAR software suite (186). To determine differential gene expression, we used the EdgeR software suite (187). Genes with 0 reads across all samples were excluded. Genes with 2-fold change and $q<0.01$ after correction for multiple testing (FDR) were considered as significantly differentially expressed. We used R software packages (CRAN project and Bioconductor) for downstream analysis of RNA-seq such as hierarchical clustering and principal component analysis. Ingenuity Pathway Analysis (Qiagen) was used to determine functional gene enrichment.

Subcellular fractionation and western blotting

Three biological replicates of 10 million Mutu-LCL per treatment group (with or without 2.5uM olaparib for 72 hours) were prepared using the Subcellular Protein Fractionation Kit for Cultured Cells from Thermo Scientific (Catalog No. 78840). Respective proteins of interest were probed via western blot using antibodies listed previously for chromatin immunoprecipitations. Samples were normalized to the following loading controls: β-tubulin (Abcam ab6046) for cytosolic extracts, lamin B1 (abcam ab16048) for nuclear soluble extracts, and histone H3 (abcam ab1791) for chromatin bound extracts.

Co-immunoprecipitation protein assays

For SMC3-immunoprecipitation (IP) assays, 10 million LCLs, with or without 72-hour 2.5uM olaparib treatment, were collected for each IP and resuspended in 1mL of RIPA buffer with protease/phosphatase inhibitor cocktail (Thermo Scientific). Before addition of 10ug of either SMC3 (abcam, ab9263) or normal rabbit IgG (Jackson, 111-005-003), 50uL of cell lysate was collected and kept as input material. Cell lysates were incubated with respective antibodies for one hour at room temperature, rotating, after which 30uL of protein A magnetic beads (Invitrogen, 10001D) were added. The mixture was left to incubate overnight at 4˚, rotating. The beads were then separated with a magnetic rack and washed three times in RIPA buffer with protease/phosphatase inhibitor, each for 10 minutes in a 4˚ thermomixer at 1000rpm. The beads were then boiled at 95˚ for 8 minutes in 50uL 2x laemmli buffer, with half of the volume ran on an immunoblot for SMC3, and half for PARP1 (abcam, ab227244) as described above. Densitometry analysis was performed on Invitrogen iBright Analysis Software, with signal density/area from IgG control lanes subtracted from IP lanes. IgG normalized IP signal was then normalized to input signal density/area. Data shown is representative of three independent co-IP assays, averaged.

EBV Copy Number Assays

LCLs were treated for 72 hours with 2.5uM DMSO, olaparib, or PDD00017273, with PDD00017273 treatment only being repeated every 24 hours. Five million cells per group were collected and

genomic DNA was extracted with GeneJET Genomic DNA Purification Kit (Thermo, Cat # K0721) as per manufacturer's protocol. Eluted DNA was quantified by nanodrop and diluted to equal concentrations. Quantitative PCR (Applied Biosystems™ 7500 Fast Dx Real-Time PCR) was performed with a master mix containing 1X Maxima SYBR Green (Thermoscientific, REF No. K0223) 0.25 µM primers, and 300ng of genomic DNA. Data were analyzed by the ΔCT method relative to host genomic control region ARRDC2. Treatment and control groups were compared via student's T-test with two-tailed distribution and equal variance.

CHAPTER 3

RESULTS

3D Chromatin Conformation Varies by Latency Type in Isogenic EBV Genomes

Previous work has shown that in type I latency, the viral OriP forms a chromatin loop with Qp, while in type III OriP forms an alternative loop with Cp (162). To extend the analysis of chromatin loops existing between other CTCF-associated regions and to explore the hypothesis that the three-dimensional structure of the viral genome differs globally between different latency types, we assessed total EBV genomic structure by *in situ* Hi-C assay, followed by enrichment for EBV-EBV interactions (Fig 3A). Sequenced reads (ligation productions of DNA-DNA interactions) were aligned to the EBV genome using Bowtie2 with iterative alignment strategy and plotted as circos graphs (Fig 3B and Fig 3C). The darkness of the blue arcs represents the strength/frequency of the interaction, with darker loops representing the higher frequency of contact between the two regions the arc connects. When looking for similarities between the latency I and III genomes, only two chromatin interactions remain entirely conserved: 1) the dense local interactions between the terminal repeat, TR, region (~170kb) and the region directly upstream of the origin of viral replication (~2.5 kb) and 2) the 10kb loop formed between the lytic transcripts BWRF1 (~35kb) and BFLF1 (~46kb) (Fig 3B and Fig 3C). The two long-range chromatin loops formed between BCRF2 (~13kb) and BKRF1 (~96.5kb), and between BWRF1 (~35kb) and the BART microRNAs (~143kb) in the type I latency genome have been completely lost in the type III genome. However, many loops and local interactions are formed in type III latency that are not observed in the type I genome. The strongest interactions in type III latency localize around the C-, Z-, and LMP- promoters, within the EBNA transcripts, and surprisingly within the BART microRNAs (Fig 2B and 2C). Overall, we observed seven total unique interactions with $p < .05$ in the type I episome and 26 in the type III (APPENDIX A), accounting for the fact that numerous overlapping and nearly-overlapping interactions visible on the circos graphs may be the same event captured multiple times. Altogether, these results indicate that the three-dimensional organization of the EBV genome differs

significantly between isogenic type I and type III latency types, with more chromatin loops existing in type III than type I.

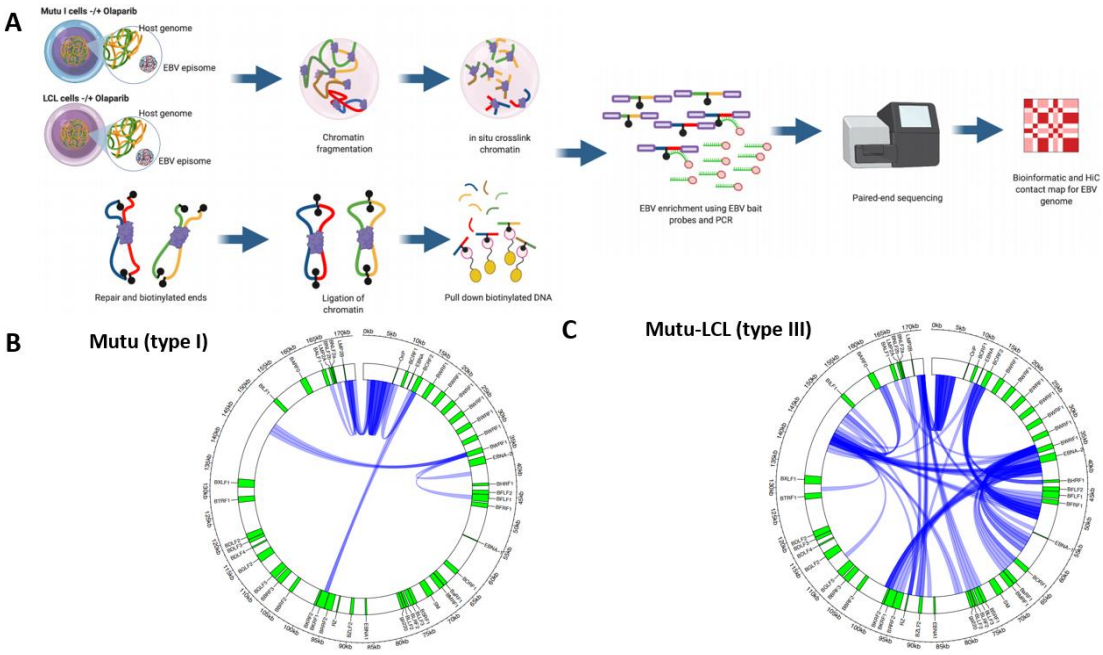

Figure 3: 3D Chromatin Conformation Varies by Latency Type in Isogenic EBV Genomes. A) 5 million Mutu (type I) or Mutu-LCL (type III) latency infected B-cells were formaldehyde fixed to preserve all DNA-DNA contacts *in situ*. Fixed chromatin was extracted, fragmented, and subsequently ligated with a biotin tag within the newly formed junction. These ligation junctions are then purified via their biotin tag. All ligations are then incubated with EBV specific “baits” to remove EBV genomic ligations from human ligation products. These EBV-specific ligations are subsequently sequenced and mapped against the genome to visualize all intragenomic interactions in the EBV episome. B-C)**:** Circos graphs generated from Hi-C contact maps, whereby each intragenomic interaction on the circularized EBV episome map is visualized with an arc. Each end point of the arc represents the physical contact of the chromatin between the two regions. Darkness of the blue arc represents strength/frequency of the interaction. Data represented are averaged from two independent Hi-C assays.

Intragenomic Interactions are Globally Altered by PARP1 Enzymatic Inhibition

Previous work has shown that the more transcriptionally active type III latency has 4-fold higher intracellular PAR (pg/mL) than the immunoevasive type I latency (121). As PARP1 has an established role in chromatin remodeling, primarily by regulation of CTCF insulator function, we investigated whether the reported increase in PARP activity was necessary for maintenance of EBV episomal 3D structure. We additionally wanted to assess if the increased PARP1 activity in type III latency will confer a dependence on PARylation to maintain the highly organized chromatin structure we observed by Hi-C. To determine the impact of PARP1 activity on EBV chromatin structure, we inhibited PARP enzymatic activity in the same EBV+ B cell lines that are isogenic with respect to the EBV genome. Both cell lines were treated with 2.5uM of the potent PARP inhibitor olaparib and PAR levels were assessed after 72 hours via ELISA. At this concentration, Mutu I PAR levels were decreased 36.06% and LCL PAR levels were decreased 86.24% (APPENDIX B). PARP1 protein levels were not impacted by olaparib treatment (APPENDIX B). Interestingly, our data using the same PAR ELISA kit showed that Mutu-LCL an even bigger difference than previously published compared to Mutu, ranging more towards 9X higher intracellular PAR (APPENDIX B). To determine the effect of the observed reduction in PARP1 activity, we assessed changes in the 3D structure of the EBV genome by Hi-C assay as described above. For both type I and type III latency, total unique intragenomic interactions (chromatin loops) with at least a significance of $p<.05$ decreased from seven to four (Fig 4A and Fig 4C) and from 26 to 18 (Fig 4B and Fig 4D), respectively, after PARP inhibition. In type I latency, long-range chromatin loops between the ~35kb region and the 145kb-150kb BART microRNA region, and ~13kb region and the 95kb-100kb region disappear, indicating that these regions are no longer interacting (Fig 4A and Fig 4C). We also observed a relatively smaller loop disappear between the 35kb region and the 45kb region. Interestingly, we observed that no new interactions are gained after olaparib treatment in type I EBV+ cells (Fig 4A and Fig 4C). For type III latency, while eight unique high-frequency loops disappear, there are also many regions where new long-range chromatin loops are formed between regions that are on average 60kb apart. (Fig 4B, Fig 4D, and APPENDIX A). Additionally, the local interactions within the 142kb-152kb region seem to be shifted after PARP

inhibition, with a dense region of local interactions now observed from 137kb-143kb. While the conformation of the type III genome is significantly altered after olaparib treatment, the strong, sequential interactions between the region within the EBNA1.1 transcript directly preceding OriLyt (~33-37kb) and the region between the lytic Zp and EBNA1.3 (~93-95kb) remain unchanged, indicating that this chromatin interaction occurs independent of PARP activity. However, when an additional statistical parameter of FDR ≤ .05 (APPENDIX A) is added atop the $p < .05$ threshold, we see that the type III genome maintains the same absolute number of intragenomic contacts. The seventeen DNA-DNA interactions are not static between the two groups though, as the identity of the fragments is distinct between treatment and control. This statistical discrepancy could indicate that the nine loops not meeting the FDR threshold could be weaker interactions, context-dependent, or that these loops are present in only a portion of the five-million cell population. Regardless, our analysis demonstrates that PARP inhibition changes the three-dimensional structure of the EBV genome, particularly in type III latently infected cells.

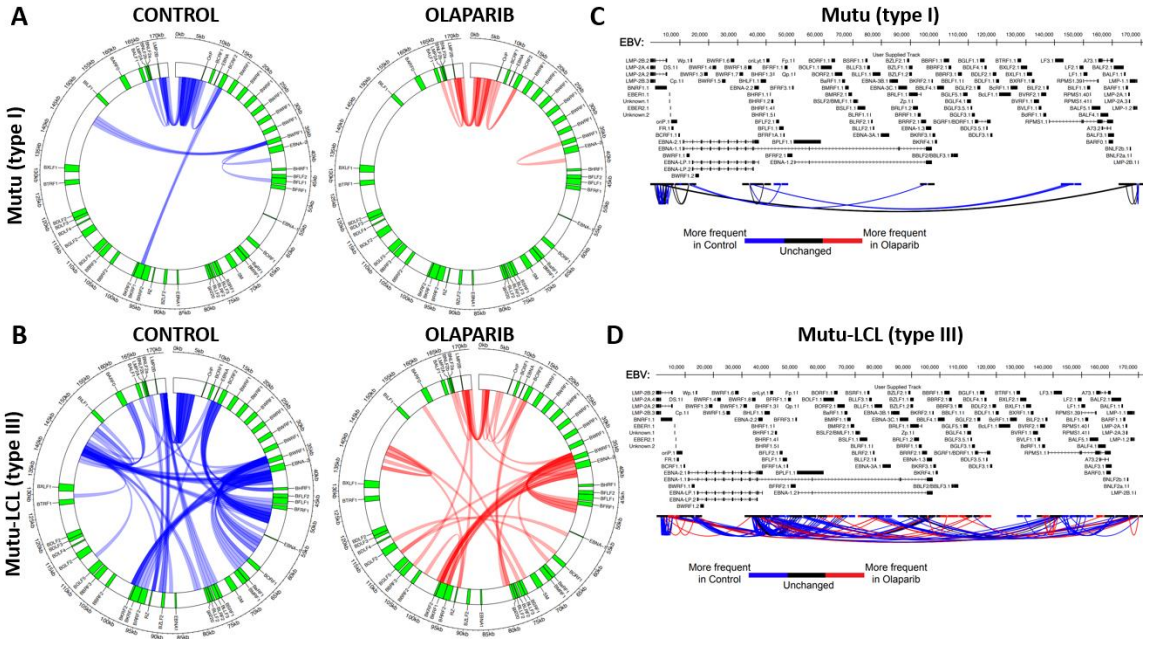

Figure 4: Intragenomic Interactions are Globally Altered by PARP1 Enzymatic Inhibition. A-B) 5 million Mutu (type I) or Mutu-LCL (type III) latency infected B-cells were either treated with 2.5uM olaparib or equal volume DMSO for 72-hours. After which time, each group was collected

as described previously for Hi-C assay followed by enrichment for EBV ligation products. Circos graphs generated from Hi-C contact maps, whereby each point of the arc represents the physical contact of the chromatin between the two regions. Darkness of the blue (control) or red (olaparib) arc represents strength/frequency of the interaction. C-D) Linearized EBV genome with arcs connecting DNA-DNA contacts derived from Hi-C matrices. Blue arcs represent chromatin loops that are more frequent in control genome, red arcs represent chromatin loops that are more frequently observed in the olaparib treated genome, and black arcs are loops that are unchanged between control and treatment. Data represented are averaged from two independent Hi-C assays.

Chromatin Folding brings EBV Regulatory Loci in Close Proximity

Our Hi-C analysis reveals for the first time at genome-wide level the intricate map of physical contacts existing between different regions of the EBV genome. *In situ* Hi-C analysis allowed us to illustrate that the type III latency EBV genome is organized into a complex network of DNA-DNA contacts that are at least in part regulated by PARP activity. We next decided to use the DNA-DNA contact interactions generated by our Hi-C analysis to delineate the 3D model of the EBV episome properly folded into the nucleus of the host cells, before and after PARP inhibition. To infer how EBV episome is folded, we used the PASTIS software package to generate the 3D model of the EBV genome for type III latency from our Hi-C datasets (Fig 5). The models of the EBV episome before and after PARP inhibition are dissimilar. In control cells, the 3D model shows that the origin of the viral replication OriP, the EBNAs promoter Cp, and the latent promoter Qp, cluster together (Fig 5). This somewhat supports previous work demonstrating OriP and Cp physical contact in the same type III latency cell line, however it is not possible at the roughly five kilobase resolution matrix input to generate the PASTIS model where the exact DNA-DNA contact is occurring (162). The 3D model also illustrates the OriP region separated from the divergent promoter region of LMP1, which appeared to interact with OriP in our Hi-C analysis and in previous work (188). This discrepancy between the 3D model and the Hi-C data could be due a lack of accuracy by the PASTIS software to model circular regions of DNA such as viral episomes. The 3D model of the EBV genome after PARP inhibition shows Orip and Qp are no longer colocalized (Fig 5).

Additionally, OriP and the LMP1 promoter are now brought in close proximity unlike the control genome. In reality, OriP and the LMP1 promoter are roughly ten kilobase apart in the circularized EBV genome. Overall, the inferred model of the EBV chromosome from type III latently infected cells show that important regulatory regions of EBV cluster together as consequence of EBV episome folding. Moreover, our 3D models underscore the importance of PARP activity in the folding of EBV episome by demonstrating the effect of PARP inhibition on 3D chromatin structure.

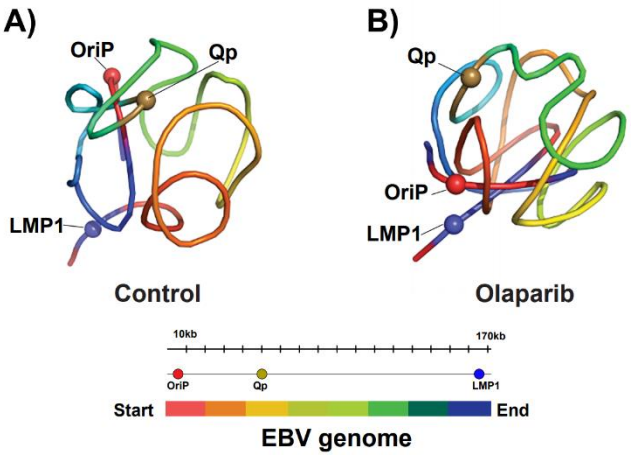

Figure 5: Chromatin Folding brings EBV Regulatory Loci in Close Proximity. PASTIS model displaying control type III EBV genome (left) or olaparib treated (right) with color-coded legend of EBV genome. Model derived from averaged Hi-C datasets (N=2) with 1kb sliding matrix.

Transcription of Viral Genes is Altered after PARP Inhibition

To determine if the differences in EBV chromatin structure observed after olaparib treatment functionally correlate to altered gene expression, we analyzed changes in viral transcription by RNA-sequencing on biological duplicates of the same type I and III cells used for our Hi-C assays, with and without PARP inhibition (Fig 5). We observed widespread dysregulation of viral gene expression with significance of $p \leq .05$ (APPENDIX C). The changes in viral gene expression are summarized by principal component analysis (PCA) (Fig 6A) and volcano plot for genes with $p \leq .05$ and FDR ≤.05 (Fig 6B and Fig 6C). Principal component 1 separates samples based on latency type, with the type III LCL samples and the type I Mutu samples diverging along the X-axis (Fig 6A). Principal component 2 separates LCL samples based on olaparib treatment but not Mutu samples, which instead grouped together regardless of treatment (Fig 6A). This is unsurprising considering olaparib treatment in type I cells only reduced intracellular PAR levels 36% compared

to type III which was reduced 86% at the same concentration (APPENDIX B). We next compared changes in the expression of viral genes in EBV+ cells before and after olaparib treatment. In type I Mutu cells, which basally have a minimal transcriptional profile, inhibition of PARP only elicits the differential expression of three genes including the two lytic genes BOLF1 and BPLF1, which code for the inner and larger tegument protein of EBV respectively (Fig 6B) (189). When we applied the same parameters to type III cells, we identified ten viral genes with a differential gene expression profile after olaparib treatment (Fig 6C). Specifically, we observed downregulated expression for all EBNA genes, including EBNA2, which we previously reported to be regulated by PARP1 (150). Olaparib treatment also triggers over-expression of four lytic genes, including BALF3 which codes for the viral translocase, BILF1 which codes for the viral G protein-coupled receptor involved in modulating host immunity, and BMRF2 encoding the viral protein responsible for EBV attachment to epithelial cells (190-193). We also observed the downregulation of the RPMS1 transcript, from which the BART microRNAs are spliced (Fig 6C). We next validated the altered expression of the viral genes identified in LCL via RT-qPCR (Fig 6D). Overall, our results demonstrate that the type III latency gene expression program of EBV is sensitive to PARP inhibition and that PARP activity supports the expression of latent genes while repressing some lytic genes.

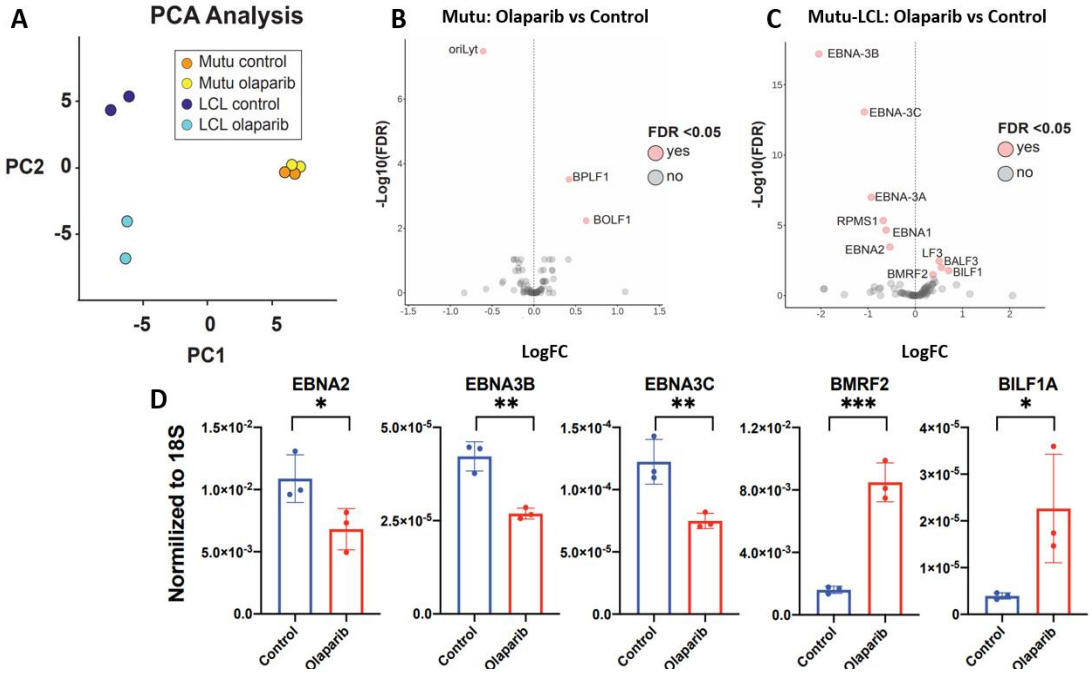

Figure 6: Transcription of Viral Genes is Altered after PARP Inhibition. A) Principle component analysis (PCA) separating type I EBV latency (Mutu) and type III EBV latency (LCL) human B-cells by treatment (control or 2.5uM olaparib). Data derived from RNA-seq dataset utilizing biological duplicates. B) Volcano plot illustrating dysregulated gene expression after olaparib treatment in Mutu cell line, with the left of the dashed line representing genes downregulated after PARP inhibition and the right representing genes upregulated after PARP inhibition. Genes displayed are dysregulated at $p<.05$ and $FDR<.05$. C) Volcano plot illustrating dysregulated gene expression after olaparib treatment in LCL, as described in B. D) RT-qPCR validation of genes shown to be dysregulated by RNA-seq in LCL after PARP inhibition. Bar graph represents the average expression of three biological replicates per treatment, each normalized to 18S expression respectively.

PARP Inhibition Alters RPMS1 Splicing

Interestingly, four of five separate primer sets used to validate the under-expression of RPMS1 showed no significant difference in expression, while one showed over-expression in olaparib treatment compared to control (Fig 7A). Because 22 pre-miRNAs are spliced from the RPMS1 transcript, and the various primer sets spanned different exons throughout the gene, we wondered if the regions we chose happened to coincide with differentially expressed microRNAs. Seven miRNAs were selected randomly and compared via RT-qPCR with highly specific locked nucleic acid primers (LNA) (Fig 7B). We found that two of the miRNAs were downregulated at values just above significance of $p<.05$, four were unaffected, and one was significantly upregulated. These data are particularly interesting as PARP1 has recently been implicated in alternative splicing (194).

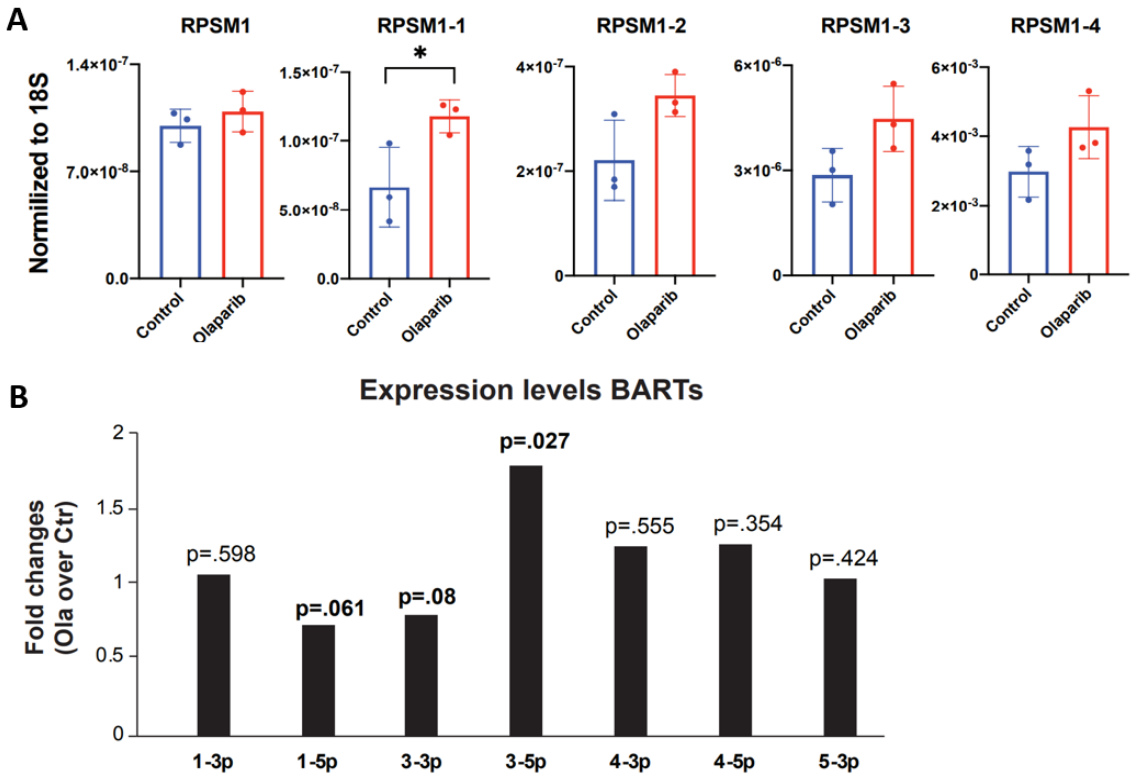

Figure 7: PARP Inhibition Alters RPMS1 Splicing. A) RT-qPCR validation of RPMS1 expression using five separate primer sets, spanning various exons in the gene. Bar graph represents the average expression of three biological replicates per treatment. B) RT-qPCR validation of seven randomly selected BART microRNAs, before and after PARP inhibition in LCL. Bar graph represents the average expression of three biological replicates per treatment, each normalized to U6 snRNA, respectively. Data displayed as fold change of olaparib treated LCL over control. (*=p ≤ .05).

CTCF and Cohesin Occupancy Does Not Vary by Latency Type

Previous studies have shown that in type III EBV latency, CTCF binds the EBV genome at several sites and disruptions to CTCF binding at specific regions alters viral gene expression (136, 138, 144, 188). We have now shown that EBV latency types display vastly different episomal conformations. As CTCF is known to regulate latency type-specific viral transcription via altered

chromatin looping at OriP and Qp/Cp, we wanted to compare CTCF binding profiles between isogenic EBV strains differing in latency status (162). To accomplish this, chromatin-immunoprecipitation and global sequencing (ChIP- seq) of CTCF was performed on human type I and type III B-cell lines. Cell lines were isogenic with respect to EBV. When the CTCF binding profiles were aligned to each latency type, we observed minimal differences (Fig 8A), except for the ~132kb peak observed in the type I Mutu genome that is absent in the type III Mutu-LCL. These data indicate that differences in CTCF binding unlikely contribute to the differences in viral gene expression observed between EBV latency types. Nor do they contribute to the altered episomal structure observed between the latency types. However, long-range chromatin loops are generally not formed by CTCF alone, but by CTCF acting as an anchor for cohesin-mediate chromatin

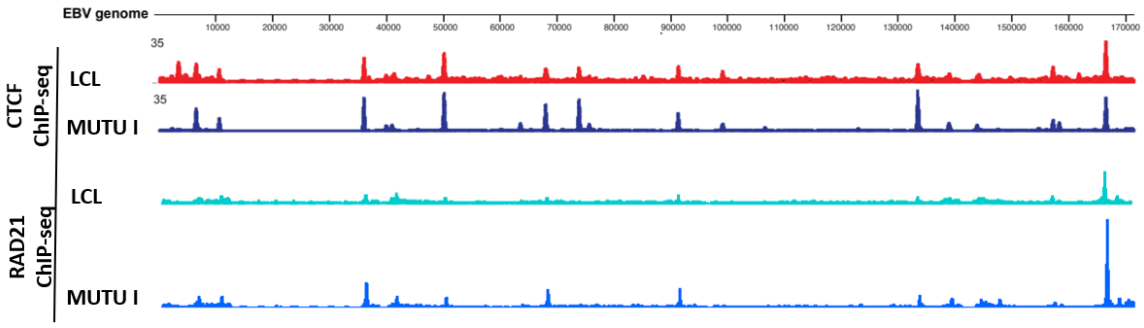

Figure 8: CTCF and Cohesin Occupancy Does Not Vary by Latency Type. A) ChIP-seq was performed on 25 million LCL or Mutu cells utilizing anti-CTCF pAB or B) anti-RAD21 pAB. Both tracks were normalized to 1% input chromatin and aligned to the EBV genome.

extrusion (67). As cohesin is known to colocalize with CTCF across at least the type III EBV genome, we also wanted to assess possible differences in binding of cohesin between isogenic type I and type III EBV genomes (Fig 8B) (143, 144). Again, no notable differences were observed between latency types. Cohesin colocalized with CTCF at virtually all its binding sites, while some independent binding sites were observed for CTCF in both genomes. We did, however, notice that RAD21 as well as CTCF seemed to bind with higher affinity to the type I latency Mutu genome than isogenic Mutu-LCL displaying type III latency, which we explored in Figure 9. To this end, it is

unlikely that altered cohesin/CTCF-chromatin binding can explain the differences in latency expressional repertoires or chromatin conformation.

EBV Copy Number Varies by Latency Type in Isogenic Strains

Previous work has indicated that PARylation seems to enhance CTCF-chromatin binding at specific regions on the human and EBV genome (150). Because of this, we were surprised to note that type I Mutu cells seemed to have higher frequency of binding across its genome than the isogenic type III LCL cells with roughly 4X the intracellular PAR levels. Due to the technical difficulty of performing chromatin-immunoprecipitation using PAR antibodies, we first set out to test a more simple hypothesis: Mutu has more EBV episomes per cell than LCL, providing more frequency of binding by virtue of more material per assay. Indeed, in three independent EBV copy number assays using four primer sets spanning the EBV genome, we found that Mutu has roughly 4X more EBV episomes per five million cell population than Mutu-LCL (Fig 9). While this is a possible explanation for the heightened signal produced in ChIP experiments in Mutu cells, we are unable to determine if the difference in EBV copy number is solely due to latency type or could be influenced by host background. Mutu and Mutu-LCL are isogenic with regard to EBV, yet the former is a Burkitt's lymphoma derived line, while the latter is an immortalized lymphoblastoid line.

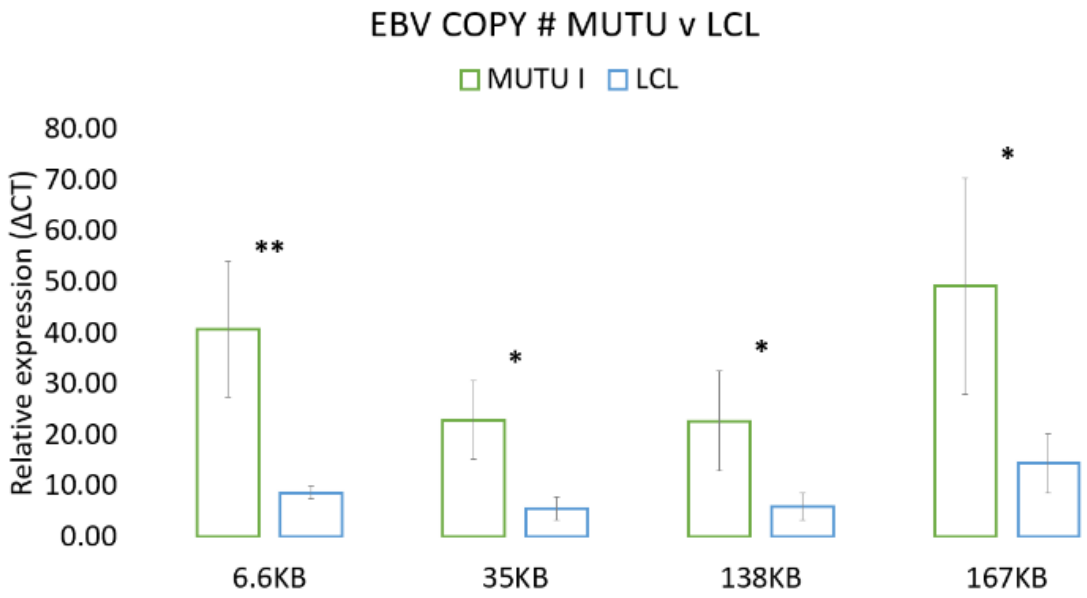

Figure 9: Mutu has significantly higher EBV copy number than isogenic Mutu-LCL. Five million Mutu or Mutu-LCL were collected for total genomic DNA. 300ng of each group was loaded for qPCR analysis with primers spanning four independent regions of the EBV genome. Values are averages of three independent experiments. (*=p ≤ .05, **=p ≤ .01).

Cohesin-Chromatin Binding is Stabilized by PARP Inhibition

Previous work demonstrated that PARP activity is necessary to stabilize CTCF binding across the EBV genome (150). The cohesin complex is known to be anchored by CTCF to promote long-range chromatin loops (77). As cohesin has been shown to colocalize with CTCF across the type III EBV genome, we wanted to determine if cohesin binding on the viral genome is also altered by PARP inhibition (143, 144). To assess cohesin binding before and after PARP inhibition, we treated type I and type III cell lines infected with isogenic EBV strains with olaparib. After 72 hours, we performed chromatin-immunoprecipitation followed by next-generation sequencing (ChIP-seq) using antibody against the RAD21 component of the cohesin complex. We normalized the RAD21 binding profile to input chromatin and used peak calling to illustrate cohesion occupancy across the EBV genome in both type I and type III cells lines (Fig 10A and Fig 10B). In the type I Mutu cell line, we observed no significant differences in RAD21 occupancy between treatment groups (Fig 10A). In the type III Mutu-LCL cells, we found that RAD21 occupancy was increased after olaparib treatment at nearly all binding sites across the type III EBV genome (Fig 10B). Since we previously reported that CTCF binding was reduced at specific regions across the type III EBV genome, we noted that after PARP inhibition, RAD21 binding is increased at those sites where CTCF binding is decreased (Fig 10D) (150). We validated increased occupancy of cohesin complex at these regions by quantitative ChIP analysis utilizing RAD21 and SMC3 antibodies, and additionally validated CTCF binding at the same regions (Fig 10D). We observed an increase in occupancy of both cohesion subunits after PARP inhibition as well as a significant decrease in CTCF binding. Our results demonstrate that cohesin occupancy increases at regions where CTCF occupancy is reduced after PARP inhibition.

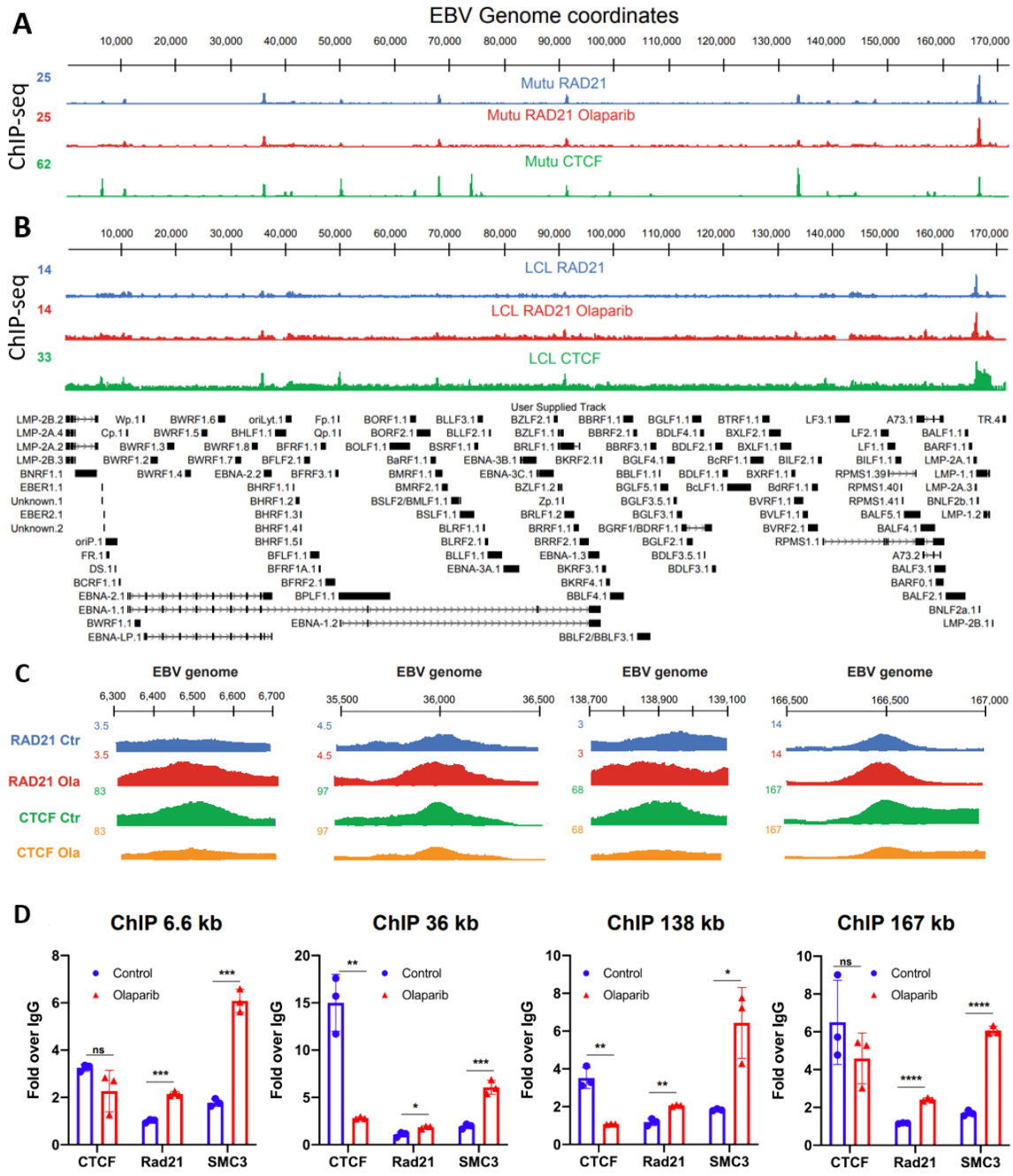

Figure 10: Cohesin-Chromatin Binding is Stabilized by PARP Inhibition. A) ChIP-seq tracks for CTCF (green), RAD21 (cohesin component, blue), and RAD21 after PARP inhibition (cohesin component, red) in type I EBV latency cell line Mutu. All ChIP-seq tracks are normalized to input chromatin and aligned to the EBV genome. B) ChIP-seq tracks (as described in A) in type III latency EBV cell line LCL. C) Magnified RAD21 binding profiles in LCL, before (blue) or after PARP inhibition (red), aligned to CTCF binding profiles before (green) or after PARP inhibition (orange)

in the same cell line. D) ChIP-qPCR validation of magnified regions of LCL ChIP-seq tracks for cohesin (RAD21, SMC3) and CTCF, normalized to input chromatin and fold change over IgG. (*=p ≤ .05, **=p ≤ .01, ***p= ≤ .001)

PARP1 binding is stabilized on the EBV genome after enzymatic inhibition

Others have reported that olaparib treatment traps PARP on DNA, therefore we assessed the "PARP-trapping" effect of olaparib at the identified CTCF/cohesin binding sites of the EBV genome by quantitative ChIP (195). We observed a slight increase that did not rise to the level of statistical significance in PARP1 binding after olaparib treatment (Fig 11). This observation supports the notion that PARP-trapping also occurs across the EBV genome as PARP1-chromatin binding is preserved by enzymatic inhibition.

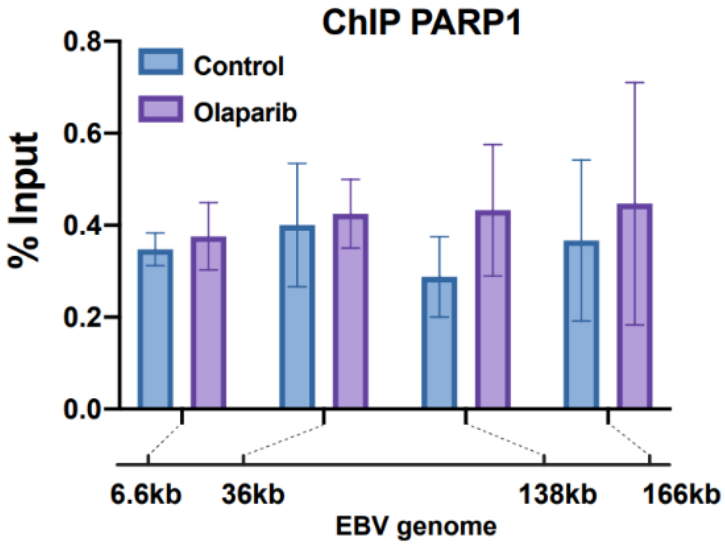

Figure 11: PARP1 Binding is Stabilized Across the EBV Genome after Olaparib Treatment. ChIP-qPCR of PARP1 binding at cohesin/CTCF colocalization sites in LCL, with and without 2.5uM olaparib treatment. ChIP data was normalized to input chromatin. Data presented are averaged from three independent experiments.

Dysregulated Viral Gene Expression is Correlated with Altered Chromatin Looping

We determined that the type III latency EBV genome establishes a complex network of intragenomic interactions and that PARP1 inhibition alters viral gene expression as well as occupancy of both CTCF and cohesin chromatin looping factors. We also noted that the viral genes

most significantly dysregulated in expression tended to correlate to the regions where intragenomic interactions were altered after PARP inhibition (Fig 12), raising the possibility that EBV chromatin conformation impacts the transcription of viral genes. To establish a correlation between changes in viral transcripts and changes in EBV 3D structure, we compared the frequency of DNA-DNA interactions from our Hi-C dataset to the number of reads per region in the EBV genome (forward and reverse) from our RNA-seq data set (Fig 12, APPENDIX A and APPENDIX C). In the top panel labeled “Hi-C”, the blue arcs represent DNA-DNA interactions that occur with higher frequency in the control samples (no olaparib treatment) between the two regions it connects. The red arcs represent DNA-DNA interactions that occur with higher frequency after olaparib treatment. Finally, the black arcs are chromatin loops that remain unchanged despite treatment group. In the bottom panel labeled “RNA-seq”, the blue peaks represent transcripts that are more abundant in the control sample (no olaparib treatment) and the red peaks represent transcripts that are more abundant after olaparib treatment (Fig 12). Starting at the beginning of the linearized episome, we observed that the red peaks along the RNA-seq tracks align perfectly with increased intragenomic contacts at the origin of replication, OriP. This corroborates previous findings showing that knock-down of PARP1 regulates OriP function (153). Moving forward along the genome, we also observed high consecutive blue peaks of RNA reads within the EBNA transcripts, which are shown to be downregulated in our RNA-seq data (Fig 6C), directly aligned with numerous blue arcs (i.e. chromatin loops that are more frequent in the untreated EBV episome). The lytic BMRF2 and BALF3 genes, which are shown to be overexpressed in olaparib treated LCLs, also have heightened RNA-seq reads that can be directly correlated to increased red arcs in the Hi-C data (Fig 6C). The latent genes EBNA3B/3C conversely are under-expressed in olaparib treatment and align with chromatin binding events that are more frequent in the control genome. Finally, though the full-length RPMS1 transcript is downregulated in olaparib treated LCLs, there are a higher number of RNA reads as displayed by the red peak on the RNA-seq track (Fig 12 and Fig 6C) that correlate with increased intragenomic contacts at the same RPMS1 transcript region. Though this seems contradictory, we observed that one of the seven tested miRNAs spliced from RPMS1 is significantly upregulated (Fig 7B). The discrepancy between our RNA-seq data and RT-qPCR

quantification of miRNA could be due to the fact that miRNAs are filtered from the RNA samples during purification before sequencing and therefore they are disregarded during data analysis. Overall, these results demonstrate that in type III latency infected EBV+ B-cells, chromatin conformation is altered after PARP inhibition, and the changes in chromatin looping correlate with dysregulation of viral genes at those regions.

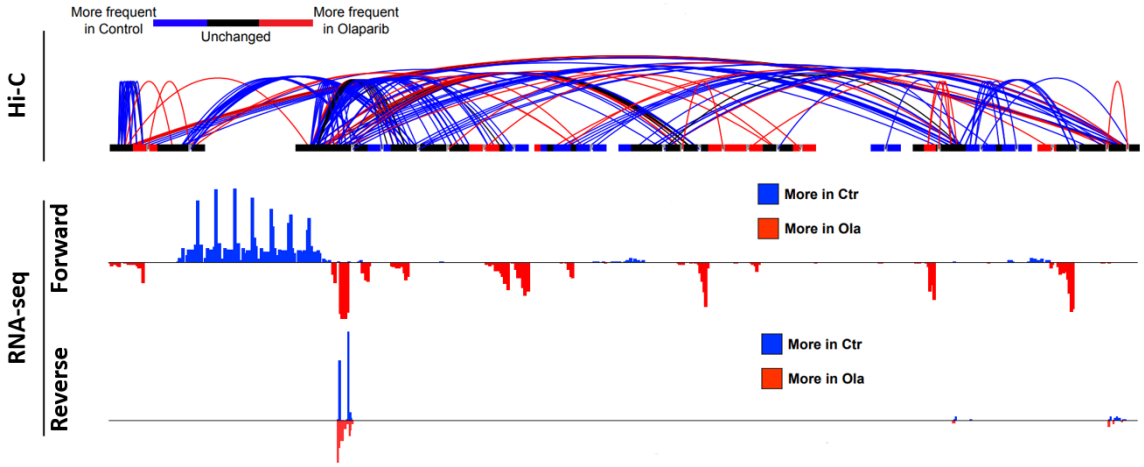

Figure 12: Dysregulated Gene Expression is Correlated with Altered EBV Chromatin Looping. Top panel "Hi-C" aligns differences in chromatin looping between control and olaparib treated LCLs to the EBV genome. Blue arcs represent chromatin loops that are more frequent in control genome, red arcs represent chromatin loops that are more frequently observed in the olaparib treated genome, and black arcs are loops that are unchanged between control and treatment. All arcs represent DNA-DNA interactions that occur at a statistical significance of $p<.05$ from averaged biological duplicates. Bottom "RNA-seq" panel displays RNA reads, forward and reverse, aligned to the EBV genome. Blue peaks pointing upward represent reads that occur more frequently in control LCLs while red peaks pointing downward represent reads occurring more frequently in olaparib treated LCLs. Genes with 2-fold change and $q<0.01$ after correction for multiple testing (FDR) were considered as significantly differentially expressed.

Altered CTCF and Cohesin Binding Frequency Correlates with Changes in EBV Chromatin Looping and Gene Expression After PARP Inhibition

Once we established that a correlation exists between changes in EBV chromatin architecture and viral gene expression after PARP inhibition, we investigated whether changes in viral chromatin loops in olaparib treated cells involved EBV genomic regions that are occupied by CTCF and cohesin. To determine the role of CTCF/cohesin occupancy in EBV chromatin conformation, we compared changes in their binding via ChIP-seq to our Hi-C and RNA-seq data. In general, we observed viral chromatin loops occurring between regions where at least one "end" of the chromatin loop is associated with CTCF/cohesin (Fig 13). Interestingly, we noted that the region between 100kb and 130kb forms short chromatin loops in the absence of CTCF and cohesin binding (Fig 13). When we compared changes in chromatin looping and CTCF/RAD21 binding (i.e. loss of CTCF occupancy and increase of RAD21 occupancy), we found that six regions of the viral genome had altered chromatin architecture correlating with loss of CTCF and increase of RAD21 occupancy after PARP inhibition (Fig 13). We also noted that changes in CTCF/RAD21 binding results in either the formation or the disruption of chromatin loops. The changes in chromatin looping due to altered CTCF/cohesin occupancy after PARP inhibition correlated to dysregulated transcription of the viral genes within the same regions (Fig 13 and Fig 6C). For example, we observed that PARP inhibition results in the disruption of the chromatin loops existing upstream the EBER microRNA encoding region located at 6.6kb, coinciding with changes in CTCF/RAD21 occupancy. However, after PARP inhibition we observed that the same region at 6.6kb now establishes a new intragenomic interaction with a region located around 35kb of the viral genome, and that both regions show changes in CTCF/RAD21 occupancy (Fig 13). The 35kb region is within the alternatively spliced EBNA transcripts, and our RNA-seq data displayed that all EBNAs are dysregulated after PARP inhibition (Fig 6C and APPENDIX C). These results demonstrate that CTCF and cohesin organize the 3D structure of the EBV episome and that their function is regulated through PARP1 activity, though perhaps in a context specific manner.

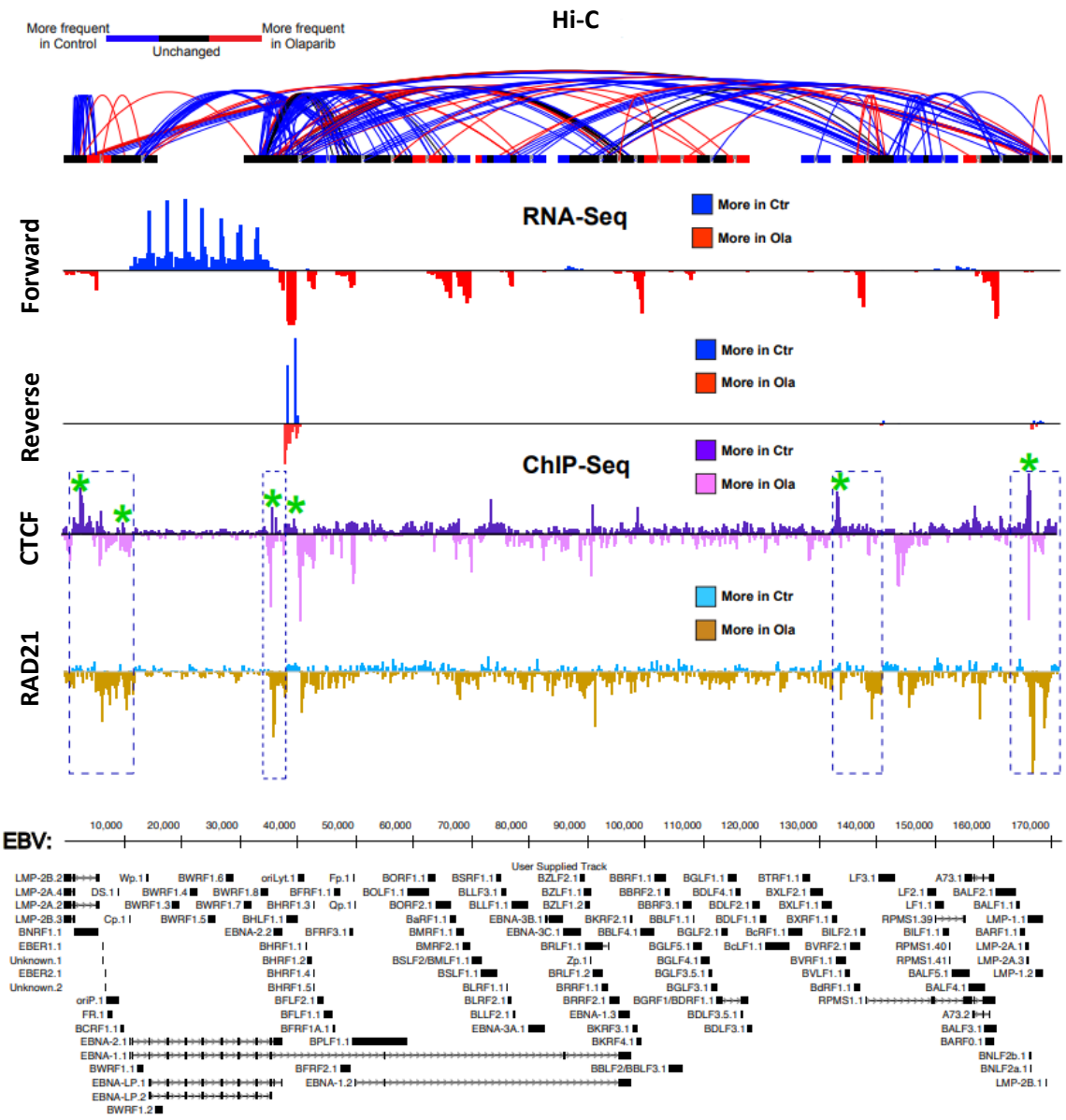

Figure 13: Altered CTCF and Cohesin Binding Frequency Correlates with Changes in EBV Chromatin Looping and Gene Expression. Top panel "Hi-C" aligns differences in chromatin looping between control and olaparib treated LCLs to the EBV genome. Blue arcs represent chromatin loops that are more frequent in control genome, red arcs represent chromatin loops that are more frequently observed in the olaparib treated genome, and black arcs are loops that are unchanged between control and treatment. All arcs represent DNA-DNA interactions that occur at a statistical significance of p<.05 from averaged biological duplicates. Middle panel "RNA-seq"

displays RNA reads, forward and reverse, aligned to the EBV genome. Blue peaks pointing upward represent reads that occur more frequently in control LCLs while Red peaks pointing downwards represent reads occurring more frequently in olaparib treated LCLs. Genes with 2-fold change and $q<0.01$ after correction for multiple testing (FDR) were considered as significantly differentially expressed. Bottom panel "ChIP-seq" aligns CTCF and cohesin (RAD21) tracks to the EBV genome, with and without PARP inhibition. The indigo peaks pointing upward represent regions of chromatin where CTCF binds more frequently in control samples while the purple peaks pointing downward represent regions where CTCF binds more frequently after PARP inhibition. The light blue peaks pointing upward represent regions of chromatin where RAD21 binds more frequently in control LCL, while the brown peaks pointing downward represent regions where RAD21 binds more frequently after PARP inhibition. MACS2 software packages were used to call reads enrichment in pull-down samples compared to input samples as peaks. Analysis of peak distribution under differentiated conditions were performed with the bedtools software package for genome arithmetic. Data was visualized with deepTools.

Global Cohesin Abundance and Localization is Unaffected by PARP Inhibition

Our data indicate that PARP1 activity regulates EBV chromatin conformation and viral gene expression by modulating CTCF and cohesin occupancy across the viral genome. To ensure the increased cohesin binding frequency observed after PARP inhibition is not merely a function of increased cohesin expression, we performed RT-qPCR on three biological replicates of each treatment group (Fig 14A). We found no differences in the expression of the cohesin subunit genes before or after PARP inhibition. Next, we assessed whether PARP inhibition affects the protein levels or the subcellular localization of each cohesin component by western blot analysis after subcellular fractionation. We found that for each cohesin component, the protein abundance and localization were unaffected by PARP inhibition (Fig 14B). As the chromatin-bound fraction showed no difference in total cohesin binding for any of the protein complex after PARP inhibition, we argue that these results indicate that PARP inhibition is stabilizing cohesin binding at specific genomic sites on the EBV genome resulting in the higher frequency of reads observed in the cohesin binding

profile. However, it is also of note that the majority of chromatin-bound cohesin in the assay is from the human genome, indicating that total cohesin binding is unaffected across both genomes, or that a global decrease in cohesin binding across the EBV genome was masked by the abundance of cohesin binding on the human genome.

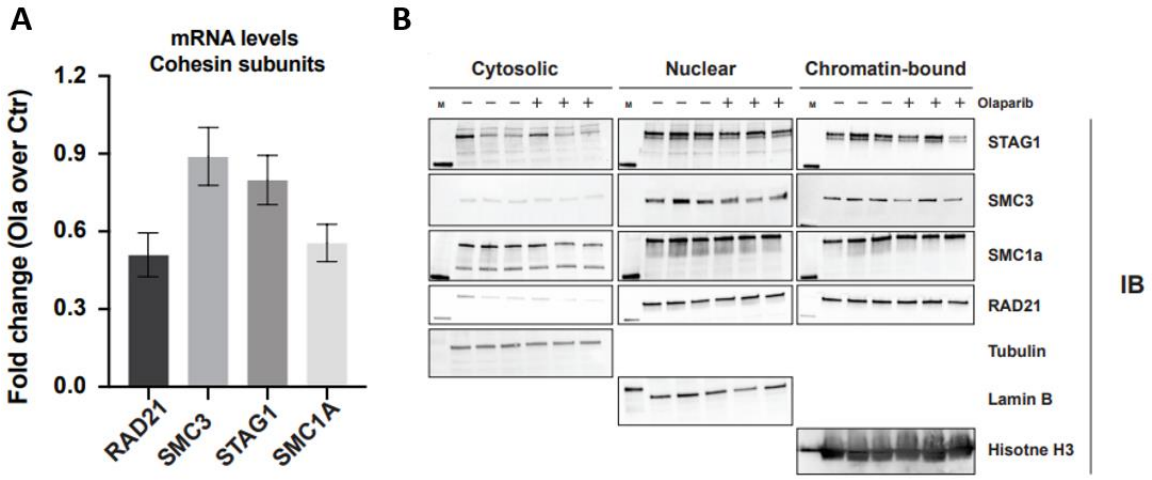

Figure 14: Global Cohesin Abundance and Localization is Unaffected by PARP Inhibition. A) RT-qPCR of each cohesin component, each normalized to 18S respectively, with and without olaparib treatment in LCL. Data displayed as fold change in expression of olaparib treated LCLs divided by control. B) Western blots of all cohesin components from control or olaparib treated LCL after subcellular fractionation.

Cohesin-PARP1 interaction is Not Altered by PARP Inhibition

To determine if cohesin binding is increased at the assessed areas on the EBV genome due to an increase in its affinity for PARP1 interaction after olaparib treatment, we performed an immunoprecipitation assay with SMC3 antibody in three biological replicates of type III LCLs, with or without olaparib treatment (Fig 15). When immunoblotted for PARP1, we found no difference in cohesin/PARP1 interaction between the groups. Taken together, this data indicates that the increased cohesin binding observed across the EBV genome after PARP enzymatic inhibition may be a function specific to the EBV genome, and that it is likely not due to an increased affinity in PARP1/cohesin interaction.

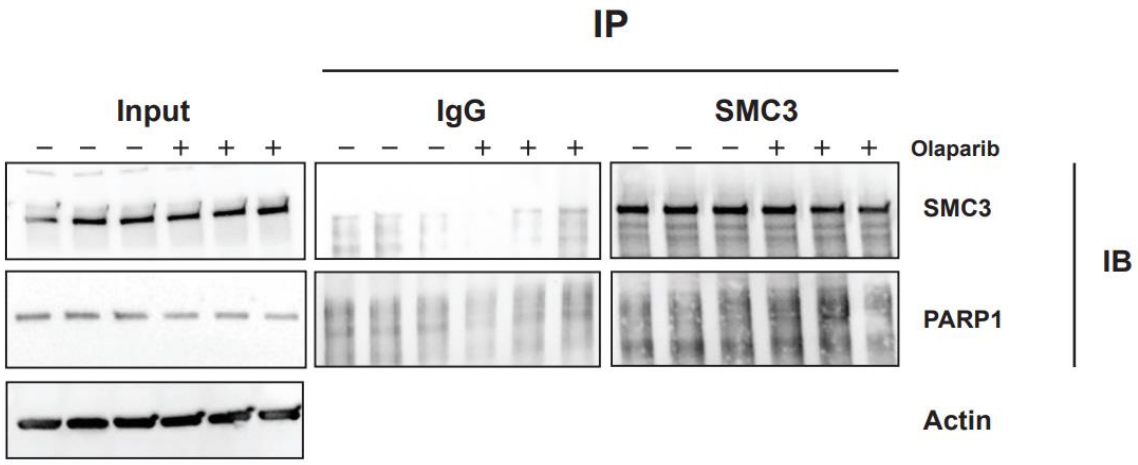

Figure 15: Cohesin-PARP1 interaction is Not Altered by PARP Inhibition. Immunoprecipitation (IP) of SMC3 component of cohesin in LCLs, with or without PARP inhibition. Input lysate was collected before IP and ran along IP material for SMC3 and PARP1 western blots.

Local Chromatin Architecture is Altered by PARP Inhibition

After PARP inhibition, every site where CTCF and cohesin bind across the EBV genome, binding was decreased and increased, respectively. There were also widespread alterations to 3D chromatin structure that seemed to perhaps be context dependent, as some regions gained where other regions lost DNA-DNA contacts despite the same alteration to CTCF/cohesin binding. To determine if PARP inhibition alters chromatin architecture in a reproducible way, ChIP-qPCR using antibodies against various histone marks and variants was performed at the previously validated regions for significantly altered CTCF/cohesin binding (Fig 16). With the exception of H4K16ac and H3.3, all other marks/variants followed the same trend at all four regions of dysregulated CTCF/cohesin binding. In agreement with previous work on the human, histone variant H1 does not colocalize with PARP1, as it is found significantly less at sites where PARP1 is trapped after olaparib treatment (113-115). Additionally, previous work has shown PARP1 has negative regulatory activity against histone methyltransferase EZH2 (121). As expected, yet to date only shown *in vitro*, H3K27me3 is found at each region with up to 4X enrichment after olaparib treatment. It is somewhat surprising, however, that PARP1 inhibition favors the accumulation of H3K9methylation at these regions, as previous work at the retinoic acid locus shows that

PARylation of demethylase KDM4D negatively regulates the enzyme, leading to accumulation of H3K9me2/3 at the locus (196). Finally, we were excited to find that histone variant H2AZ was enriched after PARP inhibition as cohesin retention (and possibly loading) in G2 phase of yeast is dependent on the presence of H2AZ (197). This finding could perhaps in part explain why cohesin binding frequency is higher after PARP inhibition, yet the link between PARP enzymatic activity and H2AZ content is yet to be established.

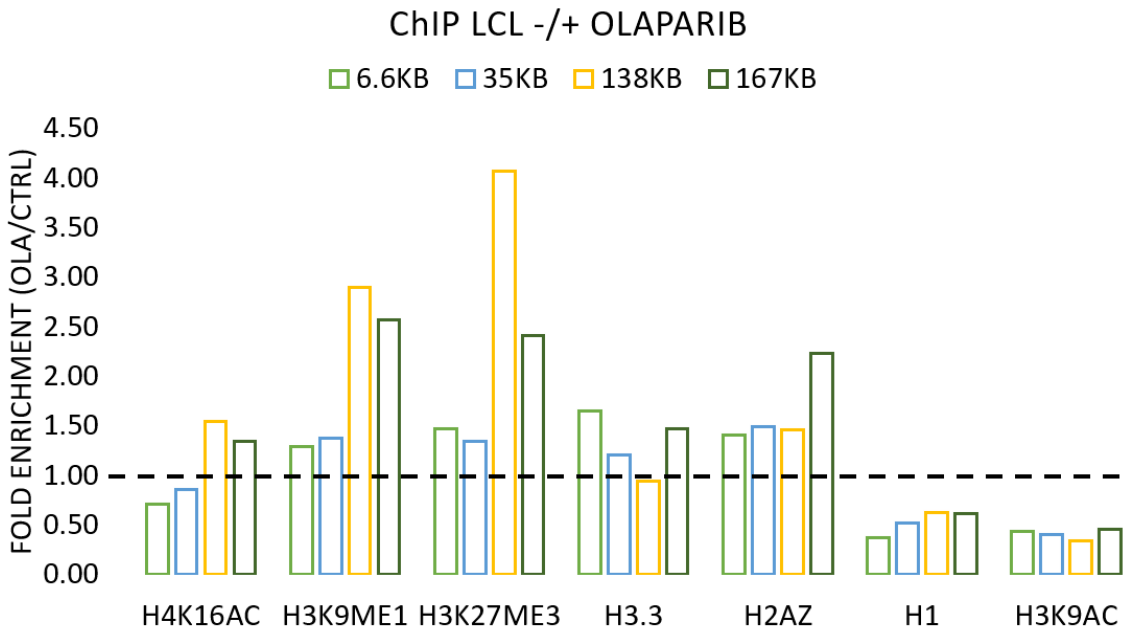

Figure 16. Local Chromatin Architecture is Altered by PARP Inhibition. ChIP-qPCR in LCL with or without olaparib treatment. Data was analyzed by ΔΔCT method, first normalized to input chromatin and then to IgG-IP. Data is displayed as fold enrichment of olaparib treatment over control and are an average of two independent experiments.

SMC3 Phosphorylation is Increased by PARP Inhibition

In addition to alterations of local histone mark and variant composition after PARP inhibition, the abundance of SMC3 serine1083 phosphorylation is also increased (Fig 17). Previous work has shown that SMC3 is phosphorylated at the same mark by ATM/ATR in response to DNA damage (96, 198). Additional studies have shown that ATM-mediated phosphorylation of SMC3 serine1083 reinforces cohesin binding at existing sites (198). It is also known that PARP inhibition, specifically

through olaparib treatment, is enough to activate ATM, likely through induction of double-strand breaks (199). Taken together, increased phosphorylation of SMC3 is likely due to downstream effects of olaparib treatment, and this phosphorylation perhaps stabilizes the binding of cohesin on the EBV genome. Additional studies will be necessary to determine how serine1083 phosphorylation impacts cohesin-chromatin dynamics and perhaps cohesin mobility.

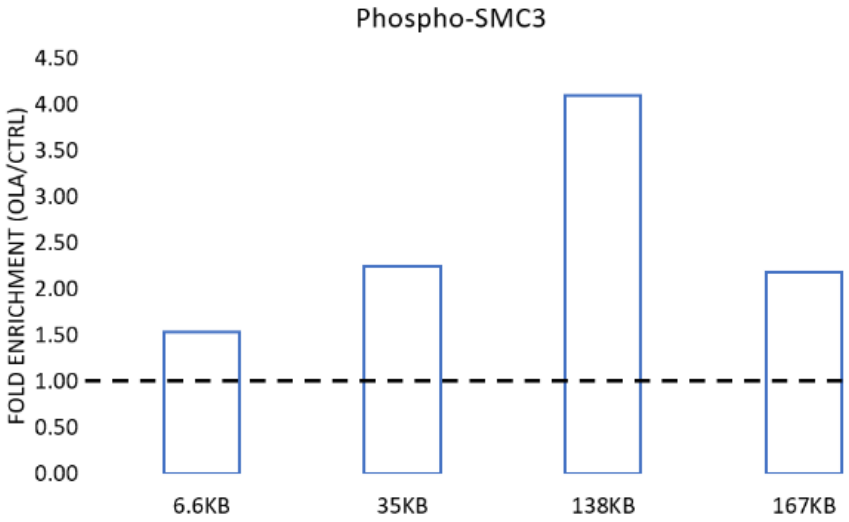

Figure 17. SMC3 Phosphorylation is Increased by PARP Inhibition. ChIP-qPCR in LCL with or without olaparib treatment. Data was analyzed by ΔΔCT method, first normalized to input chromatin and then to IgG-IP. Data is displayed as fold enrichment of olaparib treatment over control and are an average of two independent experiments.

EBV Copy Number Increases with PARP Inhibition

To determine if PARP enzymatic activity is necessary for stability of the latent EBV episome, genomic DNA was extracted from LCLs treated with the PARP1 enzymatic inhibitor olaparib, the Poly-(ADP-ribose) glycohydrolase (PARG) inhibitor PDD 00017273, or an equal volume of DMSO. PARG degrades ribose-ribose bonds within PAR moieties, though is unable to remove the terminal ester bound ADP-ribose from target residues rendering proteins mono-ribosylated (200). Treatment with PARG inhibitor dramatically increases intracellular PAR levels above endogenous levels and has no impact on PARP1 protein abundance (APPENDIX A). Previous work in type 293 cells expressing EBV-bacmid demonstrated that PARP1 is a negative regulator of viral replication

by PARylation of viral transcription factor EBNA1 as well as direct binding of PARP1 to OriP (153). A more recent study using the type I latency B-cell line “Akata” also showed that PARP inhibition through olaparib increased EBV copy number as well as expression of lytic genes (152). To ensure PARP1 has the same effect in a type III lymphoblastoid cell line, we performed an EBV copy number assay utilizing three separate primer sets spanning the EBV genome, which were then averaged (Fig 18). Olaparib treatment significantly increased the number of EBV episomes in LCLs, however the PARG inhibitor had no significant impact on copy number. While it was somewhat surprising that PDD did not have the opposite effect of increasing copy number as PARylation is known to negatively regulate EBNA1, PARG inhibition would likely have no impact on PARP1-episome binding, which is also repressive when physically associating with OriP (153).

Figure 18. PARP inhibition increases EBV copy number. Five million LCL per treatment group were collected for total genomic DNA. 300ng of each group was loaded for qPCR analysis with primers spanning three independent regions of the EBV genome. Values are averages of three independent experiments. (**=p ≤ .01).

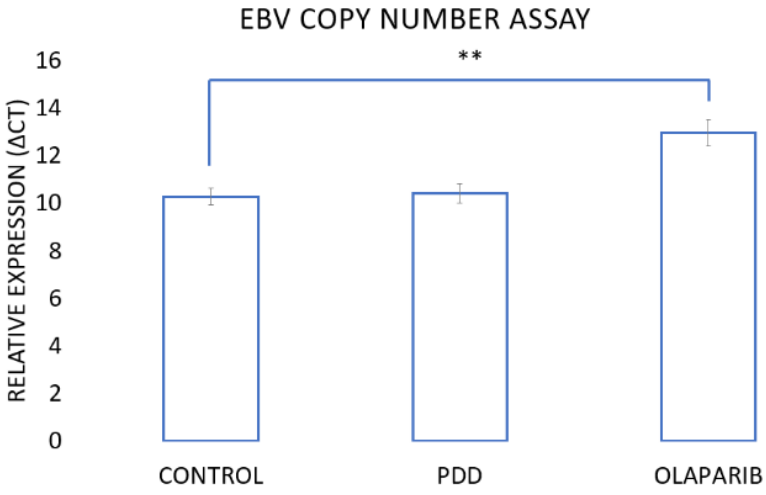

CHAPTER 4

Discussion

In this work, we set out to determine if 3D structure of the EBV episome 1) differs between latency types 2) is dependent upon PARP1 enzymatic activity and 3) can be correlated to latency-type specific gene expression. To answer these questions, we have generated the first complete 3D model of the EBV episome in type I and type III latency states, as assayed through statistical modeling of *in situ* Hi-C matrices from two biological replicates. Interestingly, despite being isogenic with respect to the EBV genome, the two latency types displayed vastly different structures. In the complete Hi-C contact matrix, there were 111 total DNA-DNA combinations with FDR < .05 and p < .05. Mutu I had 31 under the same statistical parameters. However, as Hi-C is a population study, it is highly probable that the random fragmentation from sonication allows for the same chromatin loop to be captured by fragments that map back to slightly different basepairs along the same region. For this reason, the dataset is run through an additional statistical bottleneck to remove all contacts that are likely capturing the same chromatin loop. After this threshold was met, Type III was still found to have significantly more intragenomic contacts than type I with 26 unique, statistically significant loops compared to only seven observed in the type I genome. Only two chromatin interactions remain entirely conserved between the two latency types: 1) the dense local interactions between the terminal repeat, TR, region (~170kb) and the region directly upstream of the origin of viral replication (~2.5 kb) and 2) the 10kb loop formed between the lytic transcripts BWRF1 (~35kb) and BFLF1 (~46kb). The two long-range chromatin loops formed between BCRF2 (~13kb) and BKRF1 (~96.5kb), and between BWRF1 (~35kb) and the BART microRNAs (~143kb) in the type I latency genome have been completely lost in the type III genome. However, many loops and local interactions are formed in type III latency that are not observed in the type I genome. The strongest interactions in type III latency localize around the C-, Z-, and LMP- promoters, within the EBNA transcripts, and surprisingly within the BART microRNAs.

Unexpectedly, we observed differences between our Hi-C analysis and the chromatin loops identified in a previous study using the same isogenic type I and type III cell lines. In that study, it

was found that the type I latency EBV genome forms a chromatin loop between OriP and Qp, the type I latency promoter (162). Alternatively, a loop is formed between OriP and the type III promoter Cp in type III latency (162). In our Hi-C analysis, the OriP-Qp loop observed in type I and the OriP-Cp loop in type III latency are both absent. This could be explained by differences in methodology between chromatin conformation capture assays (3C) and *in situ* Hi-C. The 3C protocol utilized by the prior study first lysed the cells, then formaldehyde fixed the cell lysate (162). It is possible that once chromatin is no longer natively folded within the host nuclei, new chromatin-chromatin interactions are possible that might not naturally occur otherwise. In contrast, *in situ* Hi-C formaldehyde fixes chromatin while still within the intact nuclei of the cell. In this way, Hi-C may provide a more accurate representation of chromatin structure.

Hi-C provides a global, unbiased view of all intragenomic interactions within the episome, but only at an average 4kb resolution in this study. Because of this, the relatively local interaction previously identified in Mutu-LCL between OriP and Cp may be too close to be identified in Hi-C analysis. Additionally, as 3C requires longer crosslinking time, predetermined primer sets, and many more PCR cycles than are required for Hi-C analysis, it is possible that prior studies may have reported chromatin loops occurring at very low frequencies. Our analysis did agree with another prior publication, however, showing strong intragenomic interactions between the region just before OriP and the LMP1/LMP2a transcript region (188). Taken together, the comparison of these datasets utilizing the same cell lines with different methodologies can underscore the importance of understanding the limitations of techniques and the need to validate results with distinct, independent assays. Regardless, our Hi-C analysis indicates that the more transcriptionally active type III EBV genome displays a more complex network of DNA-DNA interactions than the transcriptionally repressed viral genome of type I latency. We are tempted to speculated that the more organized structure of the EBV genome in type III latency allows the virus to express more latent genes while simultaneously repressing lytic transcripts, though functional studies disrupting specific chromatin loops will be necessary to support this.

When comparing the distinct 3D contact maps between latency types with their respective CTCF ChIP-seq profiles, it is clear the differences cannot be accounted for by differences in CTCF binding. Type I and type III CTCF profiles were found to be highly similar. This was initially surprising, as Mutu has roughly 9X less intracellular PAR than Mutu-LCL, and previous work has shown that PARylation is necessary to stabilize CTCF binding across the type III EBV genome (150). Taken together, though CTCF has been shown to play a critical role in the establishment and maintenance of latency repertoires, this chromatin modifier alone likely cannot account for the distinct structures of the EBV episome found via global Hi-C analysis (201). An important caveat to this, however, is that CTCF binding was assessed and compared, but the many known PTMs of CTCF were not. As PTM of CTCF is known to alter its insulator function and possible loop-formation capacity, it is not out of the realm of possibility that CTCF may be differentially regulated between the two latency types, allowing for different 3D structures despite nearly identical CTCF occupancy (58, 63). However, as isogenic EBV strains, these dissimilar structures do support the idea that chromatin structure may play a role in latency type stability.

When comparing the binding profiles of CTCF between the latency types, we also noticed that CTCF binding frequency seemed to be considerably higher in type I than type III. Again, as PARylation seems to be necessary for CTCF binding in prior studies, we were surprised by this result (150). However, when considering that much time had passed between the CTCF ChIP-seq in type I latency and type III, it is also worth noting that different batches of antibody were used for the immunoprecipitation, and antibodies are known to display batch effects. Additionally, the amount of starting material, i.e. chromatin available for antibody binding, can alter the output of chromatin in the immunoprecipitation. This seems a plausible explanation, as we found Mutu to have roughly 4X more EBV episomes per cell population than the isogenic Mutu-LCL, which contextualizes previous work demonstrating higher affinity CTCF binding in type I cells compared to type III at a specific CTCF binding site on the EBV genome (137). While this can likely account for the difference in CTCF binding strength between the two cell lines, it is unclear why there is a large difference in copy number. Besides difference in latency type, they also differ in cell type, as

Mutu is a Burkitt's lymphoma cell line and Mutu-LCL is a lymphoblastoid cell line. Mutu has another isogenic counterpart, however, in a clonal outgrowth known as Mutu III displaying type III latency in a Burkitt background. Comparing copy number between these cell lines would be a promising way to distinguish between latency type and background differences, considering these two lines are isogenic with regard to host and EBV.

Next, we analyzed how the total intragenomic contact map is altered by PARP enzymatic inhibition, enabling us to view on a total chromosome scale at average 4kb resolution the role PARP1 plays in chromosome structural maintenance. As PARP1's role in chromatin modification has been well established in various systems, we sought to determine if post-translational modification, specifically PARylation, of CTCF may account for the differences in chromatin looping between type I and III latency, perhaps by impeding CTCF's interaction with the chromatin looping factor cohesin. We have previously reported that PARP1 activity is significantly higher in type III latency compared to type I, and that knock-down or enzymatic inhibition of PARP1 destabilizes CTCF binding across the EBV genome, both with direct impact on latency type-specific transcription (150-152). However, with global knockout or pharmacological inhibition of PARP1, CTCF binding was only modestly decreased on a global scale across the EBV genome, with significant drops only validated at select loci- i.e. the Cp and BZLF1 promoter regions (150, 152). Additionally, when studying lytic reactivation by disrupting PARylation at the BZLF1 promoter, depletion of CTCF had no significant impact on lytic reactivation, suggesting the presence of an additional structural protein regulating the EBV episome (152). Importantly, changes in 3D chromatin structure were not accessed in either study.

For these reasons, we performed an additional Hi-C assay, this time with the PARP enzymatic inhibitor olaparib, to determine the extent to which PARP1 regulates the episome structure globally. We found that both the type I and type III genome had a decrease in total unique intragenomic interactions after inhibition. In the control type I genome, there are seven unique DNA-DNA interactions at $p<.05$, and six when $FDR<.05$ is also added. With olaparib treatment, there are only

four unique interactions with the same statistical parameters. In type III at p<.05, the 26 unique interactions in control LCL were decreased to 17. At p<.05 and FDR<.05, however, total number of interactions are preserved, with both equaling 17 DNA-DNA contacts. The 17 interactions are not static between the two groups though as the identity of the fragments are distinct between treatment and control, underscoring the central point that PARP enzymatic inhibition destabilizes the 3D EBV genome structure. This statistical discrepancy could indicate that the nine loops not meeting the FDR threshold could be weaker interactions, context-dependent, or that these loops are present in only a portion of the five-million cell population.

Interestingly, while type I exclusively lost chromatin loops, type III gained new chromatin contacts not seen in the control genome. In type I latency, long-range chromatin loops between the ~35kb region and the 145kb-150kb BART microRNA region, and ~13kb region and the 95kb-100kb region disappear, indicating that these regions are no longer interacting. A relatively smaller loop also disappeared between the 35kb region and the 45kb region. For type III latency, while eight unique high-frequency loops disappear, there are also many regions where new long-range chromatin loops are formed between regions that are on average 60kb apart. Additionally, the local interactions within the 142kb-152kb region seem to be shifted after PARP inhibition, with a dense region of local interactions now observed from 137kb-143kb. While the conformation of the type III genome is significantly altered after olaparib treatment, the strong, sequential interactions between the region within the EBNA1.1 transcript directly preceding OriLyt (~33-37kb) and the region between the lytic Zp and EBNA1.3 (~93-95kb) remain unchanged, indicating that this chromatin interaction occurs independent of PARP activity. Regardless, our analysis demonstrates that PARP inhibition changes the three-dimensional structure of the EBV genome, particularly in type III latently infected cells, providing the first example of PARylation impacting 3D chromatin structure on a whole-chromosome scale.

Next, we wanted to assess whether the widespread alterations to chromatin structure may impact EBV episome stability and capacity to faithfully replicate along with the host. Previous work in type

293 cells expressing EBV-bacmid demonstrated that PARP1 is a negative regulator of viral replication by PARylation of viral transcription factor EBNA1 as well as direct binding of PARP1 to OriP (153). A more recent study also showed that PARP inhibition through olaparib increased EBV copy number as well as expression of lytic genes in type I latency Akata B-cells (152). In agreement, olaparib treatment significantly increased the number of EBV episomes in LCLs. However, the PARG inhibitor PDD had no significant impact on copy number. While it was somewhat surprising that PDD did not have the opposite effect of increasing copy number as PARylation is known to negatively regulate EBNA1, PARG inhibition would likely have no impact on PARP1-episome binding, which is also repressive when physically associating with OriP (153). As PARP1 was shown to increase binding after olaparib treatment in a "PARP trapping" effect, the repressive binding at OriP would be preserved. As the previous studies were conducted in 293 cells, perhaps regulation of endogenous EBV episomal replication within latently infected host B-cells is more heavily regulated by PARP1-OriP binding than PARylation of EBNA1.

To determine the effect of altered chromatin looping after PARP inhibition on viral gene expression, RNA-seq was performed on type III Mutu-LCL and isogenic type I Mutu cells with or without PARP enzymatic inhibition. Mutu grouped together via PCA regardless of treatment while treated LCLs tightly clustered away from control LCLs. The altered gene expression observed after treatment was mapped as an unsupervised, hierarchical heat map as well as a volcano plot. Type I cells displayed significant dysregulation of only three viral genes. The OriLyt noncoding transcript was downregulated in olaparib treatment, however, two genes typical of the lytic transcriptional repertoire were simultaneously upregulated. The relatively small number of genes impacted by olaparib treatment is unsurprising though as intracellular PAR levels were only decreased ~30% by treatment. At the same olaparib concentration, LCL PAR levels were decreased ~80%, which makes sense considering type III cells basally have 9X more PARP activity than type I. In fact, at the same concentration of olaparib, LCLs still have slightly higher intracellular PAR than untreated Mutu cells. With 80% less PARylation, widespread transcriptional dysregulation was observed in treated Mutu-LCLs. Genes indicative of type III latency, namely the EBNAs, were significantly

downregulated, agreeing with prior work demonstrating that olaparib treatment decreases expression of EBNA2 (150). Lytic genes including BMRF2, BILF1, and BALF3, are upregulated in addition to the EBV early gene LF3. The upregulation of lytic genes in both cell types aligns well with prior work demonstrating that PARP1 knock-down increases viral copy number and lytic reactivation (152, 153). This data also supports our hypothesis that PARylation helps maintain latency-specific transcriptional repertoires.

CTCF has been shown to colocalize with cohesin across the type III EBV genome (143, 144). As cohesin physically forms long-range chromatin loops while CTCF acts as an anchor to recruit cohesin binding, we also performed ChIP-seq of the RAD21 component of cohesin. Again, we were surprised to observe very similar binding profiles between the type I and type III genomes. Recent work has identified ~10,000 chromatin loops within the human genome and shown that anywhere from 50-80% are bound by both CTCF and cohesin, while others seem to be regulated by the binding of various transcription factors depending on cell type (6, 49, 63). Our results indicate that in the context EBV, the chromatin loops we observed involved CTCF and cohesin, except for a small number that occur in the 100-130kb region of the viral genome. It is possible that these loops simply reflect the natural folding of the viral genome within the nucleus and therefore can form without the help of CTCF and cohesin. Much work is needed to elucidate the factors involved in chromatin looping in the EBV genome, may they be host or viral transcription factors, or other host proteins with known roles in higher order chromatin organization such as condensin or mediator (144, 201).

With the inhibition of PARP enzymatic activity, the cohesin binding pattern was unchanged. However, the frequency of binding at the majority of cohesin binding sites was significantly increased as CTCF binding was decreased. As no relationship has previously been published to the best of our knowledge regarding PARP1 regulation of cohesin-chromatin binding outside of DNA damage response, we were excited by this finding (202). Cohesins are recruited during post-replicative double-strand break repair possibly through recruitment by local histone PARylation or

by chromatin decompaction induced by PARylation making the region more accessible (202).To date, no publications have cited PARP1 having a functional relationship with cohesin under physiological conditions.

As we were surprised to find stabilization of cohesin-chromatin binding after PARP inhibition, we wanted to assess various possible explanations. The most straightforward possibility was that PARP inhibition led to more cohesin being expressed, and thus more cohesin was available to bind. After RT-qPCR and western blot of each cohesin subunit, we were able to rule out this explanation. Though cohesin was known to localize in the nucleus, we additionally wanted to rule out that PARP inhibition led to differences in cohesin protein localization, making it more concentrated near the EBV episome. We found that this was also not the case. We also ruled out the possibility that PARP enzymatic inhibition rendered it able to bind cohesin with higher affinity by co-immunoprecipitation, as PARP1 was shown to bind SMC3 with roughly equal frequency with or without olaparib treatment. Finally, as olaparib treatment has been shown to “trap” PARP1 to DNA through prevention of auto-PARylation and thus DNA-dissociation, it is possible that both decrease in PAR and increased PARP1 binding could impact cohesin-chromatin binding (195). Through PARP1 ChIP-qPCR, we determined that there is no significant difference in PARP1 binding at regions where cohesin binding is increased after olaparib treatment, though there is a trend of increased PARP1 binding not quite reaching statistical significance at the low drug concentration used in this study. As such, it is unlikely though not impossible that the presence of PARP1 alone at cohesin binding sites may stabilize cohesin-chromatin binding.

Moving past the straightforward possibilities, we also wanted to assess if local chromatin environment might make cohesin binding sites more or less accessible to the complex after PARP inhibition. By ChIP-qPCR of various histone marks and variants, we determined that, with the exception of H4K16ac and H3.3, all other marks/variants followed the same trend at regions of dysregulated CTCF/cohesin binding, i.e. all binding with higher or lower frequency after inhibition at each of the regions assessed. In agreement with previous work on the human genome, histone

variant H1 is found with mutual exclusivity to PARP1, as it is found significantly less at sites where PARP1 is trapped after olaparib treatment, despite relatively low binding even in the control (113-115). Additionally, previous work has shown PARP1 has negative regulatory activity against histone methyltransferase EZH2 (121). As expected, H3K27me3 is found at each region with up to 4X enrichment after olaparib treatment. As H3K27me3 is characteristic of less accessible chromatin, it is possible that cohesin mobility may be negatively impacted by chromatin compaction. It is somewhat surprising, however, that PARP1 inhibition favors the accumulation of H3K9methylation at these regions, as previous work at the retinoic acid locus shows that PARylation of demethylase KDM4D negatively regulates the enzyme, leading to accumulation of H3K9me2/3 at the locus (189). Regardless, H3K9me2/3 is also characteristic of condensed chromatin state, perhaps also hindering cohesin mobility. Finally, we were excited to find that histone variant H2AZ was enriched after PARP inhibition as cohesin retention (and possibly loading) in G2 phase of yeast is dependent on the presence of H2AZ (197). This finding could perhaps in part explain why cohesin binding frequency is higher after PARP inhibition, yet the link between PARP enzymatic activity and H2AZ content is yet to be established.

Perhaps another explanation for cohesin retention on the EBV genome after PARP inhibition may be the direct PTM of the complex. In particular, we found that phosphorylation of SMC3 serine1083 is increased after olaparib treatment at each of the cohesin binding sites accessed via ChIP-qPCR. Previous work has shown that SMC3 is phosphorylated at the same mark by ATM/ATR in response to DNA damage (96, 198). Additional studies have shown that ATM mediated phosphorylation of SMC3 serine1083 reinforces cohesin binding at existing sites (198). It is also known that PARP inhibition, specifically through olaparib treatment, is enough to activate ATM, likely through induction of double-strand breaks (199). Taken together, increased phosphorylation of SMC3 is likely due to downstream effects of olaparib treatment, and this phosphorylation perhaps stabilizes the binding of cohesin on the EBV genome. Additional studies will be necessary to determine how serine1083 phosphorylation impacts cohesin-chromatin dynamics and perhaps cohesin mobility,

especially since DNA damage and particularly double-strand break accumulation were not accessed in the current study.

It would also be interesting to access other cohesin complex PTMs. As cohesin dynamics have primarily been studied in the context of mitosis and sister chromatid cohesion, many questions remain on how PTMs may influence cohesin mobility along DNA or its ability to faithfully form loops with CTCF. In particular, acetylation of SMC3 is essential for sister chromatin cohesion and perhaps for cohesin's stable association to DNA in general, though it remains unclear if acetylation is necessary for initial loading or persistence on DNA (91). This may be due in part by SMC3 acetylation destabilizing association with cohesin DNA-release factor WAPL (92). Prior work has also established that phosphorylation of the STAG1/2 and RAD21 components of cohesin must be phosphorylated in order to separate from sister chromatids during mitosis, though it is unclear how their phosphorylation may impact cohesin binding on interphase DNA (93, 94). Assessing these cohesin PTMs after PARP inhibition may provide clues as to the increased binding frequency of the complex after olaparib treatment.

In the current study, nor any prior studies, was possible direct PARylation of cohesin assessed. PAR chains are held together by relatively unstable 2′,1″-O-glycosidic ribose-ribose bonds, making them technically challenging to study. Adding to the technical challenges, antibodies against the moiety are highly variable, as PAR chains themselves can be one to dozens of monomers long. For this reason, resins conjugated to PAR-binding motifs can be used in place of antibody-conjugated resins in immunoprecipitation assays. In the future, it would be interesting to assess potential PARylation of the cohesin complex itself or the histones within its binding sites. We do know, however, that CTCF can be directly PARylated (103). It would also be worth investigating whether PARylation of CTCF can alter its ability to interact with cohesin and thus form chromatin loops.

Of note, while the PARP1-mediated destabilization of cohesin was surprising, it is also not incompatible with the currently accepted loop-extrusion model of cohesin/CTCF loop formation. CTCF depletion reduces cohesin enrichment at colocalization sites but does not disrupt the binding of cohesin to chromatin overall, implying that the persistence of CTCF binding is necessary for proper distribution of cohesin but not its loading or physical interaction with chromatin (70). Prior studies have shown that inducible knockout of CTCF results in cohesin relocation outside of CTCF binding sites, but not a significant increase in dissociation from chromatin (70). Our study differs in that CTCF is still able to bind to its usual sites along the EBV genome, just with lower frequency. Perhaps time-course assays with inducible CTCF knockout would better illustrate how long cohesin is able to remain bound to its CTCF colocalization sites without the anchor present. Until then, it is tempting to speculate that PARP induced stabilization of chromatin is enough to increase its residency at these sites despite decreased anchor presence.

In the current work, we were also interested in the correlation between altered episomal structure and altered gene expression. We noted that the viral genes most significantly dysregulated in expression tended to correlate to the regions where intragenomic interactions were altered after PARP inhibition. To establish a correlation between changes in viral transcripts and changes in EBV 3D structure, we compared the frequency of DNA-DNA interactions from our Hi-C dataset to the number of reads per region in the EBV genome from our RNA-seq data set. For example, after PARP inhibition, we observed a dense region of decreased RNA reads within the EBNA transcripts, which are shown to be downregulated in our RNA-seq data, directly aligned with region of lost chromatin binding. Additionally, the lytic BMRF2 and BALF3 genes, which are shown to be overexpressed in olaparib treated LCLs, also have heightened RNA-seq reads that can be directly correlated regions of increased DNA-DNA contacts in the Hi-C data. The latent genes EBNA3B/3C conversely are under-expressed in olaparib treatment and align with chromatin binding events that are more frequent in the control genome. These examples serve to illustrate that differences in chromatin binding do not seem to be the only factors contributing to dysregulated gene expression, as some transcripts are upregulated in regions of disrupted chromatin looping while others are

downregulated. In reality, while chromatin organization does seem to impact gene expression, it is likely in a complex, context-dependent manner.

RPMS1 was shown to be upregulated in olaparib treated LCLs in our RNA-seq dataset, yet four primers spanning the gene did not show any significant downregulation via RT-qPCR. Interestingly, there are regions within the relatively long gene with a higher number of RNA reads in the treatment group when analyzing the total read count across the EBV genome. These increased reads also correlate with increased intragenomic contacts at the same RPMS1 transcript region. Though this seems contradictory, we observed that one of the seven tested miRNAs spliced from RPMS1 is significantly upregulated. The discrepancy between our RNA-seq data and RT-qPCR quantification of miRNA could be due to the fact that miRNAs are filtered from the RNA samples during purification before sequencing and therefore they are disregarded during data analysis. However, this result is nonetheless exciting as it seems to validate a study in the human genome showing that inhibition or depletion of PARP1 can alter how genes are alternatively spliced (194).

We additionally wanted to assess how altered CTCF/cohesin binding may factor into the correlation between transcription and chromatin looping. To accomplish this, we compared changes in CTCF and RAD21 binding via ChIP-seq to our Hi-C and RNA-seq data. In general, we observed viral chromatin loops occurring between regions where at least one “end” of the chromatin loop is associated with CTCF/cohesin, supporting the basic idea that not only do these proteins bind the EBV genome and regulate gene expression, they also form viral chromatin loops. Interestingly, we noted that the region between 100kb and 130Kb forms short chromatin loops in the absence of CTCF and cohesin binding. When we compared changes in chromatin looping and CTCF/RAD21 binding, we found that six regions of the viral genome had altered chromatin architecture correlating with loss of CTCF and increase of RAD21 occupancy after PARP inhibition. We also noted that changes in CTCF/RAD21 binding results in either the formation or the disruption of chromatin loops. The changes in chromatin looping due to altered CTCF/cohesin occupancy after PARP inhibition correlated to dysregulated transcription of the viral genes within the same regions. For example,

we observed that PARP inhibition results in the disruption of the chromatin loops existing upstream the EBER microRNA encoding region located at 6.6kb, coinciding with changes in CTCF/RAD21 occupancy. However, after PARP inhibition we observed that the same region at 6.6kb now establishes a new intragenomic interaction with a region located around 35kb of the viral genome, and that both regions show changes in CTCF/RAD21 occupancy. The 35kb region is within the alternatively spliced EBNA transcripts, and our RNA-seq data displayed that all EBNAs are dysregulated after PARP inhibition. While demonstrating a direct causal relationship between gene expression and particular chromatin interactions would require the mutation/deletion of cohesin binding sites, we are excited that this global, correlational study provides the rationale for future studies of EBV genome structure and maintenance of latency repertoires.

An important distinction between our study and previous publications examining cohesin/CTCF in 3D chromatin structure is that our study is respectively stabilizing or destabilizing cohesin and CTCF binding to chromatin. Prior publications have utilized knock-down or knock-out of these DNA-binding proteins to investigate impacts on host chromatin structure as outlined in detail by Rowley and Corces (6). In summary, CTCF depletion reduces cohesin enrichment at colocalization sites but does not disrupt the binding of cohesin to chromatin overall, results in loss of CTCF-mediated TADs and contact domains but not chromatin compartments (6, 70-72). In comparison, deletion of cohesin results in better segretion of chromatin compartments and loss of CTCF-mediated chromatin loops, though CTCF localization remained unchanged (71, 73, 74). Our study relied upon the decrease of one PTM which consequently decreased frequency/strength of binding of CTCF and had the opposite impact on cohesin. A caveat to our study would be that ChIP-seq is not able to distinguish between increased frequency of binding, increased affinity of binding or increase in actual protein abundance at a location, which would be interesting to explore in the future.

To date, studies in the EBV genome have utilized the disruption of specific CTCF binding sites, often in 293 cells infected with EBV bacmid which may not fully recapitulate chromatin dynamics of latency infected B-cells (136, 137, 188). This study outlines the drastic, global impact of PARP1

inhibition in an *in situ*, unbiased method. There has only been one explicit example published of PARP1 directly altering 3D chromatin structure in an analysis PARP1/CTCF mediated recruitment of circadian loci to the nuclear lamina (131). The data presented here correlate the enzymatic inhibition of PARP1 to widespread alterations in chromatin conformation, particularly in type III cell lines which basally have high levels of PARP1 activity. As human chromatin conformation as well as intracellular PAR levels basally vary between cell types, it is interesting to speculate if differences in PARylation help maintain tissue-type specific chromatin conformation (203, 204).

Finally, we would be remiss to not include the major limitations in this study as points of consideration. The major conclusions of this project were outlined by our Hi-C analysis and models made from EBV chromatin extracted from populations of five-million cells per treatment group. It has long been established that EBV episome copy number varies not only by strain and viral lifecycle, but also by genetic variation between host B-cells (205-207). Because of this, we do wonder whether different EBV strains exhibiting the same latency type would have similar episomal conformation as those we have elucidated in this project. Additionally, our type I and type III cell lines are not only from different hosts, but they also differ in pathology, as Mutu is a Burkitt's lymphoma cell line and Mutu-LCL is a lymphoblastoid cell line. It is interesting to speculate if the same strain of EBV in a different donor B-cell background would display the same chromatin conformation. For example, differences in EBV copy number can be positively correlated to host expression of CXCL16 and AGL, and negatively correlated with ADARB2 expression (207). In a cohort of 62 immortalized B-cells from different donors, there were clearly defined groups of "permissive LCLs" and "nonpermissive LCLs", with the former having stably high EBV copy number, relatively low latent gene expression, and tendency for spontaneous lytic reactivation (208). Permissive LCLs correlated to higher host expression of unfolded protein response genes and plasma cell markers. Non-permissive LCLs had relatively low EBV copy number and rarely induced lytic reactivation. These LCLs were correlated with higher expression of host transcription factors involved in maintaining B cell lineage, specifically EBF1. If we are to argue in this paper that chromatin conformation, at least in part, regulates viral gene expression through the host enzyme

PARP1, other host factors may also impact chromatin conformation, and that those factors may be differentially expressed between hosts.

Additionally, while we believe the chromatin dynamics explored here in the EBV genome may also be applicable to the human genome, our observations could be biased due to the limited size of the EBV genome. Because of this, EBV may not fully recapitulate the interactions between CTCF, cohesin, and PARP1, observed in mammalian genomes at megabase scales. With that in mind, many chromatin studies today are first conducted in yeast, with a genome only totaling 12 million bases spread across 16 chromosomes (209). In fact, the yeast genome was the first eukaryotic genome sequenced (209). The EBV genome at roughly 170 kilobases on a single chromosome is comparable in size to many of *Saccharomyces cerevisiae's* 16 chromosomes. While many human proteins have homologues in yeast, we argue that the EBV episome may also be a good model for the study of genomics on a smaller scale as the EBV genome is endogenously surrounded by host proteins.

On a technical level, the *in situ* Hi C method utilized in this paper can only generate an inferred 3D chromatin structure from a population dataset, meaning these results cannot determine if individual episomes within the same human B-cell display different chromatin conformations. The models generated here can only illustrate the most frequently occurring and robust DNA-DNA interactions as a generalized chromatin conformation for the population. While the limitations outlined here should certainly be taken into consideration, we are still excited to report that isogenic EBV genomes displaying different latency types have vastly different chromatin conformations, with type III latency depending on PARP enzymatic function to maintain its structure and latency-specific expression profile.

To conclude, when considering the translational relevance of this work, we first must evaluate the merit of evicting EBV from the host. The herpesvirus family arose 180 to 220 million years ago, with gammaherpes diverging into a distinct subfamily roughly 80 to 60 million years ago (210). Though

evolutionary studies for gammaherpes is lagging, it is estimated that at least herpes simplex virus-1 infected hominids before their evolutionary split from chimpanzees (211). EBV is a nearly ubiquitous virus with rare complications, many of which only arise during co-infection or comorbidities. Treating asymptomatic latent infection, particularly through lytic activation induced by PARP inhibition followed by antivirals, may simply be more trouble than it is worth in immunocompetent carriers.

REFERENCES

1. Kovalchuk I, Kovalchuk O. Genome stability : from virus to human application. xxii, 690 pages p.

2. Iwasaki W, Miya Y, Horikoshi N, Osakabe A, Taguchi H, Tachiwana H, et al. Contribution of histone N-terminal tails to the structure and stability of nucleosomes. FEBS Open Bio. 2013;3:363-9.

3. Bonifer C, Cockerill PN. Chromatin mechanisms regulating gene expression in health and disease. Adv Exp Med Biol. 2011;711:12-25.

4. Li G, Zhu P. Structure and organization of chromatin fiber in the nucleus. FEBS Lett. 2015;589(20 Pt A):2893-904.

5. Essentials of Cell Biology Scitable: Nature Education; 2014. Available from: https://www.nature.com/scitable/ebooks/essentials-of-cell-biology-14749010/122996796/.

6. Rowley MJ, Corces VG. Organizational principles of 3D genome architecture. Nat Rev Genet. 2018;19(12):789-800.

7. Bird AW, Yu DY, Pray-Grant MG, Qiu Q, Harmon KE, Megee PC, et al. Acetylation of histone H4 by Esa1 is required for DNA double-strand break repair. Nature. 2002;419(6905):411-5.

8. Ikura T, Ogryzko VV, Grigoriev M, Groisman R, Wang J, Horikoshi M, et al. Involvement of the TIP60 histone acetylase complex in DNA repair and apoptosis. Cell. 2000;102(4):463-73.

9. Huyen Y, Zgheib O, Ditullio RA, Gorgoulis VG, Zacharatos P, Petty TJ, et al. Methylated lysine 79 of histone H3 targets 53BP1 to DNA double-strand breaks. Nature. 2004;432(7015):406-11.

10. Wang H, Wang L, Erdjument-Bromage H, Vidal M, Tempst P, Jones RS, et al. Role of histone H2A ubiquitination in Polycomb silencing. Nature. 2004;431(7010):873-8.

11. Hurd PJ, Bannister AJ, Halls K, Dawson MA, Vermeulen M, Olsen JV, et al. Phosphorylation of histone H3 Thr-45 is linked to apoptosis. J Biol Chem. 2009;284(24):16575-83.

12. Bannister AJ, Kouzarides T. Regulation of chromatin by histone modifications. Cell Res. 2011;21(3):381-95.

13. Watson JD. Molecular biology of the gene. 6th ed. San Francisco

Cold Spring Harbor, N.Y.: Pearson/Benjamin Cummings ;

Cold Spring Harbor Laboratory Press; 2008. xxxii, 841 pages p.

14. Längst G, Manelyte L. Chromatin Remodelers: From Function to Dysfunction. Genes (Basel). 2015;6(2):299-324.

15. Petty E, Pillus L. Balancing chromatin remodeling and histone modifications in transcription. Trends Genet. 2013;29(11):621-9.

16. Phillips T, Shaw K. Chromatin Remodeling in Eukaryotes. Gene expression and regulation [Internet]. 2008; 1(1):[209 p.]. Available from: https://www.nature.com/scitable/topicpage/chromatin-remodeling-in-eukaryotes-1082/#:~:text=In%20eukaryotes%2C%20DNA%20is%20tightly%20wound%20into%20a%20complex%20called%20chromatin.&text=Therefore%2C%20a%20cell's%20chromatin%20must,functioning%20of%20all%20eukaryotic%20cells.

17. Beagan JA, Phillips-Cremins JE. On the existence and functionality of topologically associating domains. Nat Genet. 2020;52(1):8-16.

18. Schoenfelder S, Fraser P. Long-range enhancer-promoter contacts in gene expression control. Nat Rev Genet. 2019;20(8):437-55.

19. Williamson I, Lettice LA, Hill RE, Bickmore WA. Shh and ZRS enhancer colocalisation is specific to the zone of polarising activity. Development. 2016;143(16):2994-3001.

20. Symmons O, Pan L, Remeseiro S, Aktas T, Klein F, Huber W, et al. The Shh Topological Domain Facilitates the Action of Remote Enhancers by Reducing the Effects of Genomic Distances. Dev Cell. 2016;39(5):529-43.

21. Williams A, Spilianakis CG, Flavell RA. Interchromosomal association and gene regulation in trans. Trends Genet. 2010;26(4):188-97.

22. Spilianakis CG, Lalioti MD, Town T, Lee GR, Flavell RA. Interchromosomal associations between alternatively expressed loci. Nature. 2005;435(7042):637-45.

23. Guerreiro I, Kind J. Spatial chromatin organization and gene regulation at the nuclear lamina. Curr Opin Genet Dev. 2019;55:19-25.

24. Szczepińska T, Rusek AM, Plewczynski D. Intermingling of chromosome territories. Genes Chromosomes Cancer. 2019;58(7):500-6.

25. Boyle S, Gilchrist S, Bridger JM, Mahy NL, Ellis JA, Bickmore WA. The spatial organization of human chromosomes within the nuclei of normal and emerin-mutant cells. Hum Mol Genet. 2001;10(3):211-9.

26. Tanabe H, Müller S, Neusser M, von Hase J, Calcagno E, Cremer M, et al. Evolutionary conservation of chromosome territory arrangements in cell nuclei from higher primates. Proc Natl Acad Sci U S A. 2002;99(7):4424-9.

27. Sun HB, Shen J, Yokota H. Size-dependent positioning of human chromosomes in interphase nuclei. Biophys J. 2000;79(1):184-90.

28. Maharana S, Iyer KV, Jain N, Nagarajan M, Wang Y, Shivashankar GV. Chromosome intermingling-the physical basis of chromosome organization in differentiated cells. Nucleic Acids Res. 2016;44(11):5148-60.

29. Parada LA, McQueen PG, Munson PJ, Misteli T. Conservation of relative chromosome positioning in normal and cancer cells. Curr Biol. 2002;12(19):1692-7.

30. Parada LA, McQueen PG, Misteli T. Tissue-specific spatial organization of genomes. Genome Biol. 2004;5(7):R44.

31. Hindorff LA, MacArthur J, Morales J, Junkins HA, Hall PN, Klemm AK, et al. A Catalog of Published Genome-Wide Association Studies. http://www.genome.gov/gwastudies: National Human Genome Research Institute; 2012.

32. Dekker J, Belmont AS, Guttman M, Leshyk VO, Lis JT, Lomvardas S, et al. The 4D nucleome project. Nature. 2017;549(7671):219-26.

33. McCord RP, Kaplan N, Giorgetti L. Chromosome Conformation Capture and Beyond: Toward an Integrative View of Chromosome Structure and Function. Mol Cell. 2020;77(4):688-708.

34. Kempfer R, Pombo A. Methods for mapping 3D chromosome architecture. Nat Rev Genet. 2020;21(4):207-26.

35. Gall JG, Pardue ML. Formation and detection of RNA-DNA hybrid molecules in cytological preparations. Proc Natl Acad Sci U S A. 1969;63(2):378-83.

36. Speicher MR, Gwyn Ballard S, Ward DC. Karyotyping human chromosomes by combinatorial multi-fluor FISH. Nat Genet. 1996;12(4):368-75.

37. Ou HD, Phan S, Deerinck TJ, Thor A, Ellisman MH, O'Shea CC. ChromEMT: Visualizing 3D chromatin structure and compaction in interphase and mitotic cells. Science. 2017;357(6349).

38. Flors C. Super-resolution fluorescence imaging of directly labelled DNA: from microscopy standards to living cells. J Microsc. 2013;251(1):1-4.

39. Gustafsson MG. Surpassing the lateral resolution limit by a factor of two using structured illumination microscopy. J Microsc. 2000;198(Pt 2):82-7.

40. Rust MJ, Bates M, Zhuang X. Sub-diffraction-limit imaging by stochastic optical reconstruction microscopy (STORM). Nat Methods. 2006;3(10):793-5.

41. van de Linde S, Löschberger A, Klein T, Heidbreder M, Wolter S, Heilemann M, et al. Direct stochastic optical reconstruction microscopy with standard fluorescent probes. Nat Protoc. 2011;6(7):991-1009.

42. Sahl SJ, Hell SW, Jakobs S. Fluorescence nanoscopy in cell biology. Nat Rev Mol Cell Biol. 2017;18(11):685-701.

43. Dekker J, Rippe K, Dekker M, Kleckner N. Capturing chromosome conformation. Science. 2002;295(5558):1306-11.

44. Simonis M, Klous P, Splinter E, Moshkin Y, Willemsen R, de Wit E, et al. Nuclear organization of active and inactive chromatin domains uncovered by chromosome conformation capture-on-chip (4C). Nat Genet. 2006;38(11):1348-54.

45. Zhao Z, Tavoosidana G, Sjölinder M, Göndör A, Mariano P, Wang S, et al. Circular chromosome conformation capture (4C) uncovers extensive networks of epigenetically regulated intra- and interchromosomal interactions. Nat Genet. 2006;38(11):1341-7.

46. Dostie J, Richmond TA, Arnaout RA, Selzer RR, Lee WL, Honan TA, et al. Chromosome Conformation Capture Carbon Copy (5C): a massively parallel solution for mapping interactions between genomic elements. Genome Res. 2006;16(10):1299-309.

47. Denker A, de Laat W. The second decade of 3C technologies: detailed insights into nuclear organization. Genes Dev. 2016;30(12):1357-82.

48. Lieberman-Aiden E, van Berkum NL, Williams L, Imakaev M, Ragoczy T, Telling A, et al. Comprehensive mapping of long-range interactions reveals folding principles of the human genome. Science. 2009;326(5950):289-93.

49. Rao SS, Huntley MH, Durand NC, Stamenova EK, Bochkov ID, Robinson JT, et al. A 3D map of the human genome at kilobase resolution reveals principles of chromatin looping. Cell. 2014;159(7):1665-80.

50. Nagano T, Lubling Y, Yaffe E, Wingett SW, Dean W, Tanay A, et al. Single-cell Hi-C for genome-wide detection of chromatin interactions that occur simultaneously in a single cell. Nat Protoc. 2015;10(12):1986-2003.

51. Nagano T, Wingett SW, Fraser P. Capturing Three-Dimensional Genome Organization in Individual Cells by Single-Cell Hi-C. Methods Mol Biol. 2017;1654:79-97.

52. Bonev B, Cavalli G. Organization and function of the 3D genome. Nat Rev Genet. 2016;17(11):661-78.

53. Schmitt AD, Hu M, Ren B. Genome-wide mapping and analysis of chromosome architecture. Nat Rev Mol Cell Biol. 2016;17(12):743-55.

54. Dixon JR, Selvaraj S, Yue F, Kim A, Li Y, Shen Y, et al. Topological domains in mammalian genomes identified by analysis of chromatin interactions. Nature. 2012;485(7398):376-80.

55. Schwartz YB, Cavalli G. Three-Dimensional Genome Organization and Function in Drosophila. Genetics. 2017;205(1):5-24.

56. Hou C, Li L, Qin ZS, Corces VG. Gene density, transcription, and insulators contribute to the partition of the Drosophila genome into physical domains. Mol Cell. 2012;48(3):471-84.

57. Matthews BJ, Waxman DJ. Computational prediction of CTCF/cohesin-based intra-TAD loops that insulate chromatin contacts and gene expression in mouse liver. Elife. 2018;7.

58. Phillips JE, Corces VG. CTCF: master weaver of the genome. Cell. 2009;137(7):1194-211.

59. Bell AC, West AG, Felsenfeld G. The protein CTCF is required for the enhancer blocking activity of vertebrate insulators. Cell. 1999;98(3):387-96.

60. Splinter E, Heath H, Kooren J, Palstra RJ, Klous P, Grosveld F, et al. CTCF mediates long-range chromatin looping and local histone modification in the beta-globin locus. Genes Dev. 2006;20(17):2349-54.

61. Cuddapah S, Jothi R, Schones DE, Roh TY, Cui K, Zhao K. Global analysis of the insulator binding protein CTCF in chromatin barrier regions reveals demarcation of active and repressive domains. Genome Res. 2009;19(1):24-32.

62. Narendra V, Rocha PP, An D, Raviram R, Skok JA, Mazzoni EO, et al. CTCF establishes discrete functional chromatin domains at the Hox clusters during differentiation. Science. 2015;347(6225):1017-21.

63. Nichols MH, Corces VG. A CTCF Code for 3D Genome Architecture. Cell. 2015;162(4):703-5.

64. Guo Y, Xu Q, Canzio D, Shou J, Li J, Gorkin DU, et al. CRISPR Inversion of CTCF Sites Alters Genome Topology and Enhancer/Promoter Function. Cell. 2015;162(4):900-10.

65. Nagy G, Czipa E, Steiner L, Nagy T, Pongor S, Nagy L, et al. Motif oriented high-resolution analysis of ChIP-seq data reveals the topological order of CTCF and cohesin proteins on DNA. BMC Genomics. 2016;17(1):637.

66. Sanborn AL, Rao SS, Huang SC, Durand NC, Huntley MH, Jewett AI, et al. Chromatin extrusion explains key features of loop and domain formation in wild-type and engineered genomes. Proc Natl Acad Sci U S A. 2015;112(47):E6456-65.

67. Fudenberg G, Imakaev M, Lu C, Goloborodko A, Abdennur N, Mirny LA. Formation of Chromosomal Domains by Loop Extrusion. Cell Rep. 2016;15(9):2038-49.

68. Alipour E, Marko JF. Self-organization of domain structures by DNA-loop-extruding enzymes. Nucleic Acids Res. 2012;40(22):11202-12.

69. Maji A, Padinhateeri R, Mitra MK. The Accidental Ally: Nucleosome Barriers Can Accelerate Cohesin-Mediated Loop Formation in Chromatin. Biophys J. 2020;119(11):2316-25.

70. Busslinger GA, Stocsits RR, van der Lelij P, Axelsson E, Tedeschi A, Galjart N, et al. Cohesin is positioned in mammalian genomes by transcription, CTCF and Wapl. Nature. 2017;544(7651):503-7.

71. Wutz G, Várnai C, Nagasaka K, Cisneros DA, Stocsits RR, Tang W, et al. Topologically associating domains and chromatin loops depend on cohesin and are regulated by CTCF, WAPL, and PDS5 proteins. EMBO J. 2017;36(24):3573-99.

72. Nora EP, Goloborodko A, Valton AL, Gibcus JH, Uebersohn A, Abdennur N, et al. Targeted Degradation of CTCF Decouples Local Insulation of Chromosome Domains from Genomic Compartmentalization. Cell. 2017;169(5):930-44.e22.

73. Rao SSP, Huang SC, Glenn St Hilaire B, Engreitz JM, Perez EM, Kieffer-Kwon KR, et al. Cohesin Loss Eliminates All Loop Domains. Cell. 2017;171(2):305-20.e24.

74. Schwarzer W, Abdennur N, Goloborodko A, Pekowska A, Fudenberg G, Loe-Mie Y, et al. Two independent modes of chromatin organization revealed by cohesin removal. Nature. 2017;551(7678):51-6.

75. Merkenschlager M, Nora EP. CTCF and Cohesin in Genome Folding and Transcriptional Gene Regulation. Annu Rev Genomics Hum Genet. 2016;17:17-43.

76. Brackley CA, Johnson J, Michieletto D, Morozov AN, Nicodemi M, Cook PR, et al. Nonequilibrium Chromosome Looping via Molecular Slip Links. Phys Rev Lett. 2017;119(13):138101.

77. Kim Y, Shi Z, Zhang H, Finkelstein IJ, Yu H. Human cohesin compacts DNA by loop extrusion. Science. 2019;366(6471):1345-9.

78. Vian L, Pękowska A, Rao SSP, Kieffer-Kwon KR, Jung S, Baranello L, et al. The Energetics and Physiological Impact of Cohesin Extrusion. Cell. 2018;175(1):292-4.

79. Stigler J, Çamdere G, Koshland DE, Greene EC. Single-Molecule Imaging Reveals a Collapsed Conformational State for DNA-Bound Cohesin. Cell Rep. 2016;15(5):988-98.

80. Davidson IF, Goetz D, Zaczek MP, Molodtsov MI, Huis In 't Veld PJ, Weissmann F, et al. Rapid movement and transcriptional re-localization of human cohesin on DNA. EMBO J. 2016;35(24):2671-85.

81. Bausch C, Noone S, Henry JM, Gaudenz K, Sanderson B, Seidel C, et al. Transcription alters chromosomal locations of cohesin in Saccharomyces cerevisiae. Mol Cell Biol. 2007;27(24):8522-32.

82. Kojic A, Cuadrado A, De Koninck M, Giménez-Llorente D, Rodríguez-Corsino M, Gómez-López G, et al. Distinct roles of cohesin-SA1 and cohesin-SA2 in 3D chromosome organization. Nat Struct Mol Biol. 2018;25(6):496-504.

83. de Wit E, Vos ES, Holwerda SJ, Valdes-Quezada C, Verstegen MJ, Teunissen H, et al. CTCF Binding Polarity Determines Chromatin Looping. Mol Cell. 2015;60(4):676-84.

84. Szabó PE, Tang SH, Silva FJ, Tsark WM, Mann JR. Role of CTCF binding sites in the Igf2/H19 imprinting control region. Mol Cell Biol. 2004;24(11):4791-800.

85. Zuin J, Dixon JR, van der Reijden MI, Ye Z, Kolovos P, Brouwer RW, et al. Cohesin and CTCF differentially affect chromatin architecture and gene expression in human cells. Proc Natl Acad Sci U S A. 2014;111(3):996-1001.

86. Yu W, Ginjala V, Pant V, Chernukhin I, Whitehead J, Docquier F, et al. Poly(ADP-ribosyl)ation regulates CTCF-dependent chromatin insulation. Nat Genet. 2004;36(10):1105-10.

87. Torrano V, Navascués J, Docquier F, Zhang R, Burke LJ, Chernukhin I, et al. Targeting of CTCF to the nucleolus inhibits nucleolar transcription through a poly(ADP-ribosyl)ation-dependent mechanism. J Cell Sci. 2006;119(Pt 9):1746-59.

88. Klenova EM, Chernukhin IV, El-Kady A, Lee RE, Pugacheva EM, Loukinov DI, et al. Functional phosphorylation sites in the C-terminal region of the multivalent multifunctional transcriptional factor CTCF. Mol Cell Biol. 2001;21(6):2221-34.

89. Del Rosario BC, Kriz AJ, Del Rosario AM, Anselmo A, Fry CJ, White FM, et al. Exploration of CTCF post-translation modifications uncovers Serine-224 phosphorylation by PLK1 at pericentric regions during the G2/M transition. Elife. 2019;8.

90. Kitchen NS, Schoenherr CJ. Sumoylation modulates a domain in CTCF that activates transcription and decondenses chromatin. J Cell Biochem. 2010;111(3):665-75.

91. Peters JM, Nishiyama T. Sister chromatid cohesion. Cold Spring Harb Perspect Biol. 2012;4(11).

92. Terret ME, Sherwood R, Rahman S, Qin J, Jallepalli PV. Cohesin acetylation speeds the replication fork. Nature. 2009;462(7270):231-4.

93. Sumara I, Vorlaufer E, Stukenberg PT, Kelm O, Redemann N, Nigg EA, et al. The dissociation of cohesin from chromosomes in prophase is regulated by Polo-like kinase. Mol Cell. 2002;9(3):515-25.

94. Alexandru G, Uhlmann F, Mechtler K, Poupart MA, Nasmyth K. Phosphorylation of the cohesin subunit Scc1 by Polo/Cdc5 kinase regulates sister chromatid separation in yeast. Cell. 2001;105(4):459-72.

95. Kitagawa R, Bakkenist CJ, McKinnon PJ, Kastan MB. Phosphorylation of SMC1 is a critical downstream event in the ATM-NBS1-BRCA1 pathway. Genes Dev. 2004;18(12):1423-38.

96. Luo H, Li Y, Mu JJ, Zhang J, Tonaka T, Hamamori Y, et al. Regulation of intra-S phase checkpoint by ionizing radiation (IR)-dependent and IR-independent phosphorylation of SMC3. J Biol Chem. 2008;283(28):19176-83.

97. Matsuoka S, Ballif BA, Smogorzewska A, McDonald ER, Hurov KE, Luo J, et al. ATM and ATR substrate analysis reveals extensive protein networks responsive to DNA damage. Science. 2007;316(5828):1160-6.

98. Stewart GS, Wang B, Bignell CR, Taylor AM, Elledge SJ. MDC1 is a mediator of the mammalian DNA damage checkpoint. Nature. 2003;421(6926):961-6.

99. Kim ST, Xu B, Kastan MB. Involvement of the cohesin protein, Smc1, in Atm-dependent and independent responses to DNA damage. Genes Dev. 2002;16(5):560-70.

100. Watrin E, Peters JM. The cohesin complex is required for the DNA damage-induced G2/M checkpoint in mammalian cells. EMBO J. 2009;28(17):2625-35.

101. McAleenan A, Cordon-Preciado V, Clemente-Blanco A, Liu IC, Sen N, Leonard J, et al. SUMOylation of the α-kleisin subunit of cohesin is required for DNA damage-induced cohesion. Curr Biol. 2012;22(17):1564-75.

102. Sanyal S, Molnarova L, Richterova J, Huraiova B, Benko Z, Polakova S, et al. Mutations that prevent methylation of cohesin render sensitivity to DNA damage in. J Cell Sci. 2018;131(13).

103. Kamaletdinova T, Fanaei-Kahrani Z, Wang ZQ. The Enigmatic Function of PARP1: From PARylation Activity to PAR Readers. Cells. 2019;8(12).

104. Lüscher B, Bütepage M, Eckei L, Krieg S, Verheugd P, Shilton BH. ADP-Ribosylation, a Multifaceted Posttranslational Modification Involved in the Control of Cell Physiology in Health and Disease. Chem Rev. 2018;118(3):1092-136.

105. Wang ZQ, Auer B, Stingl L, Berghammer H, Haidacher D, Schweiger M, et al. Mice lacking ADPRT and poly(ADP-ribosyl)ation develop normally but are susceptible to skin disease. Genes Dev. 1995;9(5):509-20.

106. Wang ZQ, Stingl L, Morrison C, Jantsch M, Los M, Schulze-Osthoff K, et al. PARP is important for genomic stability but dispensable in apoptosis. Genes Dev. 1997;11(18):2347-58.

107. d'Adda di Fagagna F, Hande MP, Tong WM, Lansdorp PM, Wang ZQ, Jackson SP. Functions of poly(ADP-ribose) polymerase in controlling telomere length and chromosomal stability. Nat Genet. 1999;23(1):76-80.

108. de Murcia JM, Niedergang C, Trucco C, Ricoul M, Dutrillaux B, Mark M, et al. Requirement of poly(ADP-ribose) polymerase in recovery from DNA damage in mice and in cells. Proc Natl Acad Sci U S A. 1997;94(14):7303-7.

109. Jubin T, Kadam A, Jariwala M, Bhatt S, Sutariya S, Gani AR, et al. The PARP family: insights into functional aspects of poly (ADP-ribose) polymerase-1 in cell growth and survival. Cell Prolif. 2016;49(4):421-37.

110. Tulin A, Spradling A. Chromatin loosening by poly(ADP)-ribose polymerase (PARP) at Drosophila puff loci. Science. 2003;299(5606):560-2.

111. Petesch SJ, Lis JT. Activator-induced spread of poly(ADP-ribose) polymerase promotes nucleosome loss at Hsp70. Mol Cell. 2012;45(1):64-74.

112. Poirier GG, de Murcia G, Jongstra-Bilen J, Niedergang C, Mandel P. Poly(ADP-ribosyl)ation of polynucleosomes causes relaxation of chromatin structure. Proc Natl Acad Sci U S A. 1982;79(11):3423-7.

113. Huletsky A, de Murcia G, Muller S, Hengartner M, Ménard L, Lamarre D, et al. The effect of poly(ADP-ribosyl)ation on native and H1-depleted chromatin. A role of poly(ADP-ribosyl)ation on core nucleosome structure. J Biol Chem. 1989;264(15):8878-86.

114. Kim MY, Mauro S, Gévry N, Lis JT, Kraus WL. NAD+-dependent modulation of chromatin structure and transcription by nucleosome binding properties of PARP-1. Cell. 2004;119(6):803-14.

115. Krishnakumar R, Gamble MJ, Frizzell KM, Berrocal JG, Kininis M, Kraus WL. Reciprocal binding of PARP-1 and histone H1 at promoters specifies transcriptional outcomes. Science. 2008;319(5864):819-21.

116. Muthurajan UM, Hepler MR, Hieb AR, Clark NJ, Kramer M, Yao T, et al. Automodification switches PARP-1 function from chromatin architectural protein to histone chaperone. Proc Natl Acad Sci U S A. 2014;111(35):12752-7.

117. Reale A, Matteis GD, Galleazzi G, Zampieri M, Caiafa P. Modulation of DNMT1 activity by ADP-ribose polymers. Oncogene. 2005;24(1):13-9.

118. Zampieri M, Guastafierro T, Calabrese R, Ciccarone F, Bacalini MG, Reale A, et al. ADP-ribose polymers localized on Ctcf-Parp1-Dnmt1 complex prevent methylation of Ctcf target sites. Biochem J. 2012;441(2):645-52.

119. Witcher M, Emerson BM. Epigenetic silencing of the p16(INK4a) tumor suppressor is associated with loss of CTCF binding and a chromatin boundary. Mol Cell. 2009;34(3):271-84.

120. Farrar D, Rai S, Chernukhin I, Jagodic M, Ito Y, Yammine S, et al. Mutational analysis of the poly(ADP-ribosyl)ation sites of the transcription factor CTCF provides an insight into the mechanism of its regulation by poly(ADP-ribosyl)ation. Mol Cell Biol. 2010;30(5):1199-216.

121. Martin KA, Cesaroni M, Denny MF, Lupey LN, Tempera I. Global Transcriptome Analysis Reveals That Poly(ADP-Ribose) Polymerase 1 Regulates Gene Expression through EZH2. Mol Cell Biol. 2015;35(23):3934-44.

122. Caruso LB, Martin KA, Lauretti E, Hulse M, Siciliano M, Lupey-Green LN, et al. Poly(ADP-ribose) Polymerase 1, PARP1, modifies EZH2 and inhibits EZH2 histone methyltransferase activity after DNA damage. Oncotarget. 2018;9(12):10585-605.

123. Krishnakumar R, Kraus WL. PARP-1 regulates chromatin structure and transcription through a KDM5B-dependent pathway. Mol Cell. 2010;39(5):736-49.

124. Sala A, La Rocca G, Burgio G, Kotova E, Di Gesù D, Collesano M, et al. The nucleosome-remodeling ATPase ISWI is regulated by poly-ADP-ribosylation. PLoS Biol. 2008;6(10):e252.

125. Beneke S. Regulation of chromatin structure by poly(ADP-ribosyl)ation. Front Genet. 2012;3:169.

126. Oei SL, Herzog H, Hirsch-Kauffmann M, Schneider R, Auer B, Schweiger M. Transcriptional regulation and autoregulation of the human gene for ADP-ribosyltransferase. Mol Cell Biochem. 1994;138(1-2):99-104.

127. Soldatenkov VA, Chasovskikh S, Potaman VN, Trofimova I, Smulson ME, Dritschilo A. Transcriptional repression by binding of poly(ADP-ribose) polymerase to promoter sequences. J Biol Chem. 2002;277(1):665-70.

128. Vidaković M, Gluch A, Qiao J, Oumard A, Frisch M, Poznanović G, et al. PARP-1 expression in the mouse is controlled by an autoregulatory loop: PARP-1 binding to an upstream S/MAR element and to a novel recognition motif in its promoter suppresses transcription. J Mol Biol. 2009;388(4):730-50.

129. Ju BG, Solum D, Song EJ, Lee KJ, Rose DW, Glass CK, et al. Activating the PARP-1 sensor component of the groucho/ TLE1 corepressor complex mediates a CaMKinase IIdelta-dependent neurogenic gene activation pathway. Cell. 2004;119(6):815-29.

130. Asher G, Reinke H, Altmeyer M, Gutierrez-Arcelus M, Hottiger MO, Schibler U. Poly(ADP-ribose) polymerase 1 participates in the phase entrainment of circadian clocks to feeding. Cell. 2010;142(6):943-53.

131. Zhao H, Sifakis EG, Sumida N, Millán-Ariño L, Scholz BA, Svensson JP, et al. PARP1- and CTCF-Mediated Interactions between Active and Repressed Chromatin at the Lamina Promote Oscillating Transcription. Mol Cell. 2015;59(6):984-97.

132. Lang F, Li X, Vladimirova O, Hu B, Chen G, Xiao Y, et al. CTCF interacts with the lytic HSV-1 genome to promote viral transcription. Sci Rep. 2017;7:39861.

133. Ertel MK, Cammarata AL, Hron RJ, Neumann DM. CTCF occupation of the herpes simplex virus 1 genome is disrupted at early times postreactivation in a transcription-dependent manner. J Virol. 2012;86(23):12741-59.

134. Washington SD, Musarrat F, Ertel MK, Backes GL, Neumann DM. CTCF Binding Sites in the Herpes Simplex Virus 1 Genome Display Site-Specific CTCF Occupation, Protein Recruitment, and Insulator Function. J Virol. 2018;92(8).

135. Washington SD, Edenfield SI, Lieux C, Watson ZL, Taasan SM, Dhummakupt A, et al. Depletion of the Insulator Protein CTCF Results in Herpes Simplex Virus 1 Reactivation. J Virol. 2018;92(11).

136. Tempera I, Wiedmer A, Dheekollu J, Lieberman PM. CTCF prevents the epigenetic drift of EBV latency promoter Qp. PLoS Pathog. 2010;6(8):e1001048.

137. Chau CM, Zhang XY, McMahon SB, Lieberman PM. Regulation of Epstein-Barr virus latency type by the chromatin boundary factor CTCF. J Virol. 2006;80(12):5723-32.

138. Day L, Chau CM, Nebozhyn M, Rennekamp AJ, Showe M, Lieberman PM. Chromatin profiling of Epstein-Barr virus latency control region. J Virol. 2007;81(12):6389-401.

139. Hughes DJ, Marendy EM, Dickerson CA, Yetming KD, Sample CE, Sample JT. Contributions of CTCF and DNA methyltransferases DNMT1 and DNMT3B to Epstein-Barr virus restricted latency. J Virol. 2012;86(2):1034-45.

140. Martínez FP, Cruz R, Lu F, Plasschaert R, Deng Z, Rivera-Molina YA, et al. CTCF binding to the first intron of the major immediate early (MIE) gene of human cytomegalovirus (HCMV) negatively regulates MIE gene expression and HCMV replication. J Virol. 2014;88(13):7389-401.

141. Paris C, Pentland I, Groves I, Roberts DC, Powis SJ, Coleman N, et al. CCCTC-binding factor recruitment to the early region of the human papillomavirus 18 genome regulates viral oncogene expression. J Virol. 2015;89(9):4770-85.

142. Pentland I, Campos-León K, Cotic M, Davies KJ, Wood CD, Groves IJ, et al. Disruption of CTCF-YY1-dependent looping of the human papillomavirus genome activates differentiation-induced viral oncogene transcription. PLoS Biol. 2018;16(10):e2005752.

143. Holdorf MM, Cooper SB, Yamamoto KR, Miranda JJ. Occupancy of chromatin organizers in the Epstein-Barr virus genome. Virology. 2011;415(1):1-5.

144. Arvey A, Tempera I, Tsai K, Chen HS, Tikhmyanova N, Klichinsky M, et al. An atlas of the Epstein-Barr virus transcriptome and epigenome reveals host-virus regulatory interactions. Cell Host Microbe. 2012;12(2):233-45.

145. Li D, Mosbruger T, Verma D, Swaminathan S. Complex Interactions between Cohesin and CTCF in Regulation of Kaposi's Sarcoma-Associated Herpesvirus Lytic Transcription. J Virol. 2020;94(2).

146. Stedman W, Kang H, Lin S, Kissil JL, Bartolomei MS, Lieberman PM. Cohesins localize with CTCF at the KSHV latency control region and at cellular c-myc and H19/Igf2 insulators. EMBO J. 2008;27(4):654-66.

147. Kang H, Lieberman PM. Cell cycle control of Kaposi's sarcoma-associated herpesvirus latency transcription by CTCF-cohesin interactions. J Virol. 2009;83(12):6199-210.

148. Kang H, Wiedmer A, Yuan Y, Robertson E, Lieberman PM. Coordination of KSHV latent and lytic gene control by CTCF-cohesin mediated chromosome conformation. PLoS Pathog. 2011;7(8):e1002140.

149. Mehta K, Gunasekharan V, Satsuka A, Laimins LA. Human papillomaviruses activate and recruit SMC1 cohesin proteins for the differentiation-dependent life cycle through association with CTCF insulators. PLoS Pathog. 2015;11(4):e1004763.

150. Lupey-Green LN, Caruso LB, Madzo J, Martin KA, Tan Y, Hulse M, et al. PARP1 Stabilizes CTCF Binding and Chromatin Structure To Maintain Epstein-Barr Virus Latency Type. J Virol. 2018;92(18).

151. Martin KA, Lupey LN, Tempera I. Epstein-Barr Virus Oncoprotein LMP1 Mediates Epigenetic Changes in Host Gene Expression through PARP1. J Virol. 2016;90(19):8520-30.

152. Lupey-Green LN, Moquin SA, Martin KA, McDevitt SM, Hulse M, Caruso LB, et al. PARP1 restricts Epstein Barr Virus lytic reactivation by binding the BZLF1 promoter. Virology. 2017;507:220-30.

153. Tempera I, Deng Z, Atanasiu C, Chen CJ, D'Erme M, Lieberman PM. Regulation of Epstein-Barr virus OriP replication by poly(ADP-ribose) polymerase 1. J Virol. 2010;84(10):4988-97.

154. Ohsaki E, Ueda K, Sakakibara S, Do E, Yada K, Yamanishi K. Poly(ADP-ribose) polymerase 1 binds to Kaposi's sarcoma-associated herpesvirus (KSHV) terminal repeat sequence and modulates KSHV replication in latency. J Virol. 2004;78(18):9936-46.

155. Chung WC, Park JH, Kang HR, Song MJ. Downregulation of Poly(ADP-Ribose) Polymerase 1 by a Viral Processivity Factor Facilitates Lytic Replication of Gammaherpesvirus. J Virol. 2015;89(18):9676-82.

156. Gwack Y, Nakamura H, Lee SH, Souvlis J, Yustein JT, Gygi S, et al. Poly(ADP-ribose) polymerase 1 and Ste20-like kinase hKFC act as transcriptional repressors for gamma-2 herpesvirus lytic replication. Mol Cell Biol. 2003;23(22):8282-94.

157. Westera L, Jennings AM, Maamary J, Schwemmle M, García-Sastre A, Bortz E. Poly-ADP Ribosyl Polymerase 1 (PARP1) Regulates Influenza A Virus Polymerase. Adv Virol. 2019;2019:8512363.

158. Ha HC, Juluri K, Zhou Y, Leung S, Hermankova M, Snyder SH. Poly(ADP-ribose) polymerase-1 is required for efficient HIV-1 integration. Proc Natl Acad Sci U S A. 2001;98(6):3364-8.

159. Ariumi Y, Turelli P, Masutani M, Trono D. DNA damage sensors ATM, ATR, DNA-PKcs, and PARP-1 are dispensable for human immunodeficiency virus type 1 integration. J Virol. 2005;79(5):2973-8.

160. Siva AC, Bushman F. Poly(ADP-ribose) polymerase 1 is not strictly required for infection of murine cells by retroviruses. J Virol. 2002;76(23):11904-10.

161. Bueno MT, Reyes D, Valdes L, Saheba A, Urias E, Mendoza C, et al. Poly(ADP-ribose) polymerase 1 promotes transcriptional repression of integrated retroviruses. J Virol. 2013;87(5):2496-507.

162. Tempera I, Klichinsky M, Lieberman PM. EBV latency types adopt alternative chromatin conformations. PLoS Pathog. 2011;7(7):e1002180.

163. Dunmire SK, Verghese PS, Balfour HH. Primary Epstein-Barr virus infection. J Clin Virol. 2018;102:84-92.

164. Vetsika EK, Callan M. Infectious mononucleosis and Epstein-Barr virus. Expert Rev Mol Med. 2004;6(23):1-16.

165. Price AM, Luftig MA. To be or not IIb: a multi-step process for Epstein-Barr virus latency establishment and consequences for B cell tumorigenesis. PLoS Pathog. 2015;11(3):e1004656.

166. Hsu JL, Glaser SL. Epstein-barr virus-associated malignancies: epidemiologic patterns and etiologic implications. Crit Rev Oncol Hematol. 2000;34(1):27-53.

167. Thorley-Lawson DA, Gross A. Persistence of the Epstein-Barr virus and the origins of associated lymphomas. N Engl J Med. 2004;350(13):1328-37.

168. Khan G, Hashim MJ. Global burden of deaths from Epstein-Barr virus attributable malignancies 1990-2010. Infect Agent Cancer. 2014;9(1):38.

169. Parkin DM. The global health burden of infection-associated cancers in the year 2002. Int J Cancer. 2006;118(12):3030-44.

170. Farrell PJ. Epstein-Barr Virus and Cancer. Annu Rev Pathol. 2019;14:29-53.

171. Kanakry JA, Ambinder RF. EBV-related lymphomas: new approaches to treatment. Curr Treat Options Oncol. 2013;14(2):224-36.

172. Graham B, Lynch D. Burkitt Lymphoma. NCBI Bookshelf: Statpearls; 2020.

173. Ansell SM. Hodgkin Lymphoma: Diagnosis and Treatment. Mayo Clin Proc. 2015;90(11):1574-83.

174. Allen PB, Lechowicz MJ. Management of NK/T-Cell Lymphoma, Nasal Type. J Oncol Pract. 2019;15(10):513-20.

175. Gupta D, Mendonca S, Chakraborty S, Chatterjee T. Post Transplant Lymphoproliferative Disorder. Indian J Hematol Blood Transfus. 2020;36(2):229-37.

176. Waldum HL, Fossmark R. Types of Gastric Carcinomas. Int J Mol Sci. 2018;19(12).

177. Chen YP, Chan ATC, Le QT, Blanchard P, Sun Y, Ma J. Nasopharyngeal carcinoma. Lancet. 2019;394(10192):64-80.

178. Langmead B, Salzberg SL. Fast gapped-read alignment with Bowtie 2. Nat Methods. 2012;9(4):357-9.

179. Zhang Y, Liu T, Meyer CA, Eeckhoute J, Johnson DS, Bernstein BE, et al. Model-based analysis of ChIP-Seq (MACS). Genome Biology. 2008;9(9):R137.

180. Feng J, Liu T, Qin B, Zhang Y, Liu XS. Identifying ChIP-seq enrichment using MACS. Nat Protoc. 2012;7(9):1728-40.

181. Quinlan AR, Hall IM. BEDTools: a flexible suite of utilities for comparing genomic features. Bioinformatics. 2010;26(6):841-2.

182. Ramirez F, Ryan DP, Gruning B, Bhardwaj V, Kilpert F, Richter AS, et al. deepTools2: a next generation web server for deep-sequencing data analysis. Nucleic Acids Res. 2016;44(W1):W160-5.

183. Tanizawa H, Kim KD, Iwasaki O, Noma KI. Architectural alterations of the fission yeast genome during the cell cycle. Nat Struct Mol Biol. 2017;24(11):965-76.

184. Imakaev M, Fudenberg G, McCord RP, Naumova N, Goloborodko A, Lajoie BR, et al. Iterative correction of Hi-C data reveals hallmarks of chromosome organization. Nat Methods. 2012;9(10):999-1003.

185. Benjamini Y, Hochberg Y. Controlling the False Discovery Rate: A Practical and Powerful Approach to Multiple Testing. Journal of the Royal Statistical Society Series B (Methodological). 1995;57(1):289-300.

186. Dobin A, Davis CA, Schlesinger F, Drenkow J, Zaleski C, Jha S, et al. STAR: ultrafast universal RNA-seq aligner. Bioinformatics. 2013;29(1):15-21.

187. Robinson MD, McCarthy DJ, Smyth GK. edgeR: a Bioconductor package for differential expression analysis of digital gene expression data. Bioinformatics. 2010;26(1):139-40.

188. Chen HS, Martin KA, Lu F, Lupey LN, Mueller JM, Lieberman PM, et al. Epigenetic deregulation of the LMP1/LMP2 locus of Epstein-Barr virus by mutation of a single CTCF-cohesin binding site. J Virol. 2014;88(3):1703-13.

189. Johannsen E, Luftig M, Chase MR, Weicksel S, Cahir-McFarland E, Illanes D, et al. Proteins of purified Epstein-Barr virus. Proc Natl Acad Sci U S A. 2004;101(46):16286-91.

190. Chiu SH, Wu MC, Wu CC, Chen YC, Lin SF, Hsu JT, et al. Epstein-Barr virus BALF3 has nuclease activity and mediates mature virion production during the lytic cycle. J Virol. 2014;88(9):4962-75.

191. Paulsen SJ, Rosenkilde MM, Eugen-Olsen J, Kledal TN. Epstein-Barr virus-encoded BILF1 is a constitutively active G protein-coupled receptor. J Virol. 2005;79(1):536-46.

192. Gill MB, Edgar R, May JS, Stevenson PG. A gamma-herpesvirus glycoprotein complex manipulates actin to promote viral spread. PLoS One. 2008;3(3):e1808.

193. Xiao J, Palefsky JM, Herrera R, Berline J, Tugizov SM. The Epstein-Barr virus BMRF-2 protein facilitates virus attachment to oral epithelial cells. Virology. 2008;370(2):430-42.

194. Matveeva E, Maiorano J, Zhang Q, Eteleeb AM, Convertini P, Chen J, et al. Involvement of PARP1 in the regulation of alternative splicing. Cell Discov. 2016;2:15046.

195. Pommier Y, O'Connor MJ, de Bono J. Laying a trap to kill cancer cells: PARP inhibitors and their mechanisms of action. Sci Transl Med. 2016;8(362):362ps17.

196. Le May N, Iltis I, Amé JC, Zhovmer A, Biard D, Egly JM, et al. Poly (ADP-ribose) glycohydrolase regulates retinoic acid receptor-mediated gene expression. Mol Cell. 2012;48(5):785-98.

197. Tapia-Alveal C, Lin SJ, Yeoh A, Jabado OJ, O'Connell MJ. H2A.Z-dependent regulation of cohesin dynamics on chromosome arms. Mol Cell Biol. 2014;34(11):2092-104.

198. Kim BJ, Li Y, Zhang J, Xi Y, Yang T, Jung SY, et al. Genome-wide reinforcement of cohesin binding at pre-existing cohesin sites in response to ionizing radiation in human cells. J Biol Chem. 2010;285(30):22784-92.

199. Aguilar-Quesada R, Muñoz-Gámez JA, Martín-Oliva D, Peralta A, Valenzuela MT, Matínez-Romero R, et al. Interaction between ATM and PARP-1 in response to DNA damage and sensitization of ATM deficient cells through PARP inhibition. BMC Mol Biol. 2007;8:29.

200. Slade D, Dunstan MS, Barkauskaite E, Weston R, Lafite P, Dixon N, et al. The structure and catalytic mechanism of a poly(ADP-ribose) glycohydrolase. Nature. 2011;477(7366):616-20.

201. Tempera I, Lieberman PM. Epigenetic regulation of EBV persistence and oncogenesis. Semin Cancer Biol. 2014;26:22-9.

202. O'Neil NJ, van Pel DM, Hieter P. Synthetic lethality and cancer: cohesin and PARP at the replication fork. Trends Genet. 2013;29(5):290-7.

203. Horvath EM, Zsengellér ZK, Szabo C. Quantification of PARP activity in human tissues: ex vivo assays in blood cells and immunohistochemistry in human biopsies. Methods Mol Biol. 2011;780:267-75.

204. Kim HJ, Yardımcı GG, Bonora G, Ramani V, Liu J, Qiu R, et al. Capturing cell type-specific chromatin compartment patterns by applying topic modeling to single-cell Hi-C data. PLoS Comput Biol. 2020;16(9):e1008173.

205. Hammerschmidt W, Sugden B. Replication of Epstein-Barr viral DNA. Cold Spring Harb Perspect Biol. 2013;5(1):a013029.

206. Mandage R, Telford M, Rodríguez JA, Farré X, Layouni H, Marigorta UM, et al. Genetic factors affecting EBV copy number in lymphoblastoid cell lines derived from the 1000 Genome Project samples. PLoS One. 2017;12(6):e0179446.

207. Houldcroft CJ, Petrova V, Liu JZ, Frampton D, Anderson CA, Gall A, et al. Host genetic variants and gene expression patterns associated with Epstein-Barr virus copy number in lymphoblastoid cell lines. PLoS One. 2014;9(10):e108384.

208. Davies ML, Xu S, Lyons-Weiler J, Rosendorff A, Webber SA, Wasil LR, et al. Cellular factors associated with latency and spontaneous Epstein-Barr virus reactivation in B-lymphoblastoid cell lines. Virology. 2010;400(1):53-67.

209. Botstein D, Chervitz SA, Cherry JM. Yeast as a model organism. Science. 1997;277(5330):1259-60.

210. McGeoch DJ, Cook S, Dolan A, Jamieson FE, Telford EA. Molecular phylogeny and evolutionary timescale for the family of mammalian herpesviruses. J Mol Biol. 1995;247(3):443-58.

211. Wertheim JO, Smith MD, Smith DM, Scheffler K, Kosakovsky Pond SL. Evolutionary origins of human herpes simplex viruses 1 and 2. Mol Biol Evol. 2014;31(9):2356-64.

APPENDICES

APPENDIX A

ALL PHYSICALLY INTERACTING DNA FRAGMENTS

A LCL

Rank	Start 1	End 1	Start 2	End 2	Distance	P-values	FDR
1	32,000	36,999	46,000	50,999	14,000	5.54E-24	6.44E-20
2	31,000	35,999	55,000	59,999	24,000	3.21E-21	1.61E-17
3	0	4,999	169,000	173,999	169,000	7.05E-17	1.64E-13
4	32,000	36,999	140,000	144,999	108,000	1.57E-10	1.52E-07
5	0	2,999	3,000	7,999	5,000	4.63E-08	3.59E-05
6	141,000	145,999	146,000	150,999	5,000	1.11E-07	7.57E-05
7	11,000	15,999	47,000	51,999	36,000	1.98E-07	0.000115
8	140,000	144,999	159,000	163,999	19,000	2.49E-07	0.000138
9	36,000	40,999	140,000	144,999	104,000	3.62E-07	0.000183
10	75,000	79,999	169,000	173,999	94,000	1.88E-06	0.000781
11	9,000	13,999	90,000	94,999	81,000	2.97E-06	0.001018
12	37,000	41,999	95,000	99,999	58,000	4.31E-06	0.001318
13	48,000	52,999	169,000	173,999	121,000	7.44E-06	0.002111
14	88,000	92,999	169,000	173,999	81,000	1.98E-05	0.004907
15	77,000	81,999	140,000	144,999	63,000	1.68E-04	0.025682
16	90,000	94,999	140,000	144,999	50,000	2.51E-04	0.032807
17	31,000	35,999	162,000	166,999	131,000	4.43E-04	0.046846
18	127,000	131,999	140,000	144,999	13,000	7.03E-04	0.068723
19	11,000	15,999	76,000	80,999	65,000	1.63E-03	0.117764
20	9,000	13,999	97,000	101,999	88,000	2.04E-03	0.133679
21	92,000	96,999	140,000	144,999	48,000	2.59E-03	0.158299
22	11,000	15,999	139,000	143,999	128,000	3.94E-03	0.202911
23	115,000	119,999	122,000	126,999	7,000	4.19E-03	0.210006
24	112,000	116,999	167,000	171,999	55,000	5.56E-03	0.242070
25	100,000	104,999	114,000	118,999	14,000	6.73E-03	0.264501
26	72,000	76,999	117,000	121,999	45,000	1.50E-02	0.428209

B LCL+olaparib

Rank	Start 1	End 1	Start 2	End 2	Distance	P-values	FDR
1	0	2,999	31,000	35,999	33,000	1.32E-54	1.54E-50
2	0	4,999	169,000	173,999	169,000	5.65E-31	2.19E-27
3	31,000	35,999	44,000	48,999	13,000	4.28E-26	9.94E-23
4	31,000	35,999	99,000	103,999	68,000	1.97E-23	3.27E-20
5	31,000	35,999	152,000	156,999	121,000	7.93E-10	6.59E-07
6	101,000	105,999	169,000	173,999	68,000	2.70E-09	1.85E-06
7	4,000	8,999	11,000	15,999	7,000	2.87E-09	0.000002
8	31,000	35,999	153,000	157,999	122,000	1.11E-08	0.000006
9	137,000	141,999	138,000	142,999	1,000	1.23E-08	0.000006
10	34,000	38,999	169,000	173,999	135,000	2.85E-07	0.000104
11	31,000	35,999	63,000	67,999	32,000	1.51E-06	0.000497
12	32,000	36,999	121,000	125,999	89,000	1.54E-06	0.000497
13	11,000	15,999	106,000	110,999	95,000	5.97E-06	0.001333
14	90,000	94,999	140,000	144,999	50,000	7.59E-06	0.001604
15	10,000	14,999	76,000	80,999	66,000	4.62E-05	0.007460
16	163,000	167,999	168,000	172,999	5,000	1.15E-04	0.016017
17	9,000	13,999	55,000	59,999	46,000	1.84E-04	0.023980
18	74,000	78,999	169,000	173,999	95,000	1.33E-03	0.110044

C Mutu

Rank	Start 1	End 1	Start 2	End 2	Distance	P-values	FDR
1	0	4,999	169,000	173,999	169,000	9.98E-87	1.14E-82
2	6,000	10,999	11,000	15,999	5,000	3.73E-11	1.42E-07
3	32,000	36,999	144,000	148,999	112,000	1.58E-08	3.03E-05
4	32,000	36,999	37,000	41,999	5,000	6.88E-07	6.58E-04
5	10,000	14,999	94,000	98,999	84,000	5.53E-06	2.89E-03
6	165,000	169,999	168,000	172,999	3,000	2.99E-05	1.07E-02
7	141,000	145,999	143,000	147,999	2,000	3.62E-03	0.265300

D Mutu+olaparib

Rank	Start 1	End 1	Start 2	End 2	Distance	P-values	FDR
1	0	4,999	169,000	173,999	169,000	2.59E-34	2.98E-30
2	4,000	8,999	11,000	15,999	7,000	1.62E-15	9.28E-12
3	32,000	36,999	37,000	41,999	5,000	1.73E-07	8.26E-05
4	163,000	167,999	168,000	172,999	5,000	6.83E-05	9.91E-03

APPENDIX A: All Physically Interacting DNA Fragments. A-D) DNA fragments forming ligation junctions during Hi-C were mapped back to the EBV genome. The location of the fragments are listed as their basepair coordinates on the linearized EBV episome, with one fragment in the ligation product as “Start 1” and “End 1” and the other as “Start 2” and “End 2”. Their separation on the linearized episome is listed under “Distance”. Significance (p value) and false discovery rate (FDR) are both in ascending order, which is how “Rank” is determined. Values listed have already been filtered for “unique ligation products”, i.e. repeated ligation products were removed.

APPENDIX B

DETERMINATION OF OLAPARIB AND PDD EFFICACY IN LCLS

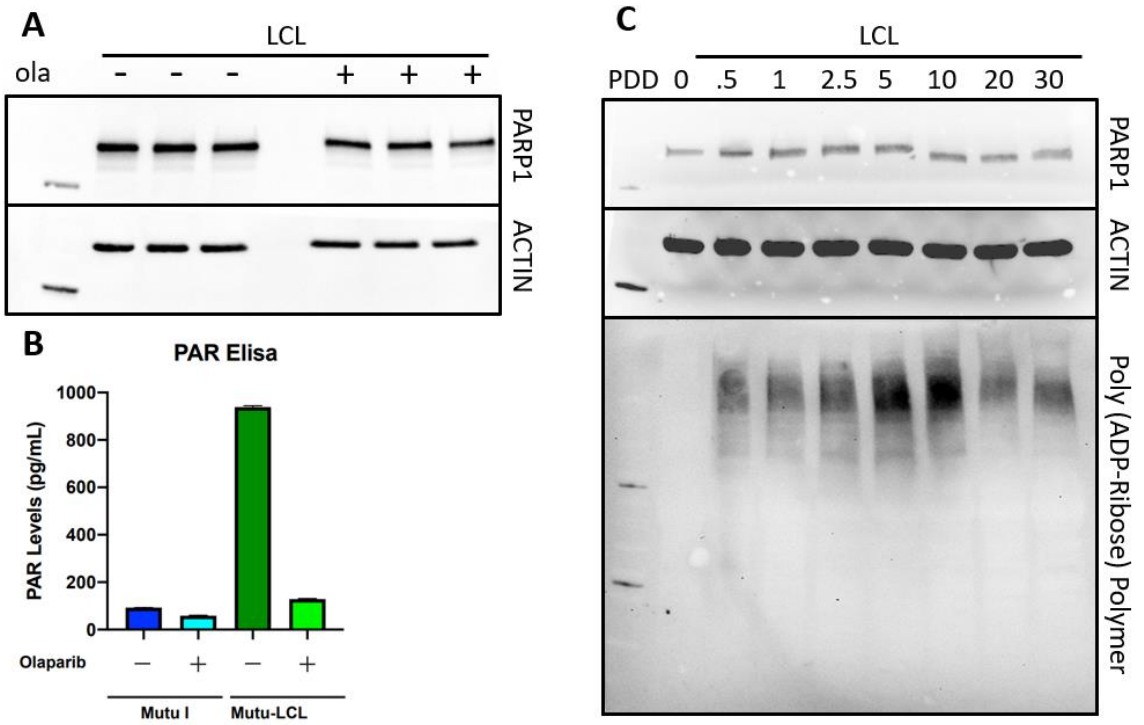

APPENDIX B: Determination of olaparib and PDD efficacy in LCLs. Three biological replicates of LCLs were treated with 2.5uM olaparib or equal volume DMSO for 72 hours. Cells were then A) collected in RIPA buffer and immunoblotted for PARP1 and actin or B) collected and quantified for intracellular PAR concentration via PAR ELISA. C) Three biological replicates of LCLs were treated with varying concentration of PDD 00017273 for 72 hours, with re-dosing every 24 hours. Cells were then collected and immunoblotted for PARP1, actin, or PAR polymer.

APPENDIX C

TOTAL RNA-SEQ DATASET AFTER PARP INHIBITION

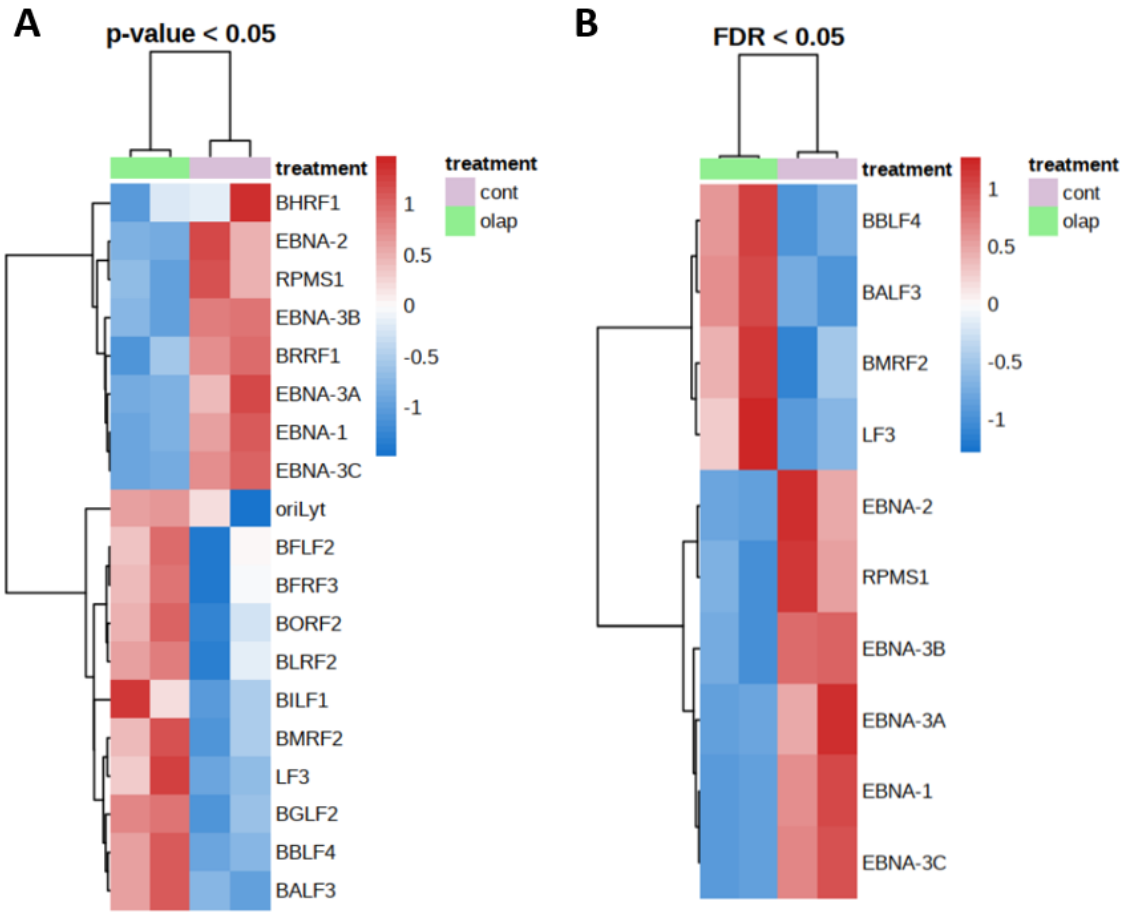

APPENDIX C: Total RNA-seq dataset after PARP inhibition. Gene expression data in LCLs treated with olaparib or equal volume DMSO for 72 hours. A) Genes dysregulated at p<.05 significance. B) Genes dysregulated at p<.05 and FDR<.05.